Nanomaterials in Water Remediation: Functionalization and Applications for Pharmaceutical Removal in Municipal Wastewater Effluent

by

Ivana Jaciw-Zurakowsky

A thesis
presented to the University of Waterloo
in fulfillment of the
thesis requirement for the degree of
Master of Applied Science
in
Mechanical and Mechatronics Engineering

Waterloo, Ontario, Canada, 2019

AUTHOR'S DECLARATION

I hereby declare that I am the sole author of this thesis. This is a true copy of the thesis, including any required final revisions, as accepted by my examiners.

I understand that my thesis may be made electronically available to the public.

Abstract

With an increasing population, there is a higher pressure on natural resources including water. Increased water consumption, altered hydrology and pollution, threaten the sustainability of aquatic ecosystems and water resources. The increasing contamination of water resources with a diversity of priority and emerging chemicals of concern has created a need for innovative water treatment solutions. Although current technologies can remove some of these chemicals new and more effective treatment solutions are still required for both water and wastewater applications. Nanomaterials have been widely studied for their potential for photocatalytic removal of contaminants in water treatment applications. Unfortunately, the low efficiency and difficulty with recovery of the catalyst material have limited implementation at the industrial or municipal scale. Functionalization of nanoparticles such as TiO_2 is a possible mechanism to improve the efficiency of the photocatalytic reactions holds considerable promise for treatment applications.

Plasmonic photocatalysis has widely been considered as a potential method to improve photocatalytic efficiency. Few studies have examined optimizations of the ratio of metal to metal-oxide in photocatalysts for improving the efficiency of photocatalytic reactions. In the current study, the ratio of silver was altered in zinc oxide nanoparticles and the photocatalytic efficiency determined. Silver-zinc oxide nanoparticles were hydrothermally synthesized beginning with zinc oxide nanoparticles blended with acid digester containing silver nitrate and methenamine (HMTA). Characterization of the synthesized nanomaterials found little difference in the bandgap (around 380 nm) of the different manufactured materials and the agglomeration levels of the nanomaterial, indicating a decrease in surface area and reactivity. However, this agglomeration was seen through all silver loadings, meaning that it is not a factor affecting the comparison of this study. A photocatalytic test was completed using six-cm collimated UV-LED beam (θ_{beam}= 4 cm) light source setup with a heat sink, placed over a four-position magnetic stir plate (10.5 cm above the surface of the water). Twenty mg of the silver-zinc oxide nanoparticles were added to a

300 mL solution of 0.5 mM terephthalic acid (TPA) to measure hydroxyl production through the conversion of TPA into hydroxyterephthalic acid (HTPA). The conversion rate constants, calculated using a zero-order reaction rate model, were compared. An increase in silver resulted in an apparent increase in the photocatalytic efficiency of the nanomaterial as indicated by increased hydroxyl production. However, this did not result in a major change in the photocatalytic activity until the silver was greater than 700,000%.

Previously published laboratory scale photocatalytic removal tests tend to use purified water as the matrix in experiments. However, actual industrial or municipal applications need to consider the natural waters and effluents that are a complex mixture of chemicals that can affect the efficiency of photocatalysts. Although nanoparticles have been proposed for the removal of emerging contaminants, such as pharmaceuticals, in water and wastewater few tests have been conducted under these actual conditions. The efficiency of TiO_2 (P25) for the removal of representative pharmaceuticals in an actual wastewater matrix (i.e. Waterloo municipal wastewater effluent) was compared to the removal efficiency in pure (Milli-Q) water. Pharmaceutical removal tests were completed under UV light irradiation, and a model photocatalyst (P25) and compared to dark and non-photocatalyst conditions. After exposure to different periods of time the pharmaceuticals were isolated from solution using solid phase extraction (SPE) and quantified using liquid chromatography mass spectroscopy (LC-MS/MS). The removal was measured by comparing the reduction in concentration using the first-order reaction rate constants. Using UV irradiation combined with a photocatalyst removal of some pharmaceuticals to below the detection limit was observed in as little as 5 minutes in Milli-Q water. In contrast, in wastewater effluent photocatalysis removed fewer of the pharmaceutical compounds and there was an apparent decrease in the photocatalytic efficiency. The decrease in efficiency is likely due to the blocking of the UV light and scavenging of the generated reactive oxygen species by the organic matter in the wastewater effluent matrix. Although photocatalysis is a useful tool for the removal of pharmaceuticals from pure water matrices, the substantial decrease of the removal rate for a wastewater effluent matrix exemplifies the need for further efficiency improvements for applications in

natural waters/effluents. The challenges surrounding the application of nanoparticles in photocatalytic treatment processes for water and wastewater treatment is explored and highlighted.

Acknowledgements

I would first like to thank my supervisors Professor Mark R. Servos and Dr. Y Norman Zhou; without whose support this work would not have been possible.

An additional thank you goes to NSERC and their support of this project as part of the Strategic Partner Grant.

I would also like to especially thank Leslie Bragg, who has been immeasurably helpful in all areas of work, including general lab support and constant assistance with data processing and acknowledgement. I would also like to thank Azar Fattahi, who has been a true friend and partner in navigating our research. Thank you Nivetha Srikanthan for assisting in the collection of wastewaters and helping me navigate the Servos lab. Thank you to Emad Shahman, who introduced me to the basis of our work, and our co-ops Olivia Schneider and Avneet Kaur who always happily lent a hand in the lab. Thanks to Robert Liang for his leadership of the team.

Thank you to my friends within and outside of CAMJ and the Servos group in Biology, who kept light perspective on the experience of being a graduate student. It would have been impossible to get through a master's without the constant support and jokes we shared throughout.

Finally, I would like to thank my family. My parents Leo and Angela Jaciw-Zurakowsky, who were always ready to accept a phone call, welcome me home for dinner and managed to keep my dear G6 alive past 419 000 km (and counting). To my siblings Renata, Natalie, Andrew, Luke and my in-law's Ante and Brandon and my precious nephew Broderick who was always there for family dinners and to keep a constant loving and joking relationship. You guys are the best.

Dedication

For my family, who were all relentless in their support and encouragement.

Table of Contents

List of Figures

List of Tables

List of Abbreviations

AOP: advanced oxidation process

DRS: diffuse reflectance spectroscopy

HMTA: Hexamethylenetetramine or methenamine

HTPA: hydroxyterephthalic acid

LSPR: Localized surface plasmon resonance

NOM: natural organic matter

PZC: point of zero charge

ROS: reactive oxygen species

SEM: scanning electron microscopy

TPA: terephthalic acid

UV: ultraviolet

UV-LEDs: ultraviolet light emitting diodes

XPS: X-ray photoelectron spectroscopy

Chapter 1
Introduction

With an increasing population, water sources are strained due to higher demand and greater contamination of a variety of emerging chemicals of concern. Innovative treatment approaches are needed to ensure protection of the environment as well as downstream drinking water intakes. Photocatalysis using nanomaterials has been explored widely as a possible approach for treatment of a broad variety of environmental contaminants in water. To use photocatalysts in water treatment, functionalization's may provide improved removal. The overall objective of this thesis is to improve the photocatalytic efficiency of zinc oxide nanomaterials through plasmonic photocatalysts and to test the efficacy of photocatalytic degradation of pharmaceuticals in wastewater effluent collected from a local wastewater treatment plant (Waterloo).

Although the use of nanomaterials for photocatalytic water treatment applications has been widely researched for nearly 40 years (Cates, 2017) this extensive research base has not been effectively translated into industrial applications. Although many scientific challenges currently limit its application in water treatment this approach continues to hold considerable promise. Titanium dioxide nanomaterials have become the benchmark for studying photocatalytic efficiency, as it is commercially available as Degussa P25, nanoparticles with a primary particle size of 21-23 nm. However, many other metal-oxides also have photocatalytic potential, such as zinc oxide. Initial trials found a significant improvement in the conversion rate constant of terephthalic acid (TPA) into hydroxyterephthalic acid (HTPA) when using zinc oxide nanoparticles over P25. Zinc oxide nanoparticles were therefore proposed for further study for improving photocatalytic efficiency.

Plasmonic photocatalysis can improve the photocatalytic efficiency by combining a metal with a metal-oxide semiconducting material. The blend of the elements enhances efficiency through both localized surface plasmon resonance (LSPR) and Schottky barrier effects. While studies are often completed using plasmonic photocatalysis, few studies have researched the optimal ratio of metal to metal-oxide nanomaterials to improve photocatalytic efficiency. In this thesis, hydrothermal synthesis methods were used with increasing silver

nitrate concentrations to create new materials and these applied in a photocatalytic reactor to find the ratio with an optimal conversion rate. Zinc oxide nanoparticles were combined with a solution of acid digester, containing silver nitrate and hexamethylenetetramine (HMTA). Different volumes of acid digester were used to load the zinc oxide with a range of silver. The photocatalytic efficiency of different silver loadings was tested by observing hydroxyl production through the conversion of terephthalic acid (TPA) into hydroxyterephthalic acid (HTPA).

Research exploring photocatalytic removal of contaminants of interest in water treatment applications typically use pure water matrices (such as Mill-Q water) spiked with a single contaminant. These studies explore the mechanisms and efficiency for contaminant removal but do not represent the complexity of water matrices where treatment would be applied. The second component of this thesis tests the relative efficiency of photocatalytic removal of selected pharmaceuticals using TiO_2 nanoparticles (P25) in both a pure water matrix and with wastewater effluent. The conversion rate constants (calculated using a first-order reaction rate), for a variety of pharmaceuticals typically found in wastewater were compared under light and dark conditions. The various properties of pharmaceuticals will affect the overall photocatalytic removal of the compound. The charge of the pharmaceutical in solution is important because there is a dependence on surface adsorption for photocatalytic removal. Oppositely charged particles should enhance electrostatic attraction. The degradation rate constants were compared with the charges of the pharmaceuticals in solution to observe whether electrostatic attraction significantly affected photocatalytic degradation rate.

1.1 Thesis Organization

This thesis is organized with a literature review and two data/experimental chapters, each describing the major experiments conducted, followed by general conclusions and recommendations chapter. A brief overview of each chapter is listed below:

- **Chapter 1. Introduction:** This chapter has an introduction to the thesis and outlines the organization of the thesis.

- **Chapter 2. Literature Review:** This chapter contains a brief introduction to the theory and challenges for application of nanoparticle photocatalytic processes for treatment of trace contaminants in water/wastewater.
- **Chapter 3. Functionalization of Zinc Oxide with Silver to Improve Efficiency of Hydroxyl Formation:** This chapter contains the project that studies the use of plasmonic photocatalysis for improved hydroxyl production.
- **Chapter 4. Removal of Pharmaceuticals from Wastewater Effluent using Titanium Dioxide based Photocatalysis:** This chapter outlines the project regarding the removal of pharmaceuticals using titanium dioxide photocatalysis from pure (Milli-Q) and wastewater effluent.
- **Chapter 5 Conclusions and Recommendations:** This chapter includes the general conclusions from and recommendations for future studies.

Chapter 2 Literature Review

This review was partially adapted from (Jaciw-Zurakowsky et al., 2019).

Over the past number of years, there has been a vast increase in the strains placed on the environment, including our water sources. For the first time in history, over half of the population lives within an urban area. With an ever-increasing population, the demands for water and the usage requirements have changed. The United Nations has established Sustainable Development Goals (SDGs) as an urgent call for global partnership. The SDGs highlight areas that must be prioritized to ensure the protection of the environment and the improvement of life in both developing and developed countries. For water protection, SDG 6, Clean Water and Sanitation, and SDG 14, Life Below Water are of interest. New challenges in water treatment have surfaced with the increased population.

Emerging contaminants, including pharmaceuticals and microtoxins, are subjects of interest due to the increased occurrence in Canadian freshwaters. These contaminants have demonstrated adverse effects on aquatic species, such as altered reproduction habits in fish species. Concentrations of less than one ng/L resulted in decreased egg fertilization and demasculinization in male fathead minnows (*Pimephales promelas*) (Parrott and Blunt, 2005). In humans, there is little knowledge surrounding the effects of chronic consumption of subtherapeutic concentrations of pharmaceuticals (Jones, Lester and Voulvoulis, 2005). Microcystins, produced by blue-green algae are common in Canada in the summer and fall months. Microcystins can have adverse effects on aquatic species and these neurotoxins can cause neurodegeneration in humans (Kotak and Zurawell, 2007). The long term, low concentration effects of emerging contaminants on human health is not fully understood but may be detrimental. Current Canadian infrastructure lacks the required technology to achieve full removal of many of these emerging contaminants. Nanomaterial-based photocatalysis may provide a unique solution for difficult to remove emerging contaminants in both large scale and decentralized applications.

2.1 Water Treatment in Canada

In Canada, advanced oxidation processes are often applied during drinking water treatment. The sources for drinking water, especially surface water, are also where treated wastewater effluent is often deposited. However, groundwater used as drinking water sources may also be contaminated by wastewaters, and the diversity of contaminants they contain. It would therefore be ideal to treat and minimize contamination 'at the source'.

The typical wastewater treatment processes employed in Canada include several stages of treatment. Primary treatment methods involve the removal of large solids via screen filtering, flocculation and coagulation steps. Secondary treatment processes remove soluble organic matter that passed primary treatment and biological matter, including bacteria and viruses. This includes methods such as biofiltration or activated sludge. Tertiary treatment is the removal methods employed to remove specific contaminants and may include disinfection. The contaminants removed during tertiary treatment can include many but not all emerging contaminants (Nathonson and Ambulkar, 2018). Tertiary treatment, including advanced oxidation processes (AOPs), are rarely employed in wastewater treatment in Canada (Government of Canada, 2017). However, there is an increasing trend to include additional treatment to protect surface waters and drinking water sources. AOPs generate highly reactive species such as (primarily but not exclusively) hydroxyl radicals which then oxidize and ultimately decompose the target pollutants. Advanced oxidation processes are potentially beneficial because they often degrade trace organic contaminants (i.e. micropollutants) that are otherwise poorly removed by other treatment processes.

2.2 Tertiary Water Treatment Methods

Many tertiary (or additional) treatment processes depend on advanced oxidation processes (AOPs). Advanced oxidation processes can remove or transform organic matter in aqueous solutions by facilitating interactions with reactive oxygen species (ROS). Dominant ROS are displayed in Figure 2-1, and includes oxygen, peroxide, the hydroxyl radical and the hydroxyl ion (Held, 2015).

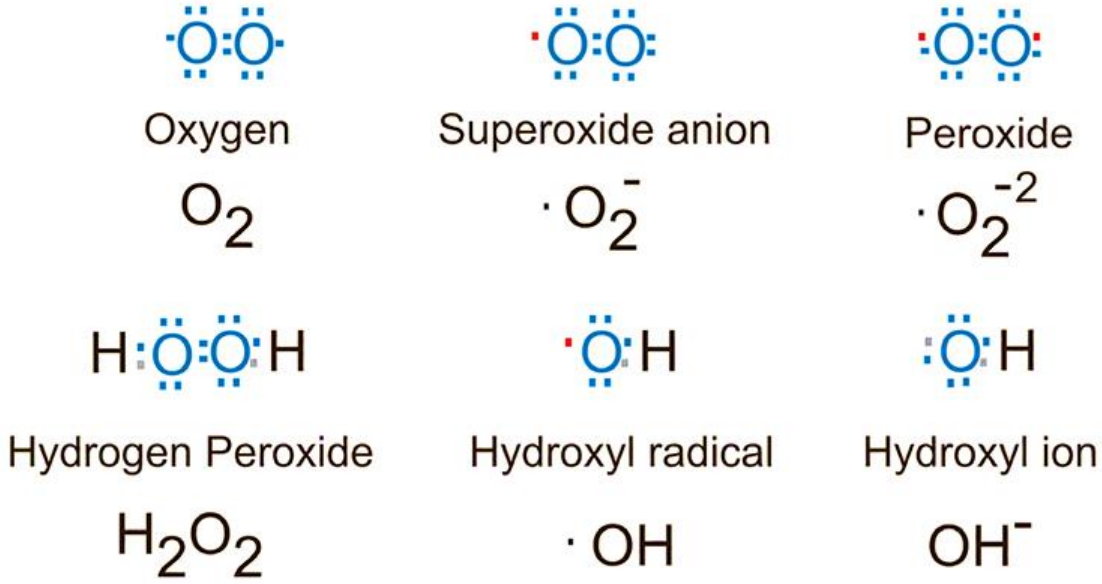

Figure 2-1 Common reactive oxygen species (ROS) and their electron structures. The red dot represents an unpaired electron. Image from Held (2015).

AOPs may employ various materials based on the individual requirements of the application. Ozonation is a standard advanced oxidation process often employed in drinking water treatment but can potentially be used in wastewater. Although ozone is highly effective, it can be costly (e.g. energy consumption), efficiency can affected by water quality and it can potentially produce toxic byproducts and be dangerous to operate (Tibbetts, 1995). Another AOP is the Fenton reaction, which involves the combination of hydrogen peroxide and a Fenton reagent (often Fe2+ or Fe3+). The Fenton reagents react with hydrogen peroxide to create two different reactive oxygen species, as demonstrated in Equation 1-1 and Equation 1-2.

$$Fe^{2+} + H_2O_2 \rightarrow Fe^{3+} + HO\cdot + OH^- \quad \textbf{Equation 1-1}$$

$$Fe^{3+} + H_2O_2 \rightarrow Fe^{2+} + HOO\cdot + H^+ \quad \textbf{Equation 1-2}$$

Industrial water treatment applications often use Fenton reactions. However, they carry limitations such as required elevated temperatures and limited operational pH (approximately 3 (Tušar *et al.*, 2011)) which leads to the need for constant acidic input, and a subsequent neutralization step. Iron also forms complexes with wastewater compounds, and the recovery of iron is limited.

While most AOPs work well on their own, a combination of various advanced oxidation processes in a single treatment step often results in higher contaminant removal. For example, one may consider combining photocatalysis with hydrogen peroxide to increase the concentration of ROS in a solution, thereby increasing the overall contaminant removal. In many cases, the addition of light irradiation also increases the degradation rate. Other advanced oxidation processes include other UV based AOPs such as UV/persulfate, UV/para-acetic acid (PAA), and UV/chlorine.

2.3 UV Based Advanced Oxidation Processes

Numerous AOPs utilize UV light irradiation, with the simplest being photolysis. Photolysis is the use of light to drive the degradation of chemicals, including contaminants, following either direct or indirect mechanisms. Direct photolysis occurs when the contaminant molecule absorbs light energy, causing the molecule to decompose. Indirect photolysis in natural waters involves the absorption of light energy by naturally occurring components in water, such as humic substances, that perform as photosensitizers to create the ROS that lead to contaminant degradation (Zepp, Baughman and Schlotzhauer, 1981). Nitrate is an example of a naturally occurring component that is a photosensitizer for the production of hydroxyl radicals (Foote *et al.*, 1996). The dissolved organic matter generates reactive species when exposed to light irradiation. These reactive species then interact with the contaminant, driving its decomposition (Santoke and Cooper, 2017). Other dissolved organic matter contains a variety of functional groups that can increase photolysis activity; these functional groups include carbonyls, nitroaromatics, n-oxides, alkenes, aryl chlorides, and products with a weak carbon-hydrogen bond (e.g., carbon-hydrogen-acidic compounds). The major

photodegradation pathways can include hydroxyl additions on alkenes and decarboxylation (Kamat and Meisel, 2002).

2.3.1.1 **Photocatalytic Mechanism**

Photocatalytic advanced oxidation processes involve the combination of a UV light source and a photocatalyst. The interaction of these two components create ROS, which interact with contaminants, driving their degradation. Photocatalysis follows a similar mechanism to photolysis. The photocatalytic nature of any material lies in the ability of the material to absorb light. Photocatalysts absorb light at specific energies that allow electrons in the valence band to 'jump' an energy level into the conduction band, leaving behind a hole. In the presence of water, the electron can react with O_2 to create $O_2\cdot$ radicals, and the hole can react with water molecules to form reactive hydroxyls, as demonstrated in Figure 2-2.

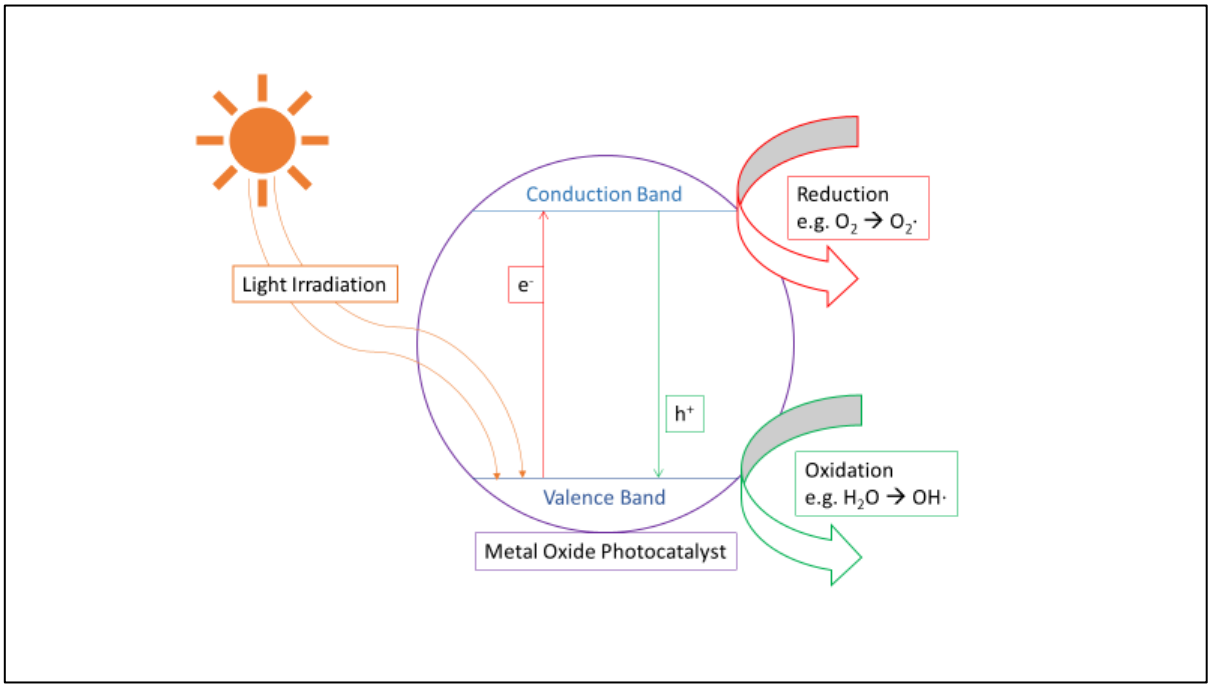

Figure 2-2-2 Photocatalysis with a metal-oxide semiconductor. The separated electrons and holes interact with water species to create reactive oxygen species (ROS).

The generated ROS in the aqueous solution, are free to degrade contaminants. There are a variety of materials employed for their photocatalytic properties, including semiconducting materials. The most commonly studied photocatalyst is TiO_2, though almost all metal-oxides can perform as photocatalytic semiconductors. The mechanism of photocatalysis was first proposed by Hermann and Folger in 1999, who divided the photocatalysis reaction into five steps, illustrated in Figure 2-3 (Herrmann, 1999; Kamat and Meisel, 2002; Chong *et al.*, 2010):

1. Mass transfer of the organic contaminants (e.g., A) in the liquid phase to the TiO_2 surface;
2. Adsorption of the organic contaminants onto the photon activated TiO_2 surface (i.e., Surface activation by photon energy co-occurs in this step);
3. Photocatalysis reaction for the adsorbed phase on the TiO_2 surface (e.g., A → B);
4. Desorption of the intermediates(s) (e.g., B) from the TiO_2 surface;
5. Mass transfer of the intermediate(s) (e.g., B) from the interface region to the bulk fluid.

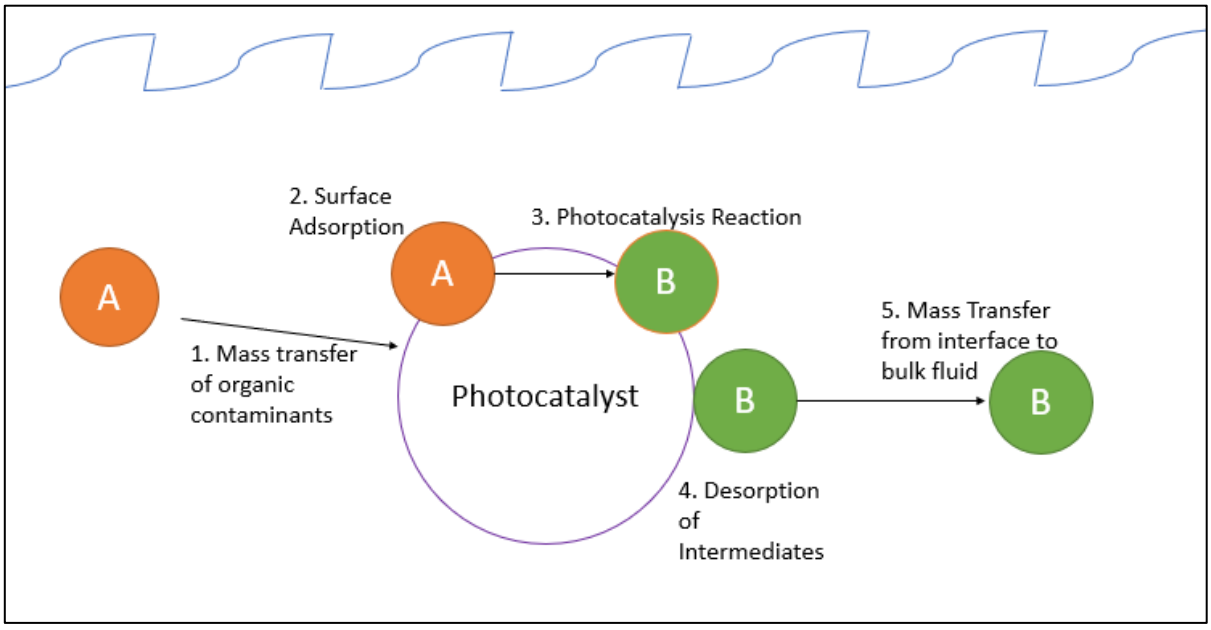

Figure 2-2-3: The five steps of the photocatalytic reaction, as proposed by Hermann and Folger. A represents the organic contaminant, and B represents the degradation intermediates, which are transferred back into the bulk fluid (Herrmann, 1999).

In this mechanism, adsorption of the contaminant onto the photocatalyst is vital. Various models are used to describe this adsorption, including the Mars- Van Krevelen model, stationary-state adsorption, the Eley Rideal, and the Langmuir- Hinshelwood models for one or two types of adsorption (Mozzanega, Herrmann and Pichat, 1979). The most commonly used photocatalytic rate models are the Langmuir- Hinshelwood models, shown in Equation 2-4. The first model describes the reaction rate, *r*, derived from the Langmuir- Hinshelwood isotherm for competition for one type of site (Equation 2-3), and the next describes the reaction rate, *r*, derived from the Langmuir-Hinshelwood isotherm for independent adsorption sites for the reductant and the oxidant (Equation 2-4) (Peral, Domènech and Ollis, 1997).

$$r = \frac{k \cdot K_{O2}^{n} \cdot K_R \cdot P_{O2}^{n} \cdot P_R}{\left(1 + K_{O2}^{n} \cdot P_{O2}^{n} + K_R \cdot P_R\right)^2} \quad \textbf{Equation 2-3}$$

$$r = \frac{k \cdot K_{O2}^{n} \cdot K_R \cdot P_{O2}^{n} \cdot P_R}{\left(1 + K_{O2}^{n} \cdot P_{O2}^{n}\right)\left(1 + K_R \cdot P_R\right)} \quad \textbf{Equation 2-4}$$

The *K* in these cases refers to a pseudo-equilibrium constant, while the *k* refers to the elementary reaction rate constant. The *P* refers to the proportion of occupied sites, of the oxygen or the reactant, depending on the subscript.

2.3.2 Mechanism of Contaminant Degradation

The hydroxyl radical is the primary oxidant in photocatalytic systems (Turchi and Ollis, 1990). There are four proposed mechanisms for hydroxyl attack. In case one, the hydroxyl is adsorbed onto the photocatalyst and reacts with the adsorbed surface contaminant. The second case involves the reaction of free hydroxyl and an adsorbed contaminant. Case three involves an adsorbed radical reacting with a free contaminant. The final hydroxyl attack case is the interaction between unbound hydroxyls and contaminants (Turchi and Ollis, 1990). While there are reactions with other radicals, Turchi and Ollis (1990) demonstrated the dominance of hydroxyls as the primary oxidizing species by detection of hydroxyls as the dominant species by electron spin resonance. They also demonstrated the necessity of

photocatalyst surface hydroxylation for organic degradation. The kinetic isotope effect was studied using D_2O and found a decrease in reaction rate when D_2O replaced H_2O in solution, demonstrating the importance of the hydroxyl formation step. Finally, the intermediates of contaminants are highly hydroxylated.

The complete degradation of a compound is called mineralization. The formed hydroxyl radicals likely continually attack the compound byproducts until they are fully mineralized. Table 1 outlines the photocatalytic reaction scheme. Other radicals can react with contaminants and cause some of the removal mechanisms. However, the reaction is often adsorption dependent, as shown in hydroxyl attack cases one to three, where with the hydroxyl, the contaminant, or both molecules are adsorbed to the surface of the photocatalyst. The fourth hydroxyl attack case refers to unbound hydroxyl and contaminant interacting without adsorption. Adsorption is profoundly affected by the charge of the contaminant, where more oppositely polarized materials are more likely to absorb.

Table 1: Mechanisms involved in the photocatalytic reaction, adapted from (Turchi and Ollis, 1990). Species in parenthesis may be adsorbed or in the aqueous phase. Oxygens with a subscript L refer to oxygens on the lattice.

Reaction Stage	Mechanism	Equation Number
Excitation	$TiO_2 \overset{h\nu}{\rightarrow} e^- + h^+$	(T1-1)
Adsorption	$O_L^{2-} + Ti^{IV} + H_2O$	(T1-2a)
	$\leftrightarrow O_L H^- + Ti^{IV} \cdot OH^-$	(T1-2b)
	$Ti^{IV} + H_2O \leftrightarrow Ti^{IV} \cdot H_2O$	(T1-3)
	$site + R_I \leftrightarrow R_{1,ads}$	(T1-4)
	$OH^{\cdot} + Ti^{IV} \leftrightarrow Ti^{IV} \lfloor OH^{\cdot}$	
Recombination	$e^- + h^+ \rightarrow heat$	(T1-5)
Trapping	$Ti^{IV} \cdot OH^- + h^+ \leftrightarrow Ti^{IV} \lfloor OH^{\cdot}$	(T1-6a)
	$Ti^{IV} \cdot H_2O + h^+ \leftrightarrow Ti^{IV} \lfloor OH^{\cdot} + H^+$	(T1-6b)

Reaction Stage	Mechanism	Equation Number
	$R_{1,ads} + h^+ \leftrightarrow R \cdot^+_{1,ads}$	(T1-7)
	$Ti^{IV} + e^- \leftrightarrow Ti^{III}$	(T1-8a)
	$Ti^{III} + O_2 \leftrightarrow Ti^{IV} \cdot O \cdot^-_2$	(T1-8b)
Hydroxyl Attack		
Case 1	$Ti^{IV}\lfloor OH^{\cdot} + R_{1,ads} \rightarrow Ti^{IV} + R_{2,ads}$	(T1-9)
Case 2	$OH^{\cdot} + R_{1,ads} \rightarrow R_{2,ads}$	(T1-10)
Case 3	$Ti^{IV}\lfloor OH^{\cdot} + R_1 \rightarrow Ti^{IV} + R_2$	(T1-11)
Case 4	$OH^{\cdot} + R_1 \rightarrow R_2$	(T1-12)
Reaction of Other Radicals	$e^- + Ti^{IV} \cdot O \cdot^-_2 + 2(H^+) \leftrightarrow Ti^{IV}(H_2O_2)$	(T1-13)
	$Ti^{IV} \cdot O \cdot^-_2 + (H^+) \leftrightarrow Ti^{IV}(HO \cdot_2)$	(T1-14)
	$(H_2O_2) + (OH^{\cdot}) \leftrightarrow (HO \cdot^-_2) + (H_2O)$	(T1-15)

2.3.3 Nanomaterial-Based Photocatalysis

Nanomaterial-based photocatalysis was first introduced in 1972 by Akira Fujishima and Kenichi Honda. This original discovery has sparked over forty years of academic research. Nanophotocatalysts are required to absorb light to create ROS. The materials considered are semiconductors, with band gaps between 0.2 and 4.0 eV, relating to absorbed light energy in wavelengths less than approximately 310 nm (ultraviolet light range). Some examples of nanomaterial photocatalysts are titanium dioxide (TiO_2), zinc oxide (ZnO), tungsten trioxide (WO_3), and other metal-oxides. The most commonly researched nanomaterial for photocatalytic application is titanium dioxide nanoparticles. A frequently used titanium dioxide nanoparticles are Degussa P25 (P25), which many authors use interchangeably with the term ‘titanium dioxide nanoparticles.

Nanomaterials used in advanced oxidation processes can be designed to consume low energy, be renewable and potentially cost effective. Nanomaterials therefore present an opportunity for enhancing water and wastewater treatment. To reduce energy consumption,

the light source, the target contaminants one wishes to remove, and the amount of pre-treatment applied to the water solution needs to be considered.

2.3.3.1 **Photocatalytic Light Sources**

Many nanomaterials that behave as photocatalysts perform best in the presence of ultraviolet (UV) light irradiation. UV light has a wavelength between 10 and 400 nm, divided into the following sub-ranges: UV-A (400 nm -315 nm), UV-B (315 nm- 280 nm) and UV-C (280 nm – 200 nm), and UV-V (200 nm- 10 nm). Sunlight provides UV light, but the source of sunlight is intermittent. UV-based reactors require additional design constraints to transmit sunlight into a reactor. The nanomaterial can be modified to improve the adsorption bandgap, or by using an alternate light source to compensate for the lack of light provided by the sun in the UV range. Commercial and industrial water treatment systems use mercury arc lamps as a UV light source. The recent developments of UV light emitting diodes (UV-LEDs) have allowed for alternative designs that can increase reactor efficiency not previously attainable using mercury arc lamps and potentially longer lifetimes. UV LEDs consume less energy than mercury arc lamps, and with advancing technology and mercury mining regulations that limit or band the use of mercury in products, the use of UV-LEDs will become more favorable and cheaper in economies-of-scale. Recent advances have also allowed for the creation of UV-C LEDs, allowing effective disinfection of bacteria and viruses as well as the potential for enhanced photocatalytic activity (Eskandarian *et al.*, 2016).

2.3.3.2 **Target Contaminants**

The arguably most crucial consideration one must make when discussing nanomaterials in advanced oxidation processes is the target contaminant one wishes to remove. In advanced oxidation processes for the treatment of drinking water, key targets include pharmaceuticals and personal care products (PPCPs), cyanotoxins, and other emerging contaminants. A pharmaceutical is any chemical used for the diagnosis, treatment, alteration or prevention of disease. The consumption of pharmaceuticals is expected to increase with research and an ageing population (Jones, Voulvoulis and Lester, 2005).

The charge of the contaminant is of crucial consideration when selecting the appropriate photocatalyst setup. Because photocatalytic efficiency is dependent on the adsorption properties of the photocatalyst, it is desirable to have a target contaminant that is of opposite charge to the photocatalyst. Opposite charges would increase electrostatic interactions, and chances of adsorption. Methods for manipulation of charges, including changing pH, are discussed further in Section 2.5.2.

2.3.3.3 **Pre-treatment of Water Matrix**

To ensure the effectiveness of photocatalytic treatment, the photocatalysis step should be applied after the water sample has undergone primary and secondary treatment steps. The influent water source, either wastewater or drinking water, contains scavenging species that decrease the efficiency of the AOP. Scavenging species refers to species that can also adsorb and react with the reactive oxygen species produced in AOPs before they interact with the target contaminant. While photocatalysis can degrade sizeable particulate matter, it would require an excessive amount of additional time and energy, being highly inefficient. The use of pre-treatment steps, such as coagulation, flocculation, and filtration, creates a more straightforward water solution for those compounds. These initial steps are necessary to ensure the efficient removal of smaller molecular size target contaminants by AOPs.

2.4 Nanomaterials in Photocatalytic Water Remediation

Numerous nanomaterials can be applied to perform water remediation. As previously mentioned, almost any metal-oxide material may perform photocatalytic water remediation. The most commonly studied nanomaterial is P25, or titanium dioxide nanoparticles. The use of P25 is likely due to their low cost, toxicity, availability and the fact that titanium dioxide was the first material considered for photocatalysis (Fujishima and Honda, 1972). Titanium dioxide has become the industry and research standard for photocatalytic treatment of both air and water.

While titanium dioxide has become the research standard, it does not mean that it is the superior photocatalyst. Photocatalytic efficiency, or the efficiency of ROS production, depends on numerous factors. For example, the introduction discussed the bandgap of materials. The bandgap is indicative of the energy that can be absorbed by a nanomaterial. Metal-oxide nanomaterials have numerous bandgaps associated with them, mostly on the range of 1.7 eV (CdSe) to 3.2 eV (ZnO, TiO_2, WO_3), as demonstrated in Figure 2-4. The nanomaterial selected should consider the light source available and be matched to the energy of the incoming light to be used.

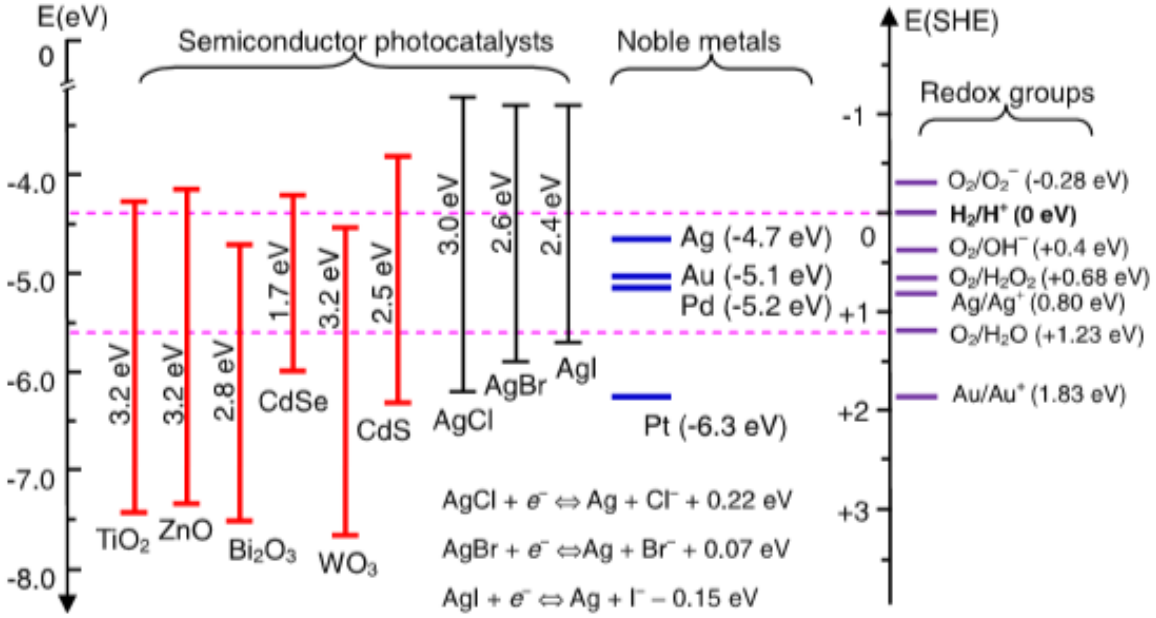

Figure 2-4: Bandgaps of Semiconductor photocatalysts and noble metal, adapted from (Zhang et al., 2013).

The wavelength of a light source is inversely correlated to the energy, as presented by Einstein's equation (Equation 2-5). In this case, λ is the wavelength of the light source (in m), h is the Planck Constant with a value of $4.135667662 \times 10^{-15}$ eV·s, and c is the speed of light with a value of 2.99×10^{8} m/s.

$$E = \frac{hc}{\lambda}$$ **Equation 2-5**

Titanium dioxide has a bandgap of 3.2 eV, illustrating that it best absorbs light at a wavelength of approximately 387 nm. Zinc oxide has a similar bandgap of 3.2-3.3 eV and therefore absorbs almost the same wavelength of light, around 391 nm (Srikant and Clarke, 1998; Zhang *et al.*, 2013). Other metal-oxides tend to have smaller bandgaps, which indicates lower energy and thus, longer wavelength light source. A longer wavelength light range approaches the visible light spectrum. A nanomaterial with a small bandgap would presumably be best for photocatalytic water remediation. However, other factors affecting the performance of ROS production show that the photocatalytic efficiency is not solely dependent on the bandgap of the photocatalyst. Section 1.5 further discusses the factors affecting photocatalytic efficiency.

Because numerous factors affecting overall photocatalytic efficiency exist, one cannot state that a single material as the best performing. Research standards have selected titanium dioxide nanoparticles as a benchmark for performance measurement. Many studies have explored the photocatalytic potential of other metal-oxide materials and have demonstrated improved performance when compared to P25 (Shafaei, Nikazar and Arami, 2010). While improved photocatalytic activity is reported comparing to titanium dioxide as a benchmark, it is difficult to compare the reports to one another. The next section discusses photocatalytic efficiency and the reporting methods used.

2.5 Photocatalytic Reaction Efficiency

Many factors are essential to consider when optimizing the efficiency of a photocatalytic setup. A water matrix is complex, and the treatment methods applied to them must be sophisticated. When referring to photocatalytic efficiency, one must consider the rate of the reaction. However, studies tend to report the reaction rate differently. There is an apparent lack of standardized reporting and testing methods and this lack of consistency makes the comparison of rates from different studies difficult (Table 2) The photocatalytic

efficiency is also affected by numerous factors, ranging from the concentration of the catalysts and contaminant to the presence of scavenging species.

Table 2: Photocatalytic Efficiency Reporting Methods. Note the variation between methods of reporting.

Reporting Method	Units	Notes
Conversion Rate (K_1, K_2)	$\frac{1}{s}, s^{-1}$	Calculated based on the order of conversion/ degradation.
Percent Degradation per unit time	$\frac{\%}{unit\ time}$	Compares the amount removed in a standardized test over a specific amount of time
Time for complete removal	s, m, hr	Measures the time required for complete removal of a compound.
Molar Degradation	$\frac{mol}{unit\ time}$	In a linear removal, compares the moles removed per unit time
Mass Degradation	$\frac{unit\ mass\ (g)}{unit\ time}$	In a linear removal, compares the mass removed per unit time
Electric Energy per Order (E_{EO})	$\frac{kWh}{m^3 \cdot order}$	Electric energy per order (EEO) is the electric energy in kilowatt hours [kWh] required to degrade a contaminant C by one order of magnitude in a unit volume [e.g., 1 m3 (1000 L)] [19] of contaminated water or air (Bolton *et al.*, 2007).

Reporting Method	Units	Notes
Photonic Efficiency ξ	$\xi = \frac{rate\ of\ reaction}{incident\ light\ intensity}$	Photonic efficiency measures the number of incident photons that productively interact with the catalytic agent (Pelaez *et al.*, 2012; Tokode *et al.*, 2016).

2.5.1 The Concentration of Catalyst and Contaminant

The concentration of the catalyst directly relates to the rate of reaction. The presence of more catalysts results in an increase in surface area and ROS, thereby increasing the degradation of the contaminants. The adsorption of the photocatalyst to the contaminant increases the overall degradation of the contaminant. With a higher presence of photocatalyst, there is a higher amount of catalyst-contaminant interactions. Similarly, the concentration of the contaminant is also essential in the overall photocatalytic efficiency. A higher concentration of the contaminant will also increase the interaction of the contaminant with the photocatalyst, and the ROS produced by the photocatalyst (Kumar, 2017).

2.5.2 pH, charge of contaminant and catalyst

The pH of the solution is a critical factor. A high pH is indicative of an acidic solution, where there are many hydrogens in solution while a low pH is indicative of a low concentration of hydrogens, and subsequently, a large concentration of hydroxyls in solution. The pH of the solution will alter the effective charges of all molecules within the solution, including the charge of the catalyst and the contaminant. Because a more opposite charge will result in a higher electrostatic attraction between molecules, an ideal pH would result in a water matrix where the contaminant and the catalyst have opposite charges, increasing their interaction. The pKa of the chemical and pH of the solution is therefore an important factor in photocatalysis.

The pH of wastewater solutions dramatically varies depending on the waste produced. The pH of some wastewater solutions can vary considerably e.g. 9.8 for textile wastes (Pekakis, Xekoukoulotakis and Mantzavinos, 2006), 8.5 for hospital wastewater (Sponza and Güney, 2017), and ranges in electronic manufacturing wastewater (stripper solution pH 9-11, developer pH 10-13 and the rinse solution can range from a pH of 4 to 10) (Chen, Ni and Chen, 2003). The charge of the photocatalyst relates to the known isoelectric point associated with the photocatalyst. The isoelectric point indicates whether a particle will have a positive or a negative charge within the solution. The isoelectric (neutral) point of titanium dioxide is 5.19, and of zinc oxide nanomaterials is 7.13 (Sayes *et al.*, 2009). Because a charge opposite to the contaminant is desirable, either the photocatalyst selected, or the pH of a waste solution may be adjusted to optimize the degradation process. The charge of the nanomaterial in the solution may also influence the agglomeration potential. Whether the pH is larger or smaller than the isoelectric point (IEP), the agglomerates are lower than when the pH is equal to the IEP, the material largely agglomerates (Sayes *et al.*, 2009).

2.5.3 Size, Shape and Structure of Photocatalyst

The reduction in the size of photocatalytic materials dramatically changes the reaction effectiveness. The primary benefit of scaling down technology is the increase in surface area that is associated with nanomaterials. Tušar et al, (2011) demonstrated that the use of nanoparticles as a Fenton-type catalyst allows for efficiency improvements associated with the application of nanoparticles due to increased surface area and decreased diffusional resistance. However, the increased benefits are no longer observed between particles in the nanometer size range. Mclaren et al., (2009), demonstrated little effect of size on photocatalytic activity for ZnO nanoparticles with primary particle sizes between 15 and 45 nanometers (Mclaren *et al.*, 2009).

The size of the particle also relates to the agglomeration potential of the photocatalyst. Agglomeration is disadvantageous due to the decrease in surface area that scaling down provided. The agglomeration of nanoparticles is best avoided to enhance the photocatalytic

ability. The agglomeration of nanoparticles in solution can be controlled by changing the pH. The variation of pH changes the zeta potential of the nanoparticles, increasing interparticle electrostatic repulsion (Li *et al.*, 2010).

The shape of the nanomaterials will also affect the photocatalytic reaction efficiency. This is demonstrated by the decreased reaction rates associated with nanorods and nanotubes when compared to nanoparticles (Pavasupree *et al.*, 2006). Finally, studies have shown that the crystal structure of the nanomaterial has an impact on photocatalytic ability. The structure of the nanomaterial will affect the bandgap of the material, the ability of the material to absorb light energy and the ability to create free oxygen radicals. For example, Degussa P25 is a blend of rutile and anatase titanium dioxide nanoparticles at a ratio of 70:30, or 80:20. For titanium dioxide, anatase is often the functional crystal structure, but rutile can be more effective in specific degradation tests (Prairie *et al.*, 1993). However, a combination of rutile and anatase crystal phases results in enhanced charge carrier separation, increasing photocatalytic activity (Djurišić, Leung and Ng, 2014).

The growth of crystal structures along different crystallographic faces can also affect the photocatalytic activity. For example, growth of zinc oxide along different crystallographic faces is demonstrated in Figure 2-5. The shortening along the [0001] direction resulted hexagonal plate-like particles over the rod-shaped morphology, which had an increasing proportion of polar faces at the surface. This shortening along the [0001] direction in zinc oxide resulted in increased reaction rate constants (Mclaren *et al.*, 2009), demonstrating that the shape of the nanoparticle will affect the photocatalytic activity.

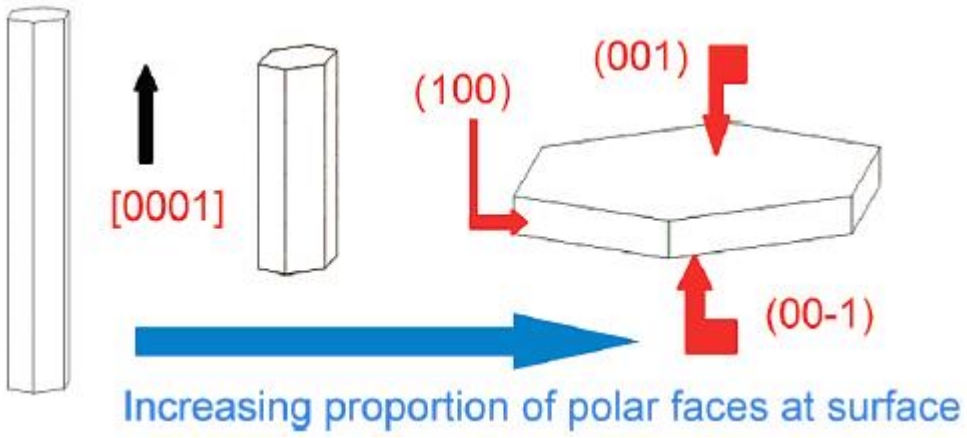

Figure 2-5: Growth patterns of ZnO structures along different crystallographic faces. A shortening of the material along the [0001] axis resulted in an increased proportion of polar faces at the surface, which demonstrated superior photocatalytic activity. Adapted from (Mclaren *et al.*, 2009).

2.5.4 Reaction Temperature

The ideal reaction temperature for photocatalytic removal of contaminants is reported by (Kumar, 2017) to be between 20℃ and 80℃. At 20℃, the apparent activation energy cannot be overcome, and over 80℃, charge carrier recombination is promoted and adsorption of contaminants to the surface is decreased (Hashimoto, Irie and Fujishima, 2005; Kumar, 2017).

2.5.5 Inorganic Ions

Inorganic ions, such as magnesium, zinc, iron, copper, bicarbonate, phosphate, nitrate, and chloride, may affect the performance of the photocatalyst due to their adsorption onto the surface of the photocatalyst. The effects of these inorganic ions vary, but both cations and anions have demonstrated some effect on photocatalytic efficiency. Copper, iron and phosphate are cations that have a substantial effect on photocatalytic ability, whereas calcium, magnesium and zinc demonstrated a little effect (Kumar, 2017). Anions, including nitrate, chlorides, carbonates and sulphates have been shown to inhibit the surface activity of the

photocatalyst. The charge of the photocatalyst in solution will determine whether cations or anions will affect the surface activity, due to electrostatic attraction forces.

2.5.6 Presence of ROS Scavengers/ Donors

Other components within the matrix may also affect photocatalytic efficiency. These components behave as scavengers or donors of the ROS produced during the photocatalytic reaction. An example is that the addition of only 0.02% (v/v) methanol in water influenced photocatalytic degradation rates of pharmaceuticals (Arlos *et al.*, 2017). Humic acids in a water matrix may act as photosensitizers, and generate additional ROS to concurrently perform indirect photolysis with photocatalysis (Zepp, Baughman and Schlotzhauer, 1981). The composition of the water matrix, therefore, can have a considerable effect of the photocatalytic reaction efficiency.

2.5.7 The Light Source: Intensity and Wavelength

Many nanomaterials that behave as photocatalysts perform best in the presence of ultraviolet (UV) light irradiation. Sunlight provides UV light, but sunlight is not consistently available in many regions. UV-based reactors require additional design constraints to transmit sunlight into a reactor. Mercury arc lamps are a common UV light source because of their high light intensity output; however, they consume a large amount of energy. The recent developments of UV light emitting diodes (UV-LEDs), mentioned in Section 2.3.3.1, have allowed for alternative designs that can increase reactor efficiency.

2.6 The TPA Test: A test for hydroxyl production

As previously mentioned, hydroxyl radicals are responsible for the bulk of contaminant removal (Turchi and Ollis, 1990). Terephthalic acid (TPA) is a probe often used to assess the generation of hydroxyl radicals in solution. Because hydroxyl radicals are the primary driver in contaminant degradation, the TPA test has become a standard to compare photocatalytic efficiency. As demonstrated in Figure 2-6, the presence of hydroxyl radicals will convert TPA into hydroxyterephthalic acid (HTPA), and other products.

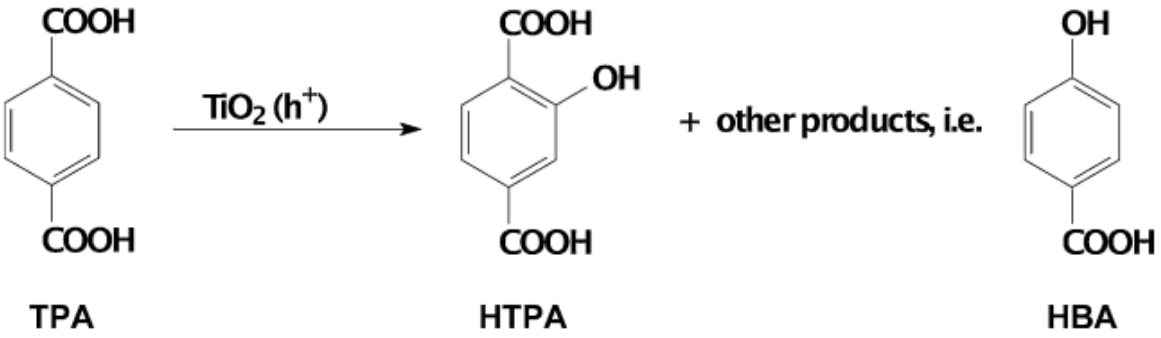

Figure 2-6: The degradation of terephthalic acid (TPA) into hydroxyterephtalic acid (HTPA) and other products including 4-hydroxybenzoic acid (HBA), as demonstrated by (Černigoj, Kete and Štangar, 2010).

HTPA can be measured using fluorescence. If samples are taken periodically, the concentration versus time curves obtained may be fit using a modified reaction model (Equation 2-6). The k_1 is the rate of formation of HTPA, while k_2 is the rate of consumption, t represents the amount of time that the reaction has undergone, published by Cernegoi et al. (Černigoj, Kete and Štangar, 2010).

$$[\boldsymbol{HTPA}] = \frac{\boldsymbol{k_1}}{\boldsymbol{k_2}}(\mathbf{1} - \boldsymbol{e}^{-\boldsymbol{k_2 \cdot t}}) \quad \textbf{Equation 2-6}$$

2.7 Commercialization Challenges and Solutions

There are two main barriers to commercialization that exist for the implementation of photocatalysis in water treatment technologies. There is a relatively low photocatalytic efficiency that currently exists when using nanomaterials as photocatalyst. Additionally, there is a need to remove the suspended nanomaterials from the water solution afterwards. Overall, there is a tradeoff between efficiency and the need to remove nanomaterials. There are methods; however, that can individually improve upon each of the limitations, as discussed below. A study completed for the Canadian Water Network in 2004 concluded that 'Ultimately, it is anticipated that photocatalyst technology will replace ultra-violet purification

in the treatment of drinking water' (Cooper Langford, 2004), encouraging the continued research on improving photocatalytic water treatment methods.

2.7.1 Photocatalyst Efficiency

There are some ways to improve the efficiency of the photocatalyst. Improving light adsorption or decreasing the charge carrier recombination are two methods of improving efficiency. Current photocatalysts tend to absorb light in the UV range, with little absorption in the visible light range, as discussed in section 2.5.7. Charge carrier recombination occurs when the generated charge carriers recombine, releasing the absorbed energy in the form of heat, rather than generating ROS. Improvements of photocatalytic activity can include sensitization with light sensors, doping, or changing the shape of the material either by engineering defects, spatial structuring or by morphology enhancement (Djurišić, Leung and Ng, 2014). Below is a discussion of methods of improving efficiency by heterojunctions offer improvements in both optimization opportunities.

2.7.1.1 **Plasmonic photocatalysts**

Increasing the hydroxyl production efficiency of the nanoparticles will increase the overall photocatalytic efficiency. One of the most studied applications of efficiency enhancement is by the creation of plasmonic photocatalysts. Plasmonic photocatalysis improves photocatalytic efficiency and assists in the remediation of a variety of efficiency challenges (Zhang *et al.*, 2013). In a plasmonic photocatalyst, noble metal nanoparticles (typically silver or gold) combine with a metal-oxide semiconductor. The blending of these two nanomaterials creates a Schottky junction and localized surface plasmon resonance (LSPR). A Schottky junction is the build-up of an electric field within the contact area between the noble metal and metal-oxide. This charge buildup forces the separation of electron and hole pairs, reducing recombination and thereby increasing the interaction of electrons and holes with the oxygen species in the aqueous environment (van Grieken *et al.*, 2009; He *et al.*, 2010). The LSPR feature of plasmonic photocatalysts provides a variety of potential benefits. First, the noble metals can be adjusted to respond to visible light, improving

the photocatalytic efficiency. The LSPR can also enhance the absorption of light. There is also a reduction in the electron-hole diffusion length, meaning that the light reacts closer to the surface of the particle, decreasing the distance that the free radicals must move to interact with oxygen species. The LSPR effect creates a strong local electric field, encourages new electron-hole pair generation, heats the surrounding environment to increase the redox reaction rate, and polarizes nonpolar molecules for better adsorption (Hofstadler *et al.*, 1994; Bohren and Huffman, 1998; Zhdanov, Hägglund and Kasemo, 2005; He *et al.*, 2010; Christopher, Xin and Linic, 2011; Linic, Christopher and Ingram, 2011; Mubeen *et al.*, 2011; Thomann *et al.*, 2011; Wang, Liu and Chen, 2012; Zhang *et al.*, 2013; Romeiro *et al.*, 2018) Figure 2-7 illustrates a summary of the theorized benefits of plasmonic photocatalysis. There are numerous improvements to the photocatalytic activity made through surface plasmon resonance.

Research has enhanced photocatalytic efficiency by using plasmonic photocatalysis (Zhang *et al.*, 2013). The fallbacks to plasmonic photocatalysis lay in the additional synthesis steps and the costs associated with using precious metal nanoparticles.

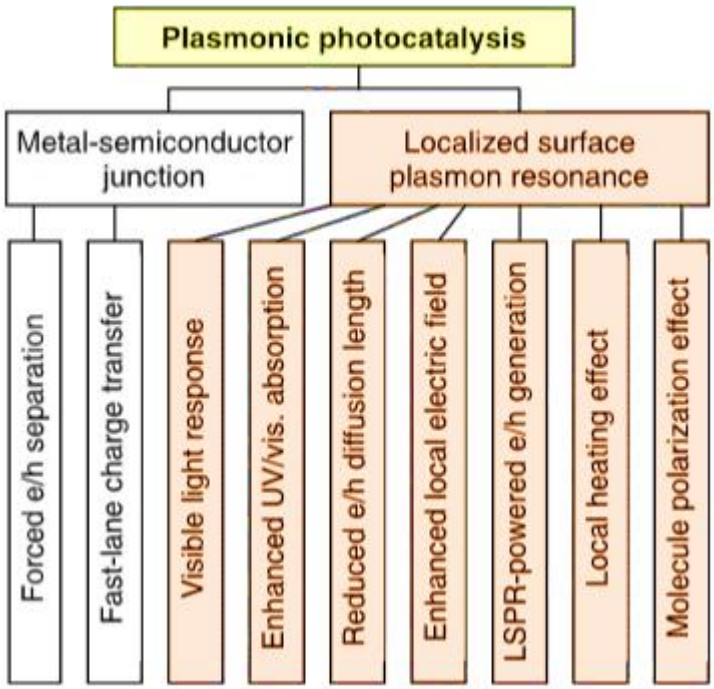

Figure 2-7: The beneficial effects and mechanisms associated with plasmonic photocatalysis. The benefits may be divided into metal-semiconductor junction (Schottky junction) and localized surface plasmon resonance (LSPR) effects. From (Zhang et al., 2013).

2.7.1.2 **Semiconductor-Semiconductor photocatalysis (p-n junctions)**

One challenge in photocatalyst efficiency is the factor of electron-hole recombination. When the charge carriers recombine, rather than interacting with external water sources or contaminants, there is a loss of energy in the form of heat. While this heat loss may be high enough to promote thermal degradation of the contaminants, it results in a much less efficient degradation method. As mentioned with plasmonic photocatalysis, the blending of two different materials may introduce four benefits. First, there is an enhanced charge carrier separation. Next, there is a rapid charge transfer and a longer lifetime of the charge carriers. Lastly, there is a separation of incompatible reduction and oxidation reactions in a small space (Wang *et al.*, 2014).

The two methods of increasing this charge carrier separation involve combining two metal-oxide semiconductors with different band gap energy levels. The difference in band gap energy levels separates the conduction and valence bands, causing the holes to travel to one material and the electrons to travel to the other. In this case, electrons move to the lower conduction band, and holes move to the higher valence band. Two metal-oxide semiconductors create a non-p-n-type heterojunction system. To further improve on this, a 'p-type' and an 'n-type' semiconductor may be combined. A 'p-type' semiconductor has the dopant missing an electron (typically group 3 elements) in its outer energy level, causing holes to be the dominant carrier. An 'n-type' semiconductor is doped with a (typically group 5) element that has an excess of electrons in its outer shell. The excess electrons become the primary charge carriers. This phenomenon is referred to as electronic p-n junctions, demonstrated in Figure 2-8 (Wang *et al.*, 2014). When excitation separates the charge carriers, electrons transfer to the conduction band (E_{CB}) of the n-type semiconductor, and the holes transfer to the valence band (E_{VB}) of the p-type semiconductor.

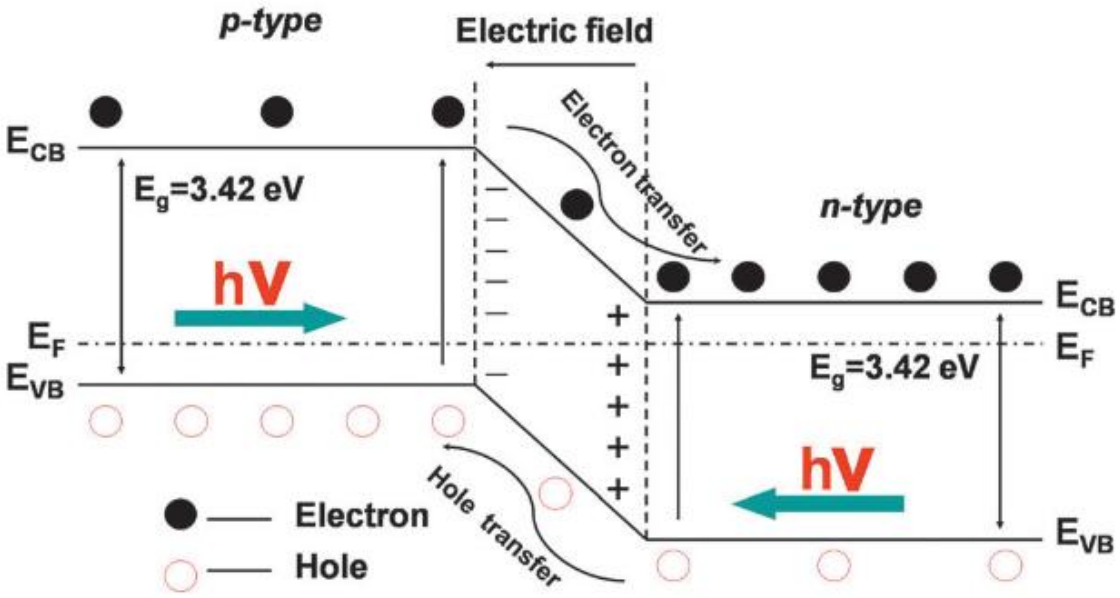

Figure 2-8: Schematic of a p-n junction. This junction may be formed by blending two doped semiconductors, or by combining a metal with a metal oxide semiconductor. From (Wang et al., 2014).

2.7.1.3 **Semiconductor- Carbon heterojunctions**

Additionally, a semiconductor combined with a carbon material adds heterojunction benefits. The carbon materials include activated carbon, graphene and carbon nanotubes (CNTs). In the case of activated carbon and CNTs, an increase in the surface area is attributed for the improvement in photocatalytic activity, namely due to the increased adsorption sites, explained by the Langmuir-Hinshelwood adsorption model, Equation 2-3 (Wang *et al.*, 2014). CNTs have the additional functionality of their electronic properties. The electronic properties indicate that they may behave as a metal-metal-oxide semiconductor as discussed in plasmonic photocatalysis. The large area also adds a capability for storage of excessive electrons. Similarly, the unique one-dimensional structure of graphene exhibits an even more advanced electron mobility, allowing for it to enhance the beneficial effects of plasmonic photocatalysis (Section 2.7.1.1) with increased adsorption sites. The increased production of

carbon-based nanomaterials has made them accessible for research of photocatalytic activity improvement with a higher chance of commercialization due to decreased production costs.

2.7.2 Recovery of Nanomaterials

Nanomaterials, while highly effective at photocatalytic based AOPs, are at times themselves considered a contaminant and are costly. The recovery of nanomaterials from the setup is a challenge due to their small size and strong dispersion properties. Three common nanomaterial recovery methods include immobilizing the nanocatalyst, filtering out the nanomaterials, or functionalizing the nanomaterials into magnetic photocatalysts.

2.7.2.1 **Immobilized Nanocatalysts**

The simplest method to address the recovery of nanomaterials issue is to immobilize the nanoparticle. However, this identifies a massive engineering trade-off to avoid the need for recovery methods versus the substantial decrease in surface area. This balance has been studied by many researchers and dates back as far as 1994, when titanium dioxide coats fused silica glass fibres (Hofstadler *et al.*, 1994). The silica glass fibres performed as optical fibres. Due to the optical nature, light irradiation immediately passes to the titanium dioxide without losing intensity by a first pass through the water matrix. The removal of the loss of light intensity compensated for the decreased surface area expected by immobilization of particles. This paper, however, notes the weakness in their comparisons due to the change in quantum yield between higher local light intensity and a decrease in illuminated photocatalyst (Hofstadler *et al.*, 1994). With current advancements in the scientific understanding of photocatalysis and the increased electrical efficiency of UV LEDs, it is likely that this study could be repeated with UV LEDs to find an improved photocatalytic degradation efficiency. Exploration of numerous other immobilization methods have been studied including the immobilization of zinc oxide on glass plates (Behnajady *et al.*, 2007), and the immobilization of titanium dioxide in a catalytic wall and a fixed bed reactor (van Grieken *et al.*, 2009). The immobilized zinc oxide on glass achieved complete removal of a dye compound, but there was no report on the rate of removal, compared with a standard sludge suspended system. A

wall reactor configuration was found to be the most optimal when compared to the fixed bed reactor setup. The success of the wall reactor configuration has been attributed to the higher specific activity of titanium dioxide, maximized radiation absorption due to the configuration, and the stability of the Ag-TiO_2 film (van Grieken *et al.*, 2009). As discussed above, immobilization of nanoparticles involves a tradeoff between the decreased surface area and the removal of a need for nanomaterial recovery. However, immobilized photocatalytic nanomaterials remain as an attractive solution for the removal of contaminants not typically removed by conventional water treatment methods.

2.7.2.2 **Membrane Filtration of Nanomaterials**

Freely suspended nanoparticles are often the most photocatalytically efficient. If a suspended nanoparticle setup is required, it may be best for the materials to be suspended and then filtered out from the treated water. The Photocat AOP+ platform, created by Purifics in London, Ontario, boasts the use of a slurry setup with titanium dioxide, followed by ceramic membrane filtration to perform multi-stage purification techniques. The setup presumably uses small photocatalysts to achieve a slurry suspension, though they do not specify a nanomaterial size. This setup exemplifies the ability to use a suspended nanomaterial for water treatment, though multi-stage filtration would be required to ensure full removal of contaminants. However, it is argued that while this filtration system may provide high contaminant removal, the process itself is not energy saving, as reported by Benotti et al. (Prairie *et al.*, 1993).

A heavily explored use of membranes combined with photocatalysts encourages the use of photocatalysts coated or blended into the material of the membrane itself. The setup not only allows for the potential of membrane filtration but also provides the advantage of reduced membrane fouling, which is currently a significant challenge in membrane technology (Damodar, You and Chou, 2009; Chong *et al.*, 2010).

2.7.2.3 **Magnetic Nanocatalysts**

Another method used to tackle the barrier associated with recovery of nanoparticles from aqueous matrices is magnetization. When the particles are magnetized, an electric field is applied to recapture nanoparticles from the treated suspension. Nanosized iron oxide particles are naturally magnetic when found in specific ratios. Fe (II) and Fe (III) at a molar ratio of 1:2 creates magnetite, a material that can perform as a Fenton catalyst and be subsequently removed by magnetic separation. In the presence of hydrogen peroxide, magnetite is not stable and is converted to maghemite in a surface to core reaction progression (Rusevova, Kopinke and Georgi, 2012). However, this does not affect the Fenton reaction efficiency. One can then conclude that it may be preferable to use maghemite initially to avoid this conversion step. Another typical application of magnetization is the use of core-shell nanostructures, where the core is magnetic, and the shell has photocatalytic activity. A prime example of core-shell magnetization is the study completed by He et al., which used a three-layer core-shell particle (He *et al.*, 2010). The core contained magnetic iron (2,3) oxide (Fe_3O_4) coated with silicon dioxide (SiO_2). The SiO_2 acts as a protective layer to avoid chemical and photo dissolution of the iron oxide. The outer shell contained titanium dioxide, which performed as the photocatalytic layer. These core-shell particles performed better than Degussa P25 and had the additional functionality of recovery from the solution. Magnetically charged nanoparticles are beneficial for two reasons. Firstly, because they can be separated and recycled from the sludge, they provide a sustainable water treatment method. Secondly, the sludge setup maximizes surface area, allowing the nanoparticle to perform photocatalysis at its highest rate.

2.8 Emerging Contaminants: Pharmaceuticals and Personal Care Products

Pharmaceuticals and personal care products (PPCPs) are widely considered to be emerging contaminants. The Food and Drugs act classifies many PPCPs as a ‘Drug.’ The Food and Drugs Act defines a ‘drug’ as:

"A drug includes any substance or mixture of substances manufactured, sold or represented for use in (a) the diagnosis, treatment, mitigation or prevention of a disease, disorder or abnormal physical state, or its symptoms, in human beings or animals, (b) restoring, correcting or modifying organic functions in human beings or animals, or (c) disinfection in premises in which food is manufactured, prepared or kept; (drogue)" (Revised Statute of Canada, 1985).

This definition encompasses numerous compounds; they have substantial variability in structure, function, and activity. The use of pharmaceuticals is expected to increase with an ageing population and the recent publishing of the human genome (Jones, Voulvoulis and Lester, 2005). The expanded use of PPCPs creates a water treatment challenge that is expanding and diverse. There are over 3000 pharmaceutical compounds licensed in the United Kingdom alone, and the term pharmaceuticals and personal care products (PPCPs) blankets thousands of unique compounds. The properties of the pharmaceutical compounds range in numerous properties, including hydrophilicity and polarity. It is therefore impossible to identify one physical property of a pharmaceutical that can be used to target removal processes for them from wastewater. However, using the physicochemical properties of the pharmaceutical will be most useful. Physiochemical properties include chemical structure, aqueous solubility, octanol/water partition coefficient and Henry's law constant (Jones, Voulvoulis and Lester, 2005). Other factors affecting the removal efficiency of these compounds include pH, retention time, temperature and amount of solids present (Jones, Voulvoulis and Lester, 2005). The range of physicochemical properties of pharmaceutical compounds contributes to a complex wastewater matrix.

2.8.1 Environmental Effects

Pharmaceuticals in the environment may impose serious toxic and other effects on aquatic species. Most effluents have a low concentrations of pharmaceuticals but approach or exceed the concentrations that have been reported to have effects in aquatic species in lab tests (Arnold *et al.*, 2014). For example, feminization of fish, identified in studies worldwide, including the demasculinization of fathead minnows. A controlled dose study of fathead minnows to 17α-ethynyl estradiol completed at the Experimental Lakes Area found a

complete collapse of the fathead minnow population in as little as two years (Kidd *et al.*, 2007). Antidepressants have also caused a decrease in fish brain serotonin levels and predation behavior at concentrations seen in wastewaters (Bisesi, Bridges and Klaine, 2014). The effect of pharmaceutical compounds in effluents will vary between the species, the gender, mobility, the breeding habits of the species as well as the characteristics of the chemical.

2.8.2 Challenges in the Treatment of Pharmaceuticals

Pharmaceuticals provide a unique challenge to water treatment due to their structural variability, their conjugation and their low concentrations. As previously mentioned, there is a large variability in the structure of pharmaceutical compounds. Variation in properties includes their size, hydrophilicity and charge. Because there is a substantial number of pharmaceuticals consumed daily, it is infeasible to create a water treatment system specialized for the removal of all pharmaceuticals. An additional problem is that PPCPs are conjugated in the body, to enhance their polarity before excretion. Once these conjugated pharmaceuticals pass through water treatment, they become deconjugated, and therefore the active compound may be released into the environment (Ternes, Joss and Siegrist, 2004). Alternatively while the body can degrade pharmaceuticals, some compounds may be excreted unchanged (Jones, Voulvoulis and Lester, 2005).

There are three proposed fates of pharmaceuticals when passing through a wastewater treatment plant. The first option is that the compound is partially degraded or mineralized. Secondly, the compound may not degrade but may partition to the sludge. The last possible fate of a pharmaceutical compound is that it passes through the wastewater treatment plant and ends up in the receiving waters (Klavarioti, Mantzavinos and Kassinos, 2009).

Numerous studies on the elimination of high to medium polarity pharmaceuticals have found that their removal is often incomplete, ranging from 60-90% (Jones, Voulvoulis and Lester, 2005). The reason for the difficulty of removal is hypothesized to be due to various reasons. For one, some pharmaceutical compounds are incredibly resistant to biological

degradation processes and usually escape intact from conventional treatment plants. Also, pharmaceuticals are typically present at minute concentrations, making them incredibly difficult to detect. The pharmaceuticals can also affect the wastewater treatment process itself. Certain pharmaceuticals, such as antibiotics have the potential to disturb the community in sewage treatment systems, as well as inhibit the wastewater bacteria although they are usually well below this concentration threshold (Jones, Voulvoulis and Lester, 2005).

2.8.3 Challenges in laboratory pharmaceutical photocatalysis setups

Many studies have been completed to assess the removal of pharmaceuticals using photocatalysis. There are however many challenges in using a laboratory setup, which makes it challenging to compare the studies and to connect the studied results to applicability in municipal treatment. Some of the challenges are identified below:

- Typical removal tests use pure water matrices, with a spike of the contaminant in question. While these tests give insight into the removal mechanisms of the contaminant, they fail to represent the surface water, or municipal wastewater where these tests would be applied. The pure water matrices do not consider the other compounds and contaminants included in a wastewater/ drinking water matrix.
- Section 1.5 Photocatalytic Reaction Efficiency discusses the most common factors associated with altering photocatalytic efficiency. Laboratory tests often isolate one factor to optimize the photocatalytic efficiency. The individual reported removal rates are incomparable. Also, as demonstrated in Table 2, the methods of reporting removal or removal efficiency are inconsistent, also making it a challenge to identify the actual usefulness of the test.
- While AOPs can be a tertiary treatment step in water treatment, scavenging species remain in the matrix that can affect the photocatalytic efficiency. Scavengers can include natural organic matter (NOM). Because many laboratory tests use pure water, the scavenging effects of NOM are not considered.

- Additionally, the pH of the solution dramatically affects the photocatalytic efficiency. The pH will affect the electrostatic charge of both the catalyst and the contaminant and will affect their electrostatic interactions. In a tertiary step, chemical addition can adjust the solution pH. The adjustment of pH may require a significant addition of chemicals, which would make the process massively inefficient. Laboratory tests that use a pH adjusting method should consider this inefficiency.
- Another challenge with standard removal tests is the lack of a standardized testing apparatus. Lack of standardization involves differences in light sources, causing changes in light intensity and emission wavelength. Even if the nanoparticle were standardized to have a similar primary particle size, differences in the bandgaps of various metal-oxides would respond differently to different wavelengths of light. Further, the concentrations of the catalyst and the contaminants are also rarely standardized. Overall, the high variability in testing conditions limit authors to conclude that their nanoparticle may show improved photocatalytic activity, but only in specific scenarios.
- As previously mentioned, pharmaceuticals have wide structural variability and physiochemical properties. While photocatalytic removal of pharmaceuticals is widely studied, the individual pharmaceuticals selected vary. A review completed on titanium dioxide based photocatalytic removal identified diclofenac, ibuprofen, naproxen, and paracetamol as commonly tested pharmaceuticals. It was concluded that while photocatalysis shows promise in pharmaceutical removal, the inconsistencies in removal rates, extent of mineralization and photoproduct formation demonstrates the extent of the complexity of the behavior of drug removal (Kanakaraju, Glass and Oelgemo, 2014). An additional review completed found 38 papers that used zinc oxide based photocatalysis for the removal of a wide variety of pharmaceuticals. This review found a similar degree of inconsistencies in the studies, but additionally identified the complexity of natural organic matter, and the low concentrations at which pharmaceuticals usually exist in wastewater (Mirzaei *et al.*, 2016). Clearly several

studies explore the photocatalytic removal of pharmaceuticals, but as the reviews identified, there is little consistency in testing and reporting that make the removal rates comparable.

Therefore, studies should aim to test pharmaceutical degradation in a manner that makes their findings comparable to other studies and represents the natural organic matter and other complexing agents that exist in wastewater and surface waters. Consideration factors should include that there is a likelihood that a preferential degradation will occur for the least stable pharmaceutical and the pharmaceutical that best adsorbs to the catalyst surface. Photocatalytic degradation studies should select a few representative pharmaceuticals based on their effective charge in solution, their typical persistence through water treatment processes and their potential adverse environmental effects.

2.9 Summary

In summary, photocatalysis continues to be a promising area of research for tertiary water treatment applications. Nanomaterials may provide a large improvement to the efficiency of ROS production due to its increased surface area. UV LEDs have provided opportunity for the exploration of energy effective photocatalytic applications. There are numerous factors affecting the photocatalytic reaction efficiency of the water matrix including the concentration of the catalyst and contaminant, the pH and electrostatic interactions between the catalyst and the contaminants, the size shape and structure of the photocatalyst, the reaction temperature, the presence of inorganic ions and scavengers and donors and the light source. The photocatalytic efficiency of materials is often assessed by the hydroxyl production, which is probed using TPA, which is converted into HTPA in the presence of hydroxyl radicals. Currently, challenges remain in the municipal use of nanomaterials in water treatment processes, including the photocatalytic efficiency and the need to remove nanomaterials from the treatment setup. The photocatalytic efficiency can be improved by creating heterojunctions between the metal-oxide photocatalyst and another material, i.e.

metals. Nanomaterials may be removed from setup by immobilization, membrane filtration or using magnetism.

Common contaminants that may be removed by nanomaterial based photocatalysis are pharmaceutical compounds. Pharmaceutical compounds cause an adverse effect on aquatic species but are difficult to remove from wastewater effluent due to their unique properties. Additionally, research completed using nanomaterial based photocatalysis for the removal of pharmaceuticals is not representative of the removal capabilities in municipal wastewater effluent. This is due to the existence of complexing agents such as NOM and inorganic ions.

Chapter 3
Functionalization of Zinc Oxide with Silver to Improve Efficiency of Hydroxyl Formation

3.1 Introduction

Photocatalysis is an advanced oxidation process that can be used to remove compounds from water matrices that are difficult to remove with other processes. The use of photocatalysts for water treatment has rarely been operationalized in industrial or utility (municipal) applications. One of the limiting factors is low photocatalytic efficiency for the removal of target chemicals. This efficiency is affected by both the ability of the nanomaterials to absorb light and the ability to produce reactive oxygen species. Plasmonic photocatalysis has been widely considered as a potential approach for improving the photocatalytic efficiency. Plasmonic photocatalysis provides improvement to the photocatalytic efficiency through both a Schottky Junction and LSPR effects (Zhang *et al.*, 2013).

While plasmonic photocatalysts is often reported to have improved photocatalytic activity when compared to an un-doped metal oxide, few tests have been performed to find the best ratio of metal: metal-oxide composition. A limited number of studies have been completed that tested silver- zinc oxide plasmonic photocatalysts for improved photocatalytic activity (Table 3) and only two studies have compared different amounts of silver loading. It is difficult to compare the studies due to differences of morphology, synthesis methods, loading percentage, and photocatalytic testing methods. The morphologies of the materials can differ and can include nanospheres or nanorods. Every study completed also used a different synthesis method. The difference in synthesis methods are of concern due to differences in how the silver loading is reported. The percentage of silver loading reported is based on the amount of silver precursor (silver nitrate, silver acetate, or pre-synthesized silver nanospheres). Different synthesis methods can result in different binding efficiencies of the silver to the zinc oxide, making the reported loading percentages incomparable with one

another. The reported photocatalytic efficiency was also tested using different methods including time for removal and percent degradation. The many differences in these studies therefore makes them difficult to compare directly.

In the study completed herein, zinc oxide-silver nanoparticles were created using a hydrothermal synthesis method beginning with zinc oxide nanoparticles and a silver precursor. The hydroxyl production capability of the synthesized nanomaterials was tested using a common photocatalytic test, the TPA conversion test to determine the conversion rate constant (i.e. the conversion of terephthalic acid (TPA) into hydroxyterephthalic acid (HTPA)).

Table 3: Studies with Ag/ZnO nanomaterials for improved photocatalytic activity.

Reported Weight Percentage	**Morphology**	**Synthesis Method**	**Optimal Photocatalytic Activity**	**Reference**
0.1% Silver nitrate	Silver decorated zinc oxide nanopowders	ZnO powder blended with silver nitrate in a quartz reactor, evaporated to dryness and treated with air	N/A	(Chen *et al.*, 2016)
1% Prepared silver nanospheres	Silver nanospheres on zinc oxide rods	Deposition precipitation	N/A	(Bensalah *et al.*, 2014)
0, 0.3, 1, 8 silver acetate (%)	Nanospheres	Precipitation	60 minute photodegradation with 1 silver acetate % (13824	(Yildirim, Unalan and Durucan, 2013)

Reported Weight Percentage	Morphology	Synthesis Method	Optimal Photocatalytic Activity	Reference
			molar %) and 8 silver acetate% (110592 molar%)	
Range of 0 to 11.7 wt% from silver nitrate	Nanorods	One-pot hydrothermal synthesis	Optimal rhodamine B degradation at 6.2 wt% (85709 molar %)	(Zhang and Mu, 2007)

3.2 Materials and Methods

3.2.1 Synthesis of Silver-Zinc Oxide Nanomaterials

Zinc oxide nanopowder (ZnO, 99+%, 10-30 nm) was purchased from US Research Nanomaterials, Inc. Silver nitrate was purchased from Alfa Aesar, and hexamethylenetetramine (HMTA) was purchased from Sigma Aldrich. The hydrothermal synthesis method is detailed in Appendix A2: Hydrothermal Synthesis. The nanoparticles were synthesized by blending an appropriate amount of acid digester solution, composed of silver nitrate and HMTA. A range of different acid digester volume was added to a constant amount of zinc oxide nanoparticles to create a range of silver: zinc oxide ratios. The HMTA served as a reducing agent for the loading of the silver with the ratios are as outlined in Table 4. The mixtures were then placed in a pressurized vessel and heated to 100℃ in a Lindberg /

Blue M furnace (Thermo Electron Corporation). The furnace was held at 100℃ for four hours and then left to cool for around three hours until the pressure decreased enough to open the vessel. The nanoparticle solution was then mixed with pure water for five minutes and purified using centrifugation and suction filtration through a 47 mm glass fiber filter (PALL Life Sciences).

Table 4: The percent ratios (in Moles and Mass) of the synthesized Ag-ZnO Particles. These ratios were calculated by dividing the amount of silver by the amount of zinc oxide and multiplying it by 100%.

Molar Percentage (%)	Mass Percentage (%)
1	7.23E-05
3	2.17E-04
5	3.62E-04
10	7.23E-04
15	1.09E-03
25	1.81E-03
50	3.62E-03
75	5.43E-03
100	7.23E-03
1000	7.23E-02
14000	0.10
42000	0.30
70000	0.51
140000	1.01
210000	1.52
350000	2.53
700000	5.06
1050000	7.60
1400000	10.13

3.2.2 Conversion Test

The photocatalytic ability of the synthesized silver-zinc oxide nanoparticles was tested using a TPA conversion test, a standard test to confirm photocatalytic efficiency. The photocatalytic test setup, demonstrated in Figure 2-1, consists of an in-house assembled six-cm collimated UV-LED beam (θ_{beam}= 4 cm) light source setup with a heat sink, placed over a four-position magnetic stir plate (10.5 cm above the surface of the water). A detailed procedure is outlined in A1: TPA to HTPA Conversion Protocol. In summary, 20 mg of the silver-zinc oxide nanoparticles were added to a 300 mL solution of 0.5 mM TPA. The solution was placed in a 400 mL beaker wrapped with foil, then left to stir on a stir plate for 60 min for adsorption to take place. At time 0, the UV lights were turned on. Samples were taken periodically for 10 min. pH was measured before and after the test, and the fluorescence of the HTPA was measured using a SpectraMax M3 plate reader. A depiction of the conversion test setup can be found in Figure 3-1. The conversion plots were then fit using a linear first order conversion rate. An ANOVA followed by Bonferroni tests were completed to determine statistical significance using SigmaPlot (Systat Software, San Jose, CA).

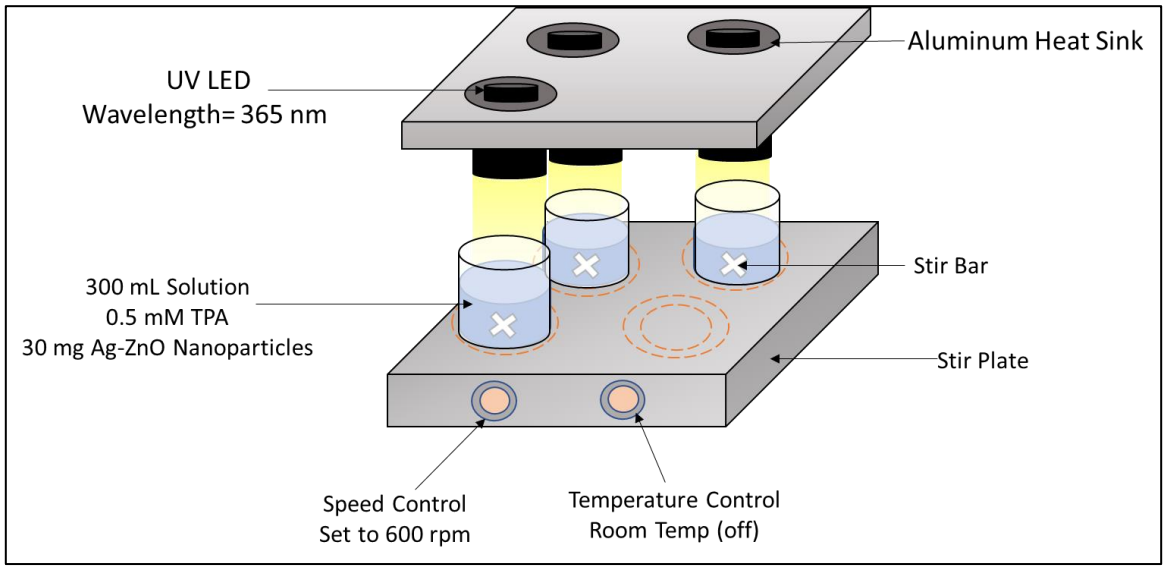

Figure 3-1 Photocatalytic setup of the TPA conversion test. The test of each nanoparticle was completed in triplicate, as demonstrated by the three beakers.

Due to the linearity of the conversion during the first 10 min of the reaction, a zero-order reaction equation (Equation 2.1) was determined using the linest function in Microsoft Excel (Office 365). k is the conversion rate constant (units: 1/min), $[A]_0$ is the initial concentration of HTPA measured in solution. A stabilization period of 60 minutes was completed before the UV-LED was turned on at time 0.

$$[\boldsymbol{A}] = [\boldsymbol{A}]_{\boldsymbol{0}} + \boldsymbol{kt}$$ **Equation 2-1: Zero Order Reaction Equation**

3.2.3 Characterization of Nanomaterials

Diffuse reflectance spectroscopy (DRS) was used to determine the bandgap of the synthesized nanoparticles. The DRS spectra was collected using a Shimadzu UV-2501PC UV-Visible-NIR spectrophotometer equipped with an integrating sphere accessory, using N2(g) as the reference. Details on the sample preparation, characterization and results can be found in Appendix A3: UV- Diffuse Reflectance Spectroscopy B3: DRS Data. Scanning Electron Microscopy (SEM) imaging was completed using a Zeiss Leo 1530 Field Emission- SEM, at

the WATLab at the University of Waterloo. An agglomeration test was also completed using a VASCO™ Particle size analyzer and NanoQ V2.5.9.0 software by Cordouan Technologies.

3.3 Results

Overall, an increased amount of silver loading on zinc oxide nanoparticles resulted in an increased hydroxyl production rate, as demonstrated by the reaction rate constant *k* (1/min) determined based on the first-order reaction rate fit the conversion of TPA into HTPA. Characterization of the nanoparticles found high agglomeration, and no change in the bandgap of various silver loadings.

3.3.1 Conversion Rates

Rapid hydroxyl formation was demonstrated by measuring the conversion of TPA into HTPA. Within the first ten minutes of the reaction, a linear conversion was observed. An example of the conversion using 100% Ag/ZnO nanoparticles is presented in Figure 3-2. Longer times for the reaction resulted in a non-linear relationship, likely as a result of the removal of HTPA once the concentrations increased and/or the depletion of the TPA. The typical pseudo-first order reaction model proposed by Černigoj et. Al (2010) could not be be fit to the data to estimate the rate constants for TPA conversion (Appendix B4) The rate constants were therefore estimated using a first order relationship (linear) during the first 10 minutes.

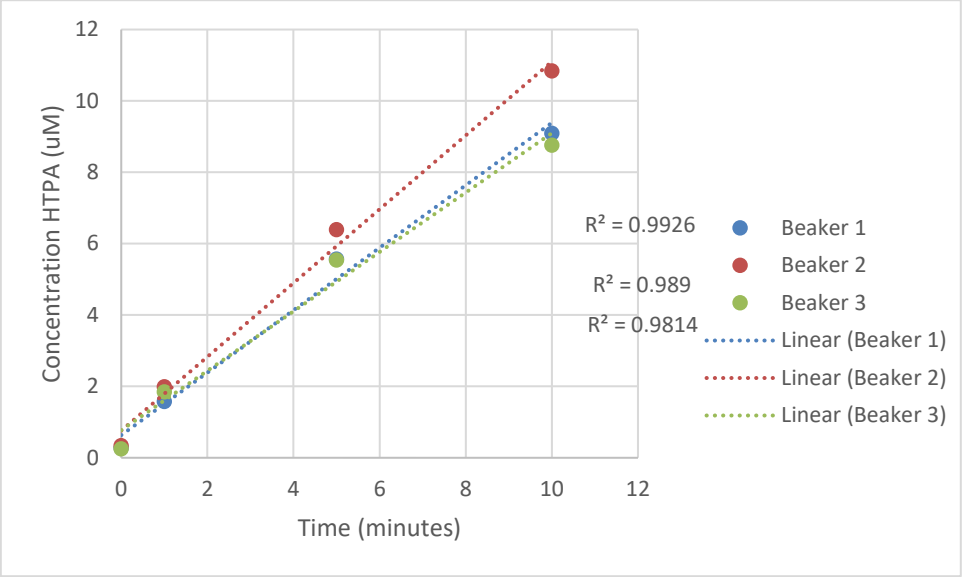

Figure 3-2: The conversion of TPA into 2-HTPA over a time of 10 minutes. The test was completed in triplicate (Beakers 1 through 3). A linear conversion is observed, as demonstrated by the high R^2 associated with the linear trendlines.

The conversion rates (*k* in Equation 2-1) for the various molar percentages of the nanomaterials is shown in Figure 3-3. Each of the tests was completed in triplicate, and the average of the three conversion rate constants is reported with the standard deviations. As can be observed, there is a general increase in the conversion rate constant with increasing silver loading on the nanoparticles. An ANOVA of the conversion rates found statistically significant differences among the treatment groups. A Bonferroni test, comparing the conversion rates to a control of pure zinc oxide, found consistent statistical improvement in the conversion values for silver mass loadings of 5.06% and higher. A general increase in conversion rates can be observed with increased silver loadings. The pattern is disrupted at 7.23E-02% and 1.01%, where a sharp increase in the conversion rate constant was observed. These increases may have occurred due to a difference in testing pH observed during the tests completed for these percentages.

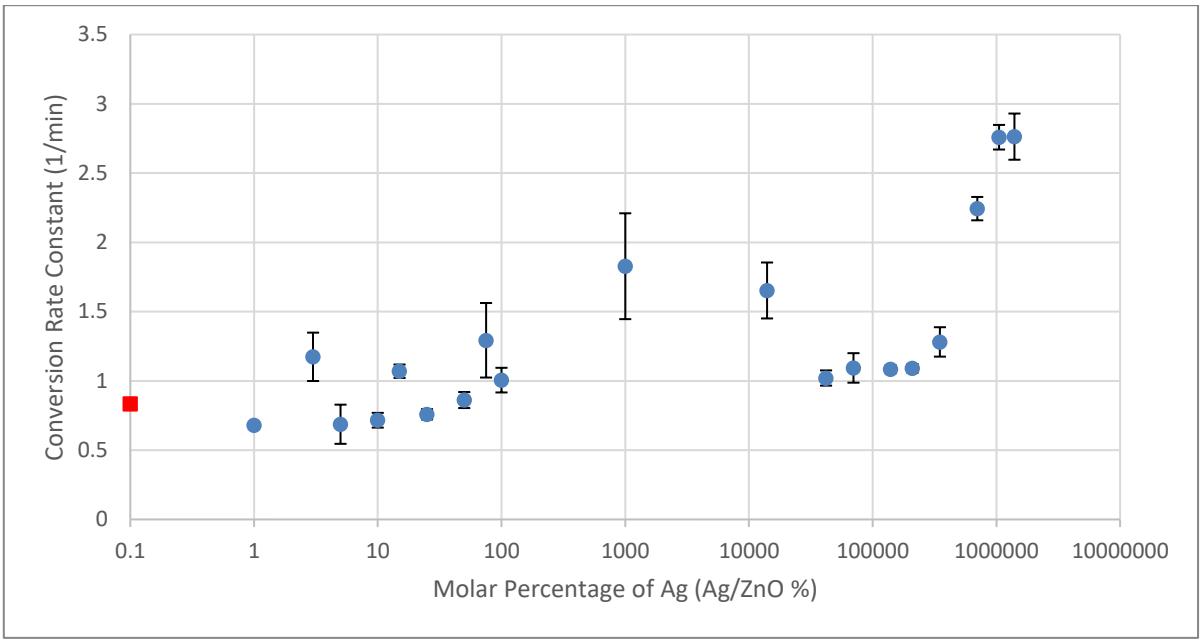

Figure 3-3: The average conversion rate constants (k) versus the molar ratios of silver: zinc oxide nanoparticles. The error bars represent the standard deviation between the three tests completed. The red square represents pure zinc oxide, as purchased, which when tested had a significantly low standard deviation.

3.3.2 Characterization of Nanomaterials

DRS measurements confirmed a bandgap ranged from 368.4 to 394.2 with a mean value of 380.2 nm for each nanoparticle configuration (Appendix B3). This is comparable with the reported bandgap of 3.3 eV (375.7 nm) for zinc oxide (Srikant and Clarke, 1998). A linear regression found that the F-statistic was not significant, and there was no correlation between the silver molar percentage and the change in bandgap. The average bandgap of 380.2 nm is close to the UV LED light source of 365 nm, indicating that the zinc oxide nanoparticles can absorb the light provided by the test setup.

SEM images displayed high agglomeration of the nanoparticles. Due to the low concentrations of silver, there was no silver peak in the XPS measurements of the 50% and 100% molar silver loadings. The SEM images in Figure 3-4 represents the 50-molar

percentage of AgZnO at low and high magnification. Figure 3-5 represents the 100-molar percentage AgZnO. As can be seen, both loadings have high levels of agglomeration, indicating a decreased surface area, and therefore reactivity of the nanoparticles. The imaging demonstrates that the shape of the synthesized nanoparticles remained spherical. This demonstrates that with a range of silver loading, the physical properties of the photocatalyst remained relatively unchanged.

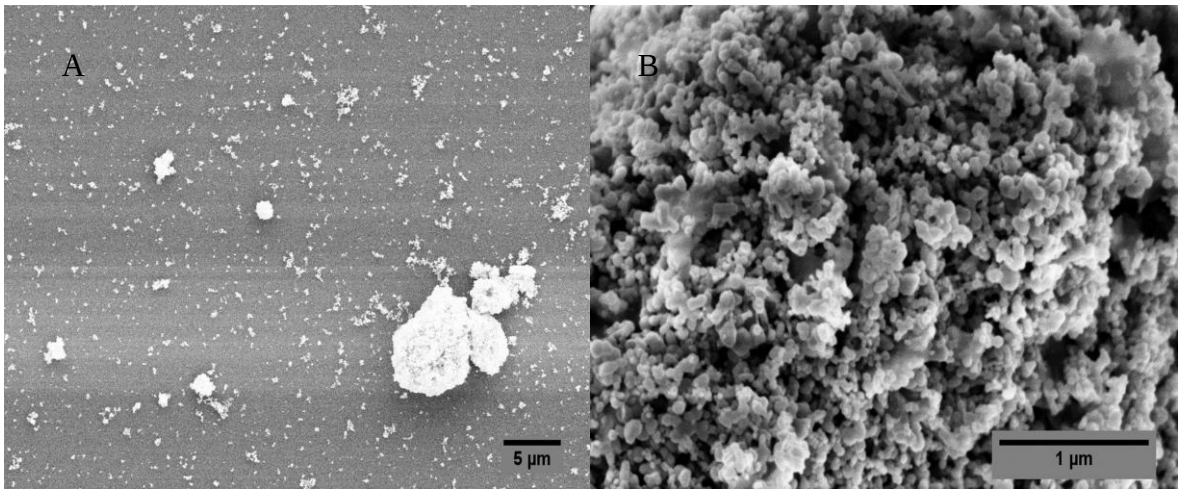

Figure 3-4: SEM images at A) 2000x magnification and B) 27 640x magnification of the 50 molar percentage of Ag-ZnO nanoparticle. High agglomeration can be seen in A, and a close up of that agglomeration can be seen in B.

.

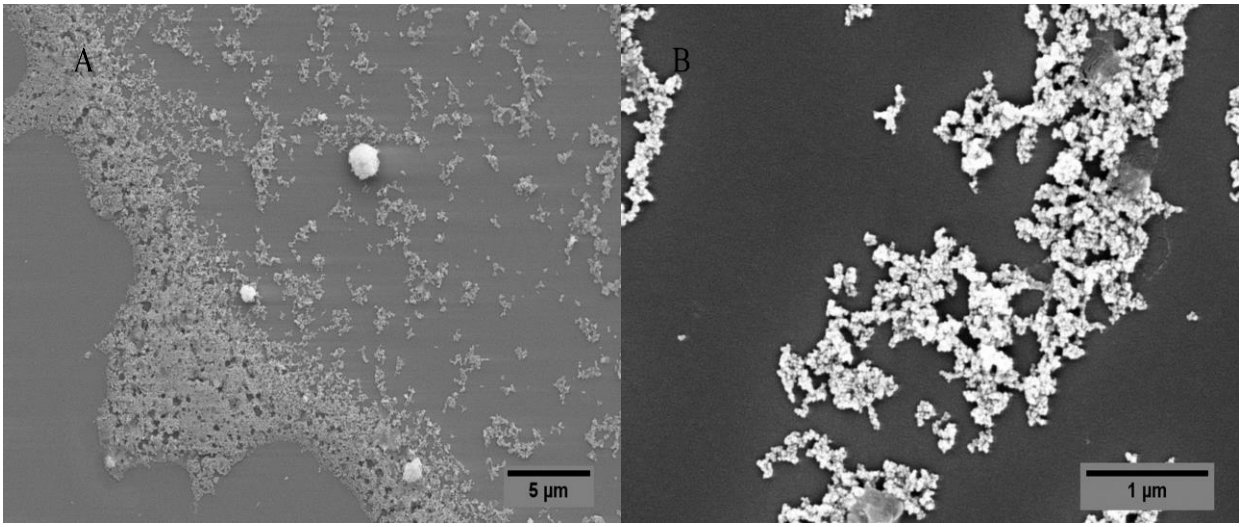

Figure 3-5: SEM images at A) 2950x magnification and B) 20 000x magnification of the 100 molar percentage Ag-ZnO nanoparticles. Agglomerated particles are still visible in A.

The agglomeration of select silver molar percentage nanoparticle blends was also tested using a NanoQ V2.5.9.0 Particle Size Analyzer. The particle sizes, reported in Table 5, are much larger than the zinc oxide precursor of 10-30 nm, indicating high levels of agglomeration. Agglomeration of nanoparticles decrease their overall surface area. The decreased surface area should result in lower overall reactivity. Since agglomeration was observed across the nanoparticles of all silver loadings, the effect of the agglomeration did not affect the observations of this study.

Table 5: The measured average particle size of zinc oxide nanoparticles with various silver loadings, as reported by the NanoQ V2.5.9.0 Particle Size Analyzer.

Molar Percentage	Average Particle Size (nm)	Standard Deviation (%)
1	894.97	94.37
3	505.19	37.92
100	1926.44	142.57
14000	492.99	51.16
42000	595.20	63.68
1400000	587.67	56.12

3.4 Discussion

As expected, an improved photocatalytic reaction rate was found with increasing silver loading. However, significant improvement, when compared to pure zinc oxide, was not found until a silver loading of 700,000%. Previous studies found immediate improvement with silver loading, though it was not stated at which point the improvement became significant (Zhang and Mu, 2007; Yildirim, Unalan and Durucan, 2013). This difference could be due to the different synthesis methods, or the different nanoparticle morphologies.

While the study completed in this thesis found improvement in hydroxyl production with increased silver loading, without a decrease in photocatalytic activity with additional

loading, other studies found an optimal silver loading, after which photocatalytic activity decreased. The optimal loading was found to be 6.2 wt.% (85,709 molar %) for the nanorod-like morphology (Zhang and Mu, 2007). Studies have attributed the decrease in photocatalytic activity to be due to the blocking of adsorption sites available by the metal (Jiang *et al.*, 2014). It is possible that the decrease in adsorption sites may be experienced by higher silver loadings not observed in the current study.

The plateau of photocatalytic improvement experienced in this study is consistent with (Yildirim, Unalan and Durucan, 2013), though they noticed that the decrease in conversion rate improvement was experienced at higher silver loadings. The synthesis method used by Yildirim et al. (2013) found a decrease in overall particle size associated with higher silver loading ratios. This decrease in particle size increased the availability of adsorption sites and oxygen defects (Yildirim, Unalan and Durucan, 2013). The work completed in the current study did not observe significant changes in particle size with silver loadings. The photocatalytic improvement therefore may not be attributed to a decrease in particle size.

Characterization of the nanoparticles found that the change in adsorption bandgap was minimal. The benefits of plasmonic photocatalysis is typically classified by two mechanisms, LSPR and Schottky junctions (Zhang *et al.*, 2013). The lack of a change in the bandgap indicates that the improved photocatalytic activity in this case may not be due to LSPR effects. In addition, it has been demonstrated that LSPR effects may decrease with Schottky effects, and the LSPR effects decrease with increased silver loading (Jiang *et al.*, 2014). The increased conversion rate can, therefore, be attributed to the increased electron-hole separation provided by the metal: metal-oxide semiconductor junction (Zhang *et al.*, 2013). The better separation leads to the higher production of reactive oxygen species. The metal component can be referred to as an electron sink (Bensalah *et al.*, 2014). This leaves the holes to freely interact with water on the surface of the metal oxide, creating hydroxyl radicals, which are responsible for the conversion of TPA into HTPA.

Both SEM imaging and particle size analysis found high levels of agglomeration. An increased level of agglomeration would decrease the surface area of the catalyst, decreasing

the levels of available adsorption sites. Since adsorption is a crucial step for photocatalytic degradation (Turchi and Ollis, 1990), agglomeration would best be avoided. The high agglomeration was consistent throughout all molar percentages of silver tests.

The nanoparticles hydrothermally synthesized with a zinc oxide nanoparticle seed resulted in a consistent sphere-like morphology. Studies that synthesized the silver-zinc oxide nanoparticles in a single step found a rod-like morphology (Zhang and Mu, 2007), due to the preferential growth of zinc oxide along the [0001] crystallographic face (Mclaren *et al.*, 2009). The differences in photocatalytic activity are possibly caused by the difference in photocatalyst shape.

The significant improvement of hydroxyl production found with high silver loading implies that the use of plasmonic photocatalysis has potential for improved contaminant removal. The metal: metal oxide junction created a Schottky barrier, which causes charge carrier separation, enhancing hydroxyl production.

3.5 Chapter Summary

The use of plasmonic photocatalysis for improved photocatalytic activity was studied in this chapter. Zinc oxide nanoparticles were loaded with a range of silver to identify the optimal ratio of metal: metal oxide. Hydrothermal synthesis provides a simple method for nanoparticle functionalization that may possibly be applied at an industrial manufacturing scale in the future. Photocatalytic activity was measured under UV light irradiation to convert TPA into HTPA. A zero-order reaction model was used to identify the conversion rate constants. There was a significant improvement in the conversion rate constant beginning at a mass percentage of 5.06% when compared to pure zinc oxide. Characterization of the synthesized nanoparticles found that the bandgap of the material did not greatly change with silver loading. The improvement in conversion rates can therefore be attributed to the increased charge carrier separation effects created by the Schottky junction. SEM imaging and particle size analysis demonstrated high agglomeration of the nanoparticles in solution, which was constant for all silver loadings imaged. Further, the nanoparticles maintained a sphere like

morphology throughout all silver loading ratios. Overall, functionalization of zinc oxide nanoparticles using plasmonic photocatalysis provides a significant improvement to hydroxyl production, indicating that it may be useful for improving contaminant removal in future water treatment applications.

Chapter 4
Removal of Pharmaceuticals from Wastewater Effluent using Titanium Dioxide based Photocatalysis

Photocatalysis has been widely considered, and accepted, as a potential method for the removal of emerging contaminants from wastewater and drinking water sources (Mirzaei *et al.*, 2016). Photocatalysis is an advanced oxidation process that uses ultraviolet (UV) light and a photocatalyst to create the reactive oxygen species (ROS). The ROS then can react with contaminants to either degrade or convert them to less harmful substances. Titanium dioxide nanoparticles are commonly used for photocatalytic reactions as they are commercially available and have demonstrated high photocatalytic activity (Friedmann, Mendive and Bahnemann, 2010).

Pharmaceuticals in wastewater effluent are of growing concern due to their potential effects on aquatic species and possibly human health. Examples of this are demonstrated by the effects that contaminants are having in fish populations. Male fish were feminized, with oocytes (eggs) developing in their testes when exposed to municipal wastewater (Tetreault *et al.*, 2011). Fish exposed to antidepressants show lethargic behavior and changes in their mating habits (Bisesi, Bridges and Klaine, 2014). The removal of pharmaceuticals from water and wastewater may therefore reduce the risks to both the environment and humans (e.g. drinking water).

Past tests of pharmaceutical contaminant removal using photocatalysis often examined the pharmaceuticals in a pure water matrix. In this study, a cocktail of 24 pharmaceuticals was spiked into actual wastewater effluent, or a pure water matrix (Milli-Q). The prepared matrices were then tested for photocatalytic degradation using an in house photocatalytic testing setup. Two UV based removal tests were completed for each of the prepared samples, along with a control test, where no UV light was added. The first test used UV light irradiation to observe whether indirect or direct photolysis was enough to degrade the pharmaceuticals. The next test used UV light combined with titanium dioxide nanoparticles to observe

photocatalytic removal. A comparison of removal efficiencies between a pure water matrix and wastewater effluent was then completed. Additional parameters were also considered for effects on photocatalytic removal including the electrostatic interactions between the catalyst and the contaminants and the degradation of natural organic matter (NOM) which was present in the wastewater effluent samples.

4.1 Materials and Methods

The materials and methods employed in this experiment involved numerous steps (Figure 4-1). First, a wastewater final effluent grab sample was collected August 14, 2018, from the Waterloo Regional Wastewater Treatment plant, following the protocol outlined in Appendix A4: Collection of Wastewater from Waterloo Wastewater Treatment Plant. Wastewater effluent was stored on ice and then filtered using a 2 µm filter (Whatman) to remove the large particulate matter. Wastewater effluent was tested within 48 hours of collection.

The wastewater effluent was then spiked from a stock solution composed of 24 different chemicals (mostly pharmaceuticals, degradation products or wastewater related contaminants), to create a suspension of 2 µg/L of each pharmaceutical compound. These are typical concentrations much higher than found in final effluent (Arlos *et al.*, 2015; Hicks *et al.*, 2017). Degradation tests were completed in six conditions outlined in Table 6. Either wastewater effluent or pure Milli-Q water was used as the test solution, spiked with pharmaceutical cocktail. Tests referred to as UV disinfection contained UV light, but no photocatalyst (x.x.UV.B). Tests referred to as photocatalytic tests contained both UV light and the photocatalyst (x.x.UV.P25). The pharmaceuticals in methanol were first evaporated in the fume hood before the water solution was added. The UV 365 lamp was turned on for constant illumination at time zero if it was used. Additionally, 30 mg of P25 (titanium dioxide nanoparticles) was spiked into each of the test setups, where necessary.

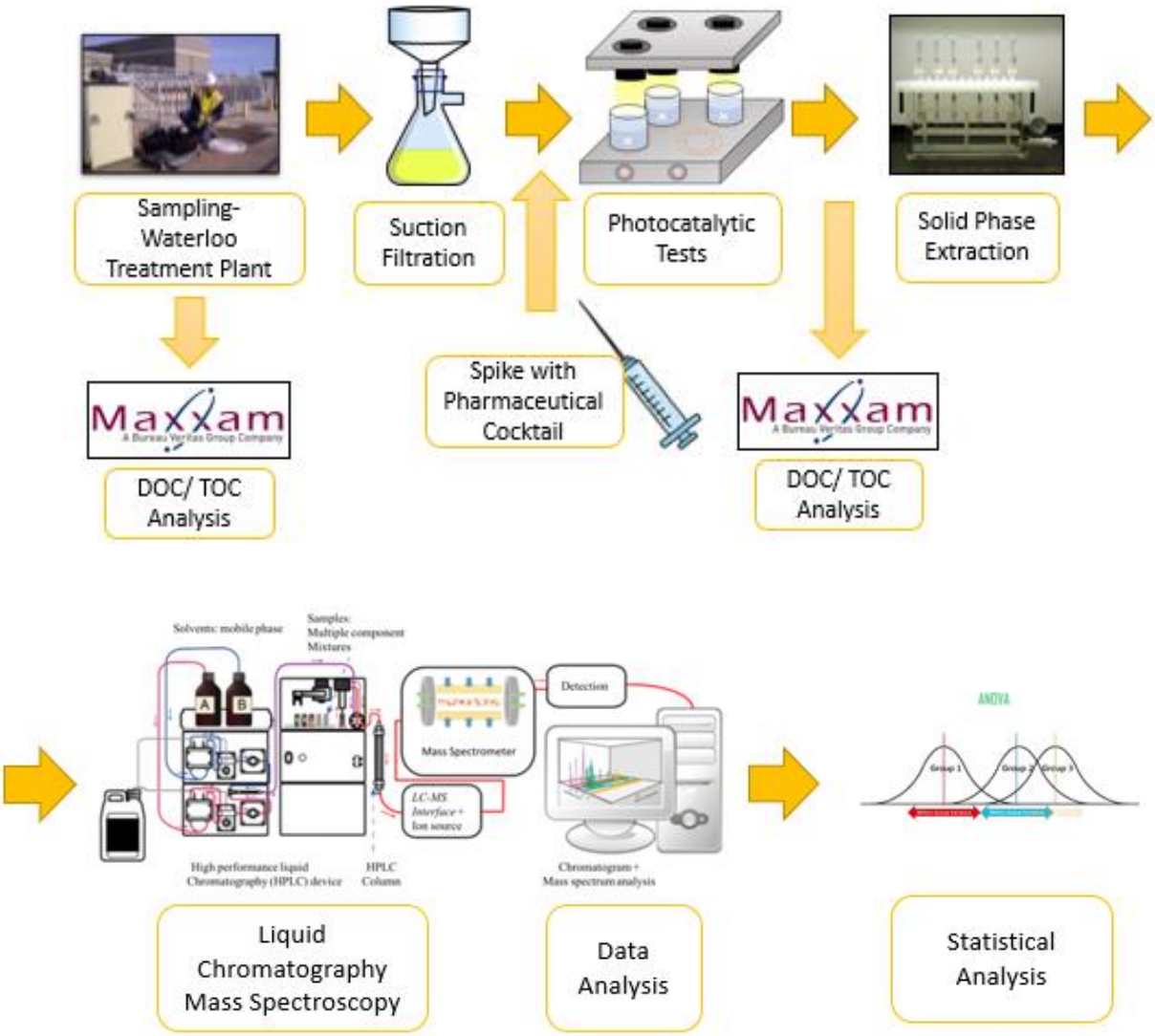

Figure 4-1: Experimental methodology of the pharmaceutical tests.

Table 6: Test conditions. Code: E= Effluent/ M= Milli-Q, U=Unspiked/ S= Spiked with Pharmaceutical Cocktail, UV= UVA Light Source/ D= Dark, P25= TiO_2 Nanoparticles included/ B=Blank (no nanoparticles added).

Plate Name	Effluent	Spiked Pharmaceutical	UV Light?	Nanoparticles?
E/S/D/B	✓	✓	✗	✗
E/S/UV/B	✓	✓	✓	✗
E/S/UV/P25	✓	✓	✓	✓
M/S/D/P25	✗	✓	✗	✓
M/S/UV/B	✗	✓	✓	✗
M/S/UV/P25	✗	✓	✓	✓

4.1.1 Photocatalyst and Pharmaceuticals

Titanium dioxide nanoparticles were purchased from Sigma-Aldrich. Pharmaceutical compounds were purchased from Sigma-Aldrich and suspended in methanol. Designated isotopically labelled standards were used for LC-MS/MS analysis and quantitation (except for monensin), and lorazepam was used as an internal standard. These standards were purchased from CDN Isotopes Inc. (Pointe-Claire, QC, Canada), except for atorvastatin-d5, which was purchased from Toronto Research Chemicals (Toronto, ON, Canada). The pharmaceutical compounds were dissolved in methanol as 1 g/L stock solutions in amber glass vials and stored at -20℃. The full list of pharmaceutical compounds and their dissociation constants and uses may be found in Table 7.

Table 7: Chemicals used in this study and some of their properties. All data was collected from TOXNET: Toxicology Data Network.

Pharmaceutical	Molecular Formula	Dissociation Constant(s)	Purpose
Acetaminophen	C8-H9-N-O2	9.38	analgesic
Atenolol	C14-H22-N2-O3	9.6	beta-blocker
Atorvastatin	C33-H35-F-N2-O5	4.3, 14.9	lipid lowering
Atrazine	C8-H14-Cl-N5	1.6	herbicide
Bisphenol A	C15-H16-O2	9.6	plastic filler
Caffeine	C8-H10-N4-O2	14	beverage
Carbamazepine	C15-H12-N2-O	13.9	anti-epileptic
Desvenlafaxine	C16-H25-N-O2	9.45, 10.66	anti-depressant
Diclofenac	C14-H11-Cl2-NO2	4.15	anti-inflammatory
Carbamazepine-10,11-Epoxide	C15-H12-N2-O	13.9	carbamazepine degradation product
Fluoxetine	C17-H18-F3-N-O	9.8	SSRI (anti-depressant)
Gemfibrozil	C15-H22-O3	4.5	lipid lowering
Ibuprofen	C13-H18-O2	5.2, 4.91	anti-inflammatory
Lincomycin	C18-H34-N2-O6-S	7.6	antibacterial
Monensin	C36-H62-O11	4.2	antibiotic
Naproxen	C14-H14-O3	4.15	anti- inflammatory
Norfluoxetine	C16-H18-F-N3-O3	6.34, 8.75	Fluoxetine degradation product
o-Atorvastatin	C33-H35-F-N2-O5	4.3, 14.9	Atorvastatin degradation product
p-Atorvastatin	C33-H35-F-N2-O5	4.3, 14.9	Atorvastatin degradation product
Sulfamethoxazole	C10-H11-N3-O3-S	1.6, 5.7	antibiotic
Sulfanilamide	C6-H8-N2-O2-S	10.43	antibacterial
Triclosan	C12-H7-Cl3-O2	7.9	antimicrobial
Trimethoprim	C14-H18-N4-O3	7.12	antimicrobial
Venlafaxine	C17-H27-N-O2	10.09	SSRI (anti-depressant)

4.1.2 Photocatalytic Setup

The photocatalytic setup may be found in Figure 3-2. Aliquots of 300 mL of spiked solution (wastewater or Milli-Q) were placed in beakers on a stir plate set to 600 rpm. The stir plate was placed below the in-house assembled six-cm collimated UV-LED beam (θ_{beam}= 4 cm) light source setup with a heat sink. The light sources were 10.5 cm above the surface of the water. The samples were stirred for 60 minutes before the light source was turned on. Samples were taken in 4.5 mL aliquots at -60, 0, 5, 10, 20, 40, 60, 90, 120 minutes. pH of the solutions was measured before and after the photocatalytic tests.

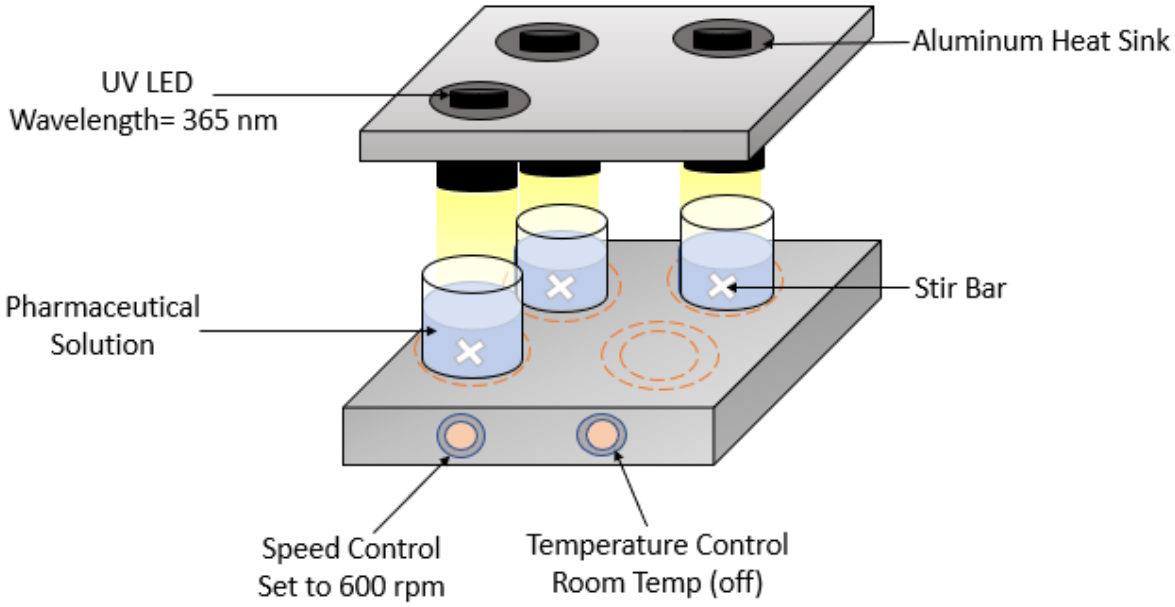

Figure 4-2: Photocatalytic degradation setup.

4.1.3 Solid Phase Extraction and LCMS

Samples were centrifuged at 3500 rpm to remove the particulate matter. Four mL of the samples were then transferred to new glass tubes, where they were spiked with 32 µL of 100 ug/L deuterated pharmaceutical standards. Solid phase extraction (SPE) was completed using Oasis HLB 1cc cartridges with 30 mg sorbent per package and a 30 µm particle size. A

detailed SPE procedure can be found in Appendix A6: Solid Phase Extraction of Pharmaceuticals.

After extraction, the samples were evaporated using the Thermo Scientific™ Rocket Synergy™ Evaporator System. The dried samples were then resuspended in 160 µL of reconstitution solution, composed of methanol containing lorazepam and chloramphenicol (75 µg/L). The samples were then stored in a -20℃ freezer until Liquid Chromatography-Mass Spectroscopy analysis. The liquid chromatography and tandem mass spectrometry (LC-MS/MS) was completed using an Agilent 1200 HPLC coupled to an Applied Biosystems 3200 QTRAP mass spectrometer (ABSciex, Concord, ON, Canada).

4.1.4 Data Analysis

Data processing was completed using Excel, and a first order linear conversion model, Equation 3-1, matched the degradation patterns of the pharmaceutical. [A] represents the concentration of the pharmaceutical, [A_0] represents the initial concentration, and *k* is the first order conversion rate constant (1/min).

$$\ln[A] = -kt + \ln[A_0]$$ **Equation 3-1**

The linest function in Excel was used to find the linear model of fit. The F-statistic was used to determine whether the null hypothesis that the values are just a random scatter of points with a slope of zero was correct. Where the null hypothesis passed, the *k* values were changed to zero for further comparisons. Similarly, if a positive slope was calculated-suggesting formation of pharmaceuticals, the *k* value was also changed to zero. Further statistical analysis was completed using SigmaPlot software (Systat Software, San Jose, CA). An ANOVA was completed to determine whether the charges of the pharmaceutical in solution effected the degradation rate constants.

4.1.5 Water Quality

Samples were sent to Maxxam analytics for a before and after analysis of total organic carbon. Measurements were also completed to measure the initial organics amount, including total ammonia, conductivity, dissolved chloride, nitrite, nitrate, and nitrate + nitrite.

4.2 Results

4.2.1 Pharmaceutical Degradation

Successful pharmaceutical degradation was achieved using photocatalysis in both Milli-Q and wastewater. In some scenarios, pharmaceutical removal to below the detection limit was achieved in as little as five minutes. In every case, even if full pharmaceutical removal was not achieved, partial degradation occurred. Additionally, some decrease in the TOC occurred when photocatalysis was applied to the wastewater effluent.

The degradation tests resulted in 2 patterns. The first, and most dominant pattern, is exemplified by ibuprofen, where only photocatalysis successfully degrades the pharmaceutical. Figure 4-3 and Figure 4-4 plots the ln(concentration) of the pharmaceutical against the time the solution was exposed to the degradation test. In the Milli-Q suspension, the photocatalytic reaction fully removed ibuprofen in an average of 20 minutes, with a reaction rate constant of 0.3878 1/min. UV alone (M/S/UV/B) provided a small amount of removal with a much lower removal rate of 0.0033 1/min. The blank control showed no removal (removal rate of 0). In wastewater effluent, the photocatalysis test (E/S/UV/P25) with ibuprofen had a much lower removal rate of 0.01136 1/min (Figure 4-4). UV disinfection and a blank test in the effluent resulted in no significant removal. Most of the other chemicals followed a case similar to this, where UV disinfection had a removal rate in Milli-Q (M/S/UV/B) of less than or equal to 0.01 1/min were acetaminophen, atenolol, atrazine, bisphenol-a, caffeine, carbamazepine, carbamazepine- 10,11-epoxide, desvenlafaxine, gemfibrozil, ibuprofen, lincomycin, naproxen, sulfamethoxazole,

sulfonamide, triclosan, trimethoprim, and venlafaxine. The degradation plots are in Appendix C1: Degradation Plots.

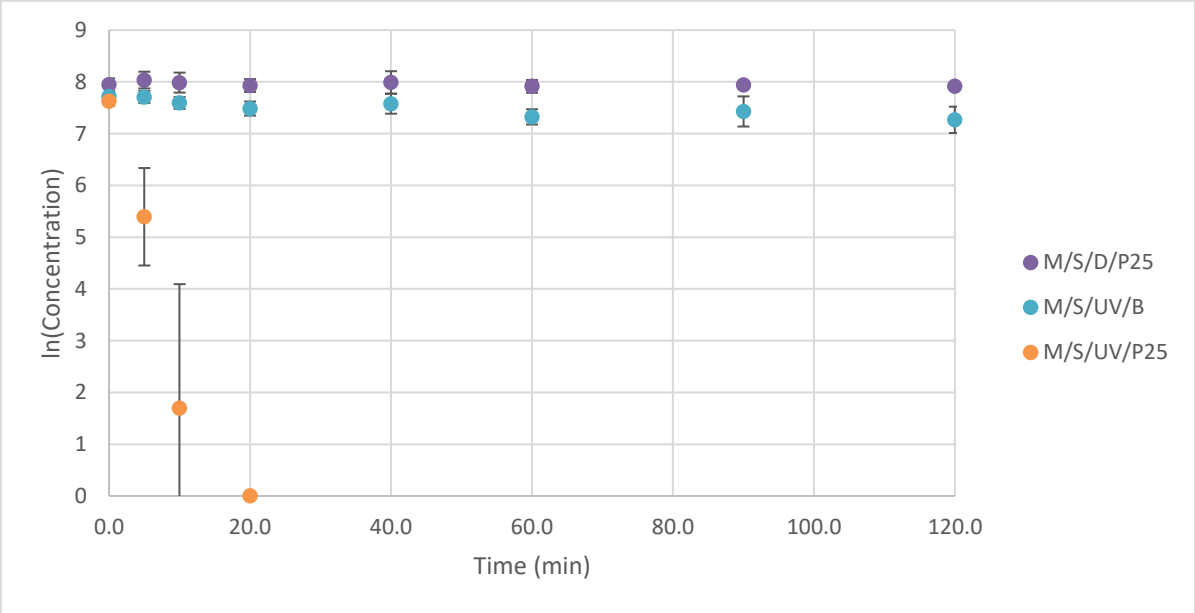

Figure 4-3: Ibuprofen degradation in pure (Milli-Q) water. This is the first category of degradation, where only photocatalysis successfully degrades the pharmaceutical. The purple dots represent the dark study with P25, the blue indicates just UV irradiation, and the orange dots represent the photocatalytic removal.

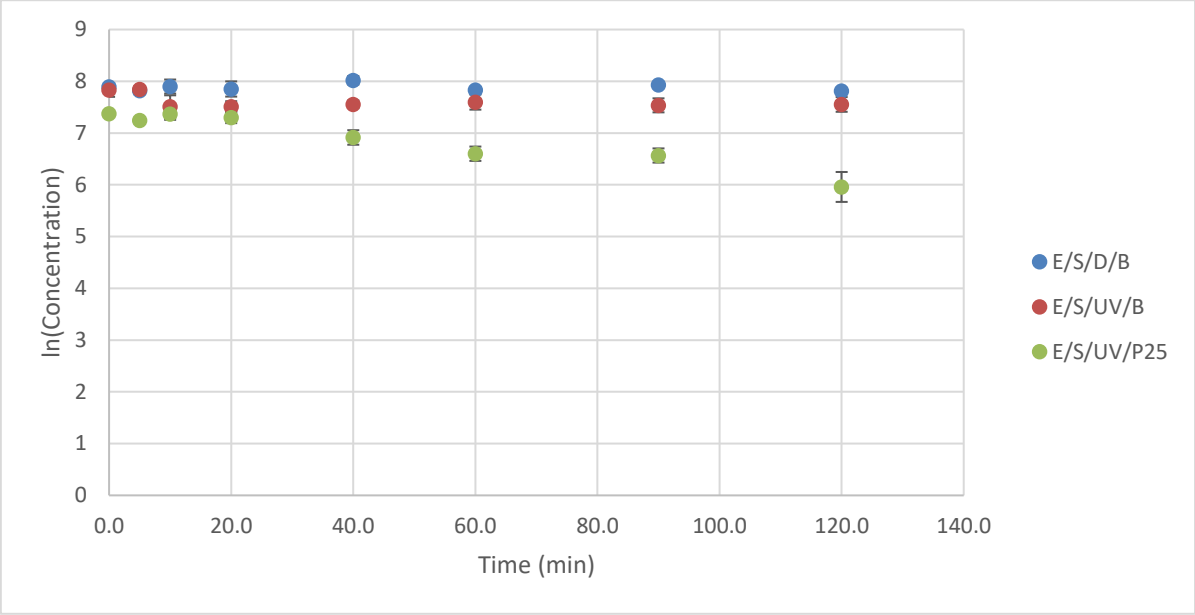

Figure 4-4: Ibuprofen degradation in wastewater effluent. Photocatalysis has little effect on pharmaceutical removal. The blue represents the dark study, red represents UV irradiation and green represents photocatalytic degradation.

The second pattern of degradation is demonstrated by monensin (Figure 3-5), where UV disinfection can partially degrade the pharmaceutical. In the pure water suspension, photocatalysis (E/S/UV/P25) achieved complete removal of the pharmaceutical in 40 min. In wastewater effluent, UV disinfection failed to remove monensin as demonstrated by Figure 3-6. In this case, photocatalysis is only marginally successful in wastewater effluent. The other pharmaceuticals that follow a degradation like monensin are atorvastatin, diclofenac, fluoxetine, norfluoxetine, o-atorvastatin and p-atorvastatin (Appendix C1: Degradation Plots).

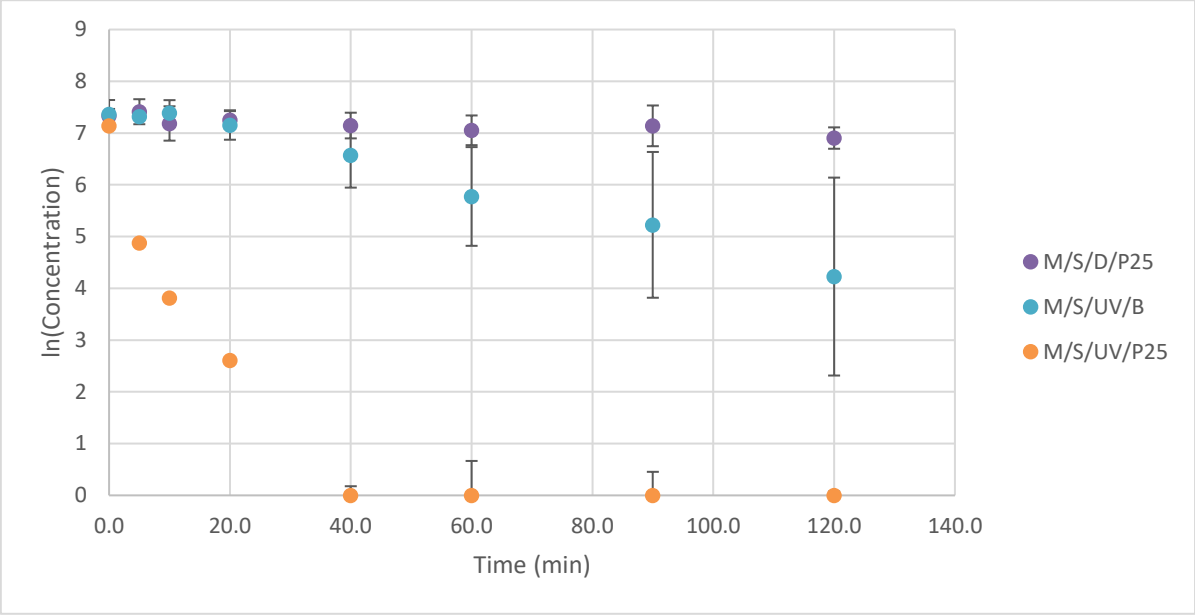

Figure 4-5: Degradation of monensin in pure (Milli-Q) water. The use of UV disinfection removes some of the pharmaceutical, and the addition of photocatalysts greatly improved the removal.

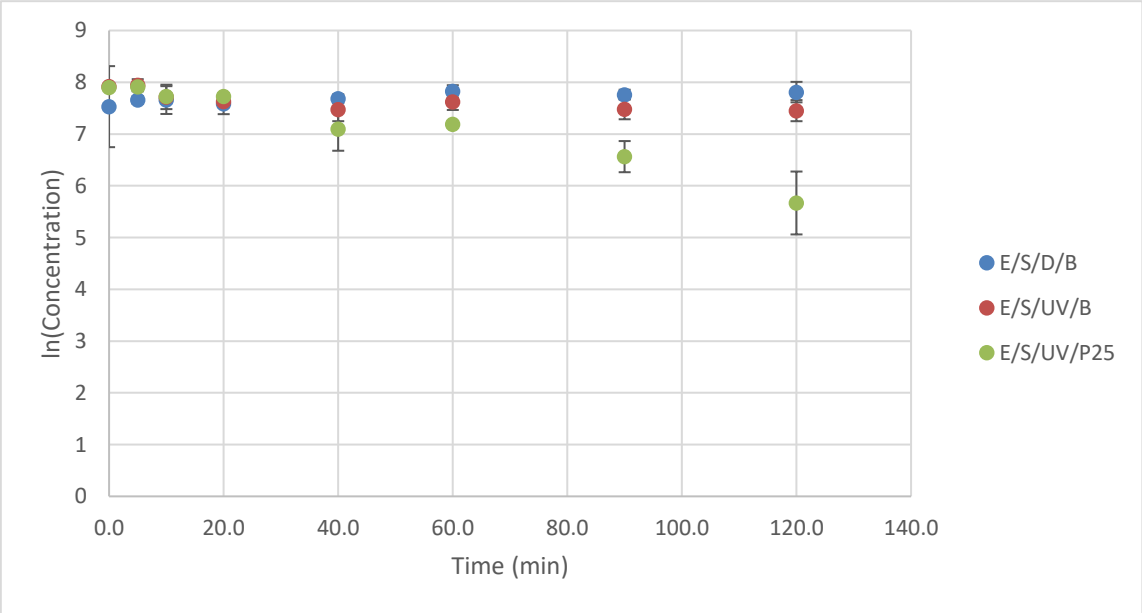

Figure 4-6: Degradation of monensin in wastewater effluent. UV disinfection is

unsuccessful at removing the pharmaceutical, and the addition of photocatalyst is only partially successful.

The degradation rate constants for all pharmaceuticals tested are reported in Table 8 and Table 9 below. A degradation rate of zero indicates that no significant removal occurred. This was common in the pure water, dark matrix with P25. As stated earlier, UV irradiation removed some of the pharmaceutical contaminants. However, the removal rates were often low (less than or equal to 0.01 1/min). The addition of the photocatalyst resulted in improvement of the pharmaceutical removal rate. When added to wastewater effluent, the removal rate was decreased compared to the Milli-Q water. This exemplifies the effects that natural organic matter has on the reactive oxygen species (scavenging and blocking light). In cases where UV irradiation was effective in the Milli-Q matrix, it did not always result in significant removal in wastewater effluent and rates were usually much reduced (Table 8, 9).

Table 8: Degradation rate constants (1/min) and the sum of residual squares of chemicals spiked in pure (Milli-Q) water for a first-order reaction model.

Sample Name	**M/S/D/P25**		**M/S/UV/B**		**M/S/UV/P25**	
	k (1/min)	**r^2**	**k (1/min)**	**r^2**	**k (1/min)**	**r^2**
Acetaminophen	0	0.3502	0.0071	0.9882	-	-
Atenolol	0	0.2670	0.0048	0.9508	0.0516	0.9399
Atorvastatin	0.0048	0.9300	0.0188	0.9067	1.4090	1.0000
Atrazine	0	0.3384	0.0024	0.9536	0.0362	0.9866
BisphenolA	0	0.0321	0.0073	0.9891	1.4668	1.0000
Caffeine	0	0.0543	0	0.4429	0	0.2724
Carbamazepine	0	0.0222	0.0043	0.9768	0.0314	0.5376
Carbamazepine-10,11-Epoxide	0	0.2052	0.0030	0.9111	0.0410	0.7409
Desvenlafaxine	0	0.8687	0.0060	0.9966	-	-
Diclofenac	0	0.1058	0.0138	0.9965	1.4506	1.0000
Flouxitine	0	0.1972	0.0185	0.9788	0.0339	0.6870
Gemfibrozil	0	0.0293	0.0066	0.9364	-	-
Ibuprofen	0	0.3546	0.0033	0.7630	0.3878	0.9142
Lincomycin	0	0.0423	0.0084	0.9920	0	0.2856
Monensin	0.0032	0.7596	0.0270	0.9868	-	-

Sample Name	M/S/D/P25		M/S/UV/B		M/S/UV/P25	
	k (1/min)	r^2	k (1/min)	r^2	k (1/min)	r^2
Naproxen	0	0.3020	0.0076	0.9427	1.1358	1.0000
Norfluoxetine	0.0018	0.5244	0.0194	0.9900	0.0321	0.7403
O-Atorvastatin	0.0145	0.8708	0.0240	0.8807	-	-
P-Atorvastatin	0.0111	0.9697	0.0231	0.9488	-	-
Sulfamethoxazole	0	0.0031	0.0066	0.9724	-	-
Sulfonamide	0	0.9178	0.0030	0.9383	-	-
Triclosan	0	0.0526	0.0094	0.9930	0.7728	0.9843
Trimethoprim	0	0.6471	0.0091	0.9950	0.0398	0.7475
Venlafaxine	0	0.6461	0.0080	0.9959	0.0454	0.7025

Table 9: The first order reaction rate constant (*k* 1/min) and the sum of residual squares for the first order model of fit for chemicals spiked in wastewater effluent.

Sample Name	E/S/D/B		E/S/UV/B		E/S/UV/P25	
	k (1/min)	R^2	k (1/min)	R^2	k (1/min)	R^2
Acetaminophen	0	0.28079	0	0.29472	-	-
Atenolol	0	0.08929	0	0.46614	0.01074	0.96091
Atorvastatin	0.00136	0.64663	0.01409	0.90040	0.05221	0.99380
Atrazine	0	0.25630	0.00176	0.32227	0.00303	0.80900
BisphenolA	0	0.02387	0.00329	0.68440	0.02963	0.96430
Caffeine	0.00206	0.54929	0	0.01589	0.00967	0.87181
Carbamazepine	0	0.00125	0.00252	0.59832	0.01612	0.98643
Carbamazepine-10,11-Epoxide	0	0.00104	0	0.40973	0.01153	0.96796
Desvenlafaxine	0	0.85351	0	0.00564	0.03262	0.96834
Diclofenac	0	0.00549	0.00547	0.90284	0.01843	0.78928
Flouxitine	0	0.00347	0	0.26222	0.01373	0.95452
Gemfibrozil	0	0.25208	0.00324	0.51081	0.01254	0.94680
Ibuprofen	0	0.01345	0	0.24262	0.01136	0.95101
Lincomycin	0	0.26061	0.00364	0.74359	0.05254	0.99209
Monensin	0	0.68527	0.00356	0.64608	0.01758	0.95568
Naproxen	0	0.02718	0.00586	0.74839	0.03916	0.96021
Norfluoxetine	0	0.10602	0.00383	0.65336	0.01455	0.93172

Sample Name	E/S/D/B k (1/min)	R^2	E/S/UV/B k (1/min)	R^2	E/S/UV/P25 k (1/min)	R^2
O-Atorvastatin	0.00076	0.57093	0.01748	0.95939	0.04987	0.79231
P-Atorvastatin	0	0.33649	0.01512	0.94916	-	-
Sulfamethoxazole	0	0.23577	0.00368	0.66885	0.03694	0.97880
Sulfonamide	0	0.44365	-	-	0.02523	0.98919
Triclosan	0	0.00063	0.00305	0.58206	0.03438	0.90501
Trimethoprim	0	0.31292	0	0.40545	0.01382	0.97954
Venlafaxine	0	0.59528	0.00021	0.01916	0.01212	0.95918

In some cases, full degradation (below the analytical detection limits) of the pharmaceutical was achieved within the testing time. Table 10 reports the time for full removal of the pharmaceutical in Milli-Q and in effluent, where it occurred. Removal as fast as five minutes occurred in four pharmaceuticals in Milli-Q (atorvastatin, bisphenol a, diclofenac, p-atorvastatin), and the fastest removal occurred in effluent in forty minutes, for sulfonamide.

Table 10: Time for full removal of pharmaceuticals (below detection limit), when it occurred. N/A indicates full removal did not occur.

Chemical	Milli-Q time for full removal (min)	Effluent time for full removal (min)
Acetaminophen	60	90
Atenolol	N/A	N/A
Atorvastatin	5	N/A
Atrazine	N/A	N/A
Bisphenol A	5	N/A
Caffeine	60	N/A
Carbamazepine	N/A	N/A
Carbamazepine-10,11- epoxide	N/A	N/A
Desvenlafaxine	120	N/A
Diclofenac	5	N/A

Chemical	Milli-Q time for full removal (min)	Effluent time for full removal (min)
Fluoxetine	N/A	N/A
Gemfibrozil	120	N/A
Ibuprofen	20	N/A
Lincomycin	N/A	N/A
Monensin	40	N/A
Naproxen	20	N/A
Norfluoxetine	N/A	N/A
o-Atorvastatin	N/A	N/A
p-Atorvastatin	5	60
Sulfamethoxazole	20	N/A
Sulfanilamide	10	40
Triclosan	10	N/A
Trimethoprim	N/A	N/A
Venlafaxine	N/A	N/A

4.2.2 Degradation Rates and Chemical Charge

A Brown-Forsythe and Tukey test (ANOVA) completed found statistical significance between the conversion rates of the negative charged pharmaceuticals and both the positive and neutral pharmaceuticals. There was no significance between the neutral and positively charged pharmaceuticals. In wastewater effluent, there was no significant differences between the conversion rates of pharmaceuticals regardless of charge.

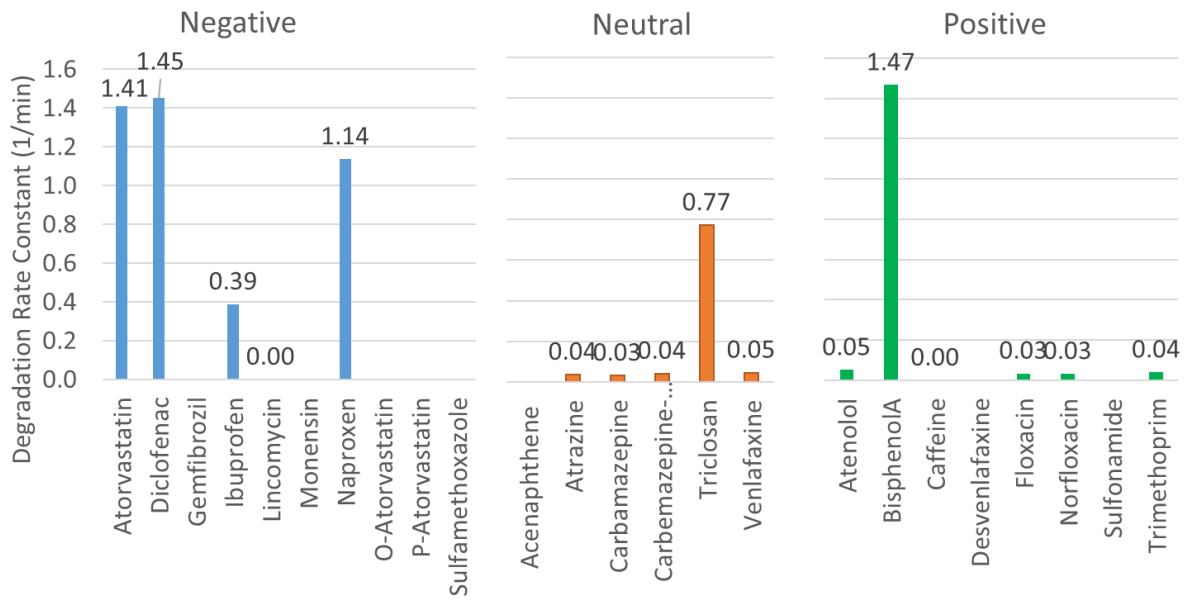

Figure 4-7: The conversion rate constants of pharmaceuticals in Milli-Q water (pH ~ 5) organized based on their charge at that pH.

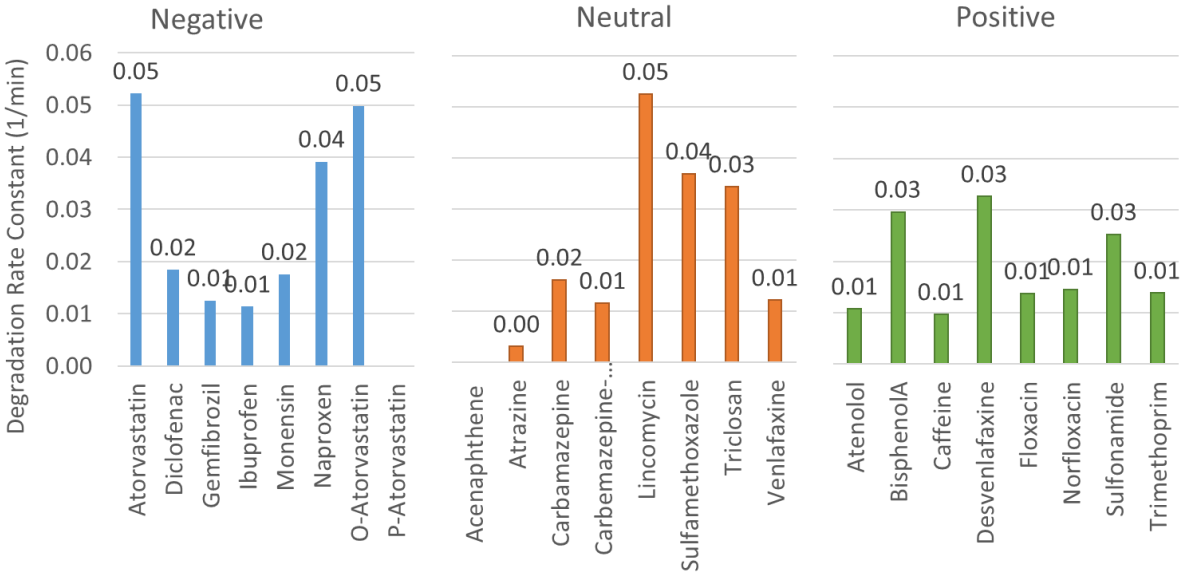

Figure 4-8: The degradation rate constants for pharmaceuticals in wastewater effluent (pH ~ 7) organized by charge.

4.2.3 Water Quality

The total organic carbon (TOC) was measured upon collection from the Waterloo wastewater treatment plant, and after pharmaceutical degradation tests were performed (Table 11, 12). The TOC values and overall percent changes are reported in Table 12. Some natural degradation of TOC occurred in the blank test (7% removal), and UV disinfection added around 5% removal. The photocatalytic test resulted in a 26% removal of TOC. This suggests that the decrease in photocatalytic degradation rates in the wastewater effluent samples can be due to the scavenging of the generated ROS by the organic matter in the solution.

Table 11: Inorganics data for wastewater effluent upon collection.

Inorganics	Units	Detection Limit	Waterloo Treatment Plant	Standard Deviation
Total Ammonia	mg/L	0.050	1.37	0.047
Conductivity	umho/cm	1.0	2400.00	0.000
Total Organic Carbon (TOC)	mg/L	0.50	9.37	0.205
Dissolved Chloride	mg/L	6.0	490.00	8.165
Nitrite	mg/L	0.010	0.53	0.009
Nitrate	mg/L	0.50	36.53	0.170
Nitrate + Nitrite	mg/L	0.50	37.07	0.189

Table 12: Total organic carbon for wastewater effluent upon collection from the Waterloo treatment plant and after photocatalytic tests were performed on the matrix.

Inorganics	Units	Waterloo Treatment Plant	E/S/D/P25	E/S/UVA/B	E/S/P25/UVA

Total Organic Carbon (TOC)	mg/L	9.37	8.70	8.20	6.90
		Percent Change	-7.12	-12.46	-26.33

4.2.4 Change in pH

Table 13 reports the pH of the test solutions, and their overall change after degradation tests. Note that the pH was measured before nanoparticles were added and after the nanoparticles were centrifuged out of the final solution. Overall, little change in pH was observed.

Table 13: Average pH values measured for the water testing conditions. Insignificant change in pH was measured between before and after the tests were applied.

	E/S/D/B	E/S/UV/B	E/S/UV/P25	M/S/D/P25	M/S/UV/B	M/S/UV/P25
Average pH	7.260	7.382	7.234	5.704	5.767	5.969
Average Change	-1.053	-0.788	-0.971	0.430	0.173	0.432
Standard Deviation	0.017	0.085	0.055	0.152	0.082	0.065

4.3 Discussion

The removal of pharmaceuticals was much more effective in pure water than in a wastewater effluent matrix. While some organic compounds can assist in indirect photolysis, the presence of organics decreased the ability of the photocatalyst to remove all the compounds. This can be due to the scavenging of the reactive oxygen species and the scattering and absorption of UV light by inorganic carbons. Doll and Frimmel (2005) attribute the decrease in photocatalytic activity in NOM to be caused by the competitive adsorption of radiation and the competitive adsorption of NOM onto the TiO_2 photocatalyst itself. Further

research completed indicates that small loading ratios of NOM (400 µg/g) can enhance the photocatalytic activity by up to 8%, by providing higher adsorption of reactants to the photocatalyst surface and serving as a photocatalytic intermediate. Higher loadings (400 mg/g) resulted in the blockage of pharmaceuticals from reaching the TiO_2 catalyst (Drosos, Ren and Frimmel, 2015). The initial TOC of 9.37 mg/L indicates an initial ratio of TOC to P25 of 104 mg/g. The general decrease in photocatalytic removal of chemicals (e.g. pharmaceuticals) reported in the literature is consistent with this study. Although NOM may produce some indirect opportunity for photolytic degradation, scavenging effects of the organic matter in wastewater greatly reduced the over photocatalysis of the chemicals of interest.

A decrease in total organic carbon was found when degradation tests were performed. There was a decrease of around 12% in the TOC with UV light irradiation (relative to controls) and over 25% in the TOC measurement after photocatalysis was applied to the matrix. This supports the conclusion that organic matter had a scavenging effect on both the formed reactive oxygen species and the UV light. A 50% mineralization of organic matter to carbon dioxide and water was reported by Eggins et al. (1997) in there experiments after one hour a mercury lamp (Eggins, Palmer and Byrne, 1997).

Dark studies of the chemicals of interest in this study did not result in significant removal. In the dark Milli-Q water study with photocatalyst added most pharmaceuticals experienced no removal, but removal rates of 0.111 (1/min) and lower were found for atorvastatin, monensin, o-atorvastatin, p-atorvastatin and norfluoxetine. Interestingly, all these compounds were negatively charged in solution except for norfluoxetine. This demonstrates some removal associated with sorption in a pure water matrix, either to the glass or the photocatalyst. In wastewater effluent without UV irradiation or photocatalysts, atorvastatin and o-atorvastatin and caffeine demonstrated degradation rates (less than 0.002 1/min), indicating some adsorption of these compounds to the NOM and/or experimental apparatus (e.g. glass). The sorption levels potentially changed with the difference in pH between Milli-Q (pH ~5) and wastewater effluent (pH ~7). No sorption effects were reported by Choi et al

(2014), although they did not study any of the pharmaceuticals where this was observed in the current study. The likelihood of chemical sorption to organic matter can be predicted using the octanol- water partition coefficient based on equilibrium partitioning of the neutral chemical form, (Cheytt *et al.*, 2005) although adsorption may also occur through charge interactions. As the pH differed in the two experimental conditions (Milli-Q and wastewater) some difference among the chemicals may be related to the dissociation constants (pK_a) and therefore the partitioning to the organic matter making them less available for chemical reactions.

Pure light irradiation by UV A LEDs did cause some removal of pharmaceutical compounds, as discussed in the results as the second case of removal. The low rates of removal by UV irradiation removal are consistent with the findings by Bielak et al. (2015), who found a much higher removal when UV light was combined with hydrogen peroxide, which served as a ROS donor (Bielak *et al.*, 2016). The removal by light irradiation indicates that these pharmaceutical compounds may not persist as long in the environment, as they may be degraded by sunlight (Santoke and Cooper, 2017). The use of a UV C light source would likely improve this UV light removal (direct photolysis), as was found by (Choi *et al.*, 2014). However, there was significant improvement in contaminant removal when a photocatalyst was added in the current study.

More oppositely charged particles have a higher chance of electrostatic interaction (Kumar, 2017). The point of zero charge of P25 has been established at a pH of 7.5 (Fernández-Nieves, de las Nieves and Richter, 1998). The P25 photocatalyst is therefore slightly positive in wastewater effluent, at a pH of 7, and even more positive in pure water at a pH of 5. It is therefore presumed that pharmaceuticals that exhibit a negative charge in solution will have a higher degradation rate constant due to electrostatic attraction to the photocatalysis (Arlos, Hatat-Fraile, *et al.*, 2016; Arlos, Liang, *et al.*, 2016). The increased attraction would increase the chance of adsorption, which is a crucial step for photocatalysis (Turchi and Ollis, 1990). The decrease in conversion rate observed in this test was significantly larger for the negatively charged pharmaceutical compounds in the Milli-Q water

sample. This effect was not significant in a wastewater effluent sample, where NOM appears to influence the degradation patterns.

4.4 Chapter Summary

The photocatalytic removal of pharmaceutical compounds in both a pure water suspension and a wastewater effluent matrix was studied. The effects of NOM, the charges of the pharmaceuticals in solution and the addition of a photocatalyst to UV light irradiation was observed. Overall, photocatalysis was demonstrated to successfully remove several pharmaceutical compounds to below the detection limit. The improvement of photocatalysis over UV irradiation was evident. UV disinfection was at times successful in removing some of the pharmaceutical, but never resulted in full removal (below analytical detection limits). In contrast, the wastewater effluent had a decrease in total organic carbon after photocatalytic tests, indicating scavenging of the UV light by organic compounds in the solution. This resulted in much reduced rates of removal of the pharmaceuticals. In a pure water matrix, many pharmaceuticals were photocatalytically degraded in as little as five minutes, demonstrating feasibility of municipal treatment scale. However, in the wastewater matrix, full removal was rarely observed. This is consistent with other studies that spiked pharmaceuticals in a wastewater effluent sample (Choi *et al.*, 2014). The slow reaction constants for contaminant removal in wastewater will remain a challenge for the application of photocatalysis treatment, especial in the presence of high levels of organic matter and where a high throughput of water is required.

Chapter 5
Conclusions and Recommendations

The objectives of this research were to explore the use of photocatalysts in water treatment applications. A large barrier in photocatalyst applications is the low efficiency of hydroxyl production. Functionalization of the nanoparticle with a metal was tested to improve photocatalytic efficiency through plasmonic photocatalysis. Photocatalytic tests of pharmaceutical removal are also typically completed in a pure water matrix that is not representative of surface waters or effluents. Photocatalytic removal of 24 different chemicals (mostly pharmaceuticals) was tested using both pure water and wastewater effluent collected from a local water treatment plant (Waterloo). Although photocatalysts (P25) can successfully remove emerging contaminants from water, wastewater still represents a major challenge. Functionalization of nanoparticles can greatly improve the photocatalytic efficiency and hold promise for future treatment applications.

In Chapter 2 it was found that an increased silver content resulted in a significant improvement in the photocatalytic efficiency of zinc oxide nanoparticles. The improvement is attributed to the improved electron-hole separation provided by the metal: metal-oxide junction in plasmonic photocatalysts. While previous studies have used plasmonic photocatalysis, few have considered the optimal ratio of metal: metal-oxide. The study completed in this thesis found significantly increased hydroxyl formation when higher silver ratios were used. Significant improvement over pure zinc oxide nanomaterials consistently began at a mass percentage of 5.06%. A different study found the same pattern of significant improvement to a certain degree of silver loading. This contrasts with another previous study, where an optimal photocatalytic efficiency was found and decreased with increasing molar ratios. The difference in optimal silver loading between that study and one completed in this thesis may be due to different nanoparticle morphology. The hydrothermal synthesis method that used a seed of zinc oxide nanoparticles maintained a sphere like morphology after synthesis to blend with silver. This synthesis method requires only a few steps, making it

promising for large scale synthesis operations. High agglomeration occurred for all molar percentages, meaning it may have had little effect on the efficiencies of hydroxyl formation. Additionally, no discernable change in bandgap occurred for the different silver loadings, indicating that the light adsorption properties of the nanomaterial were unchanged with silver loading.

Chapter 3 tested the photocatalytic removal of pharmaceuticals from both wastewater effluent and a pure (Milli-Q) water matrix. Photocatalysis greatly improved the removal of pharmaceuticals from the Milli-Q water matrix, when compared to just UV light irradiation. However, when applied in wastewater effluent, the photocatalysis became less active. This is likely due to the scavenging of reactive oxygen species and the scavenging of and shielding of UV light caused by the organic compounds, as demonstrated by the high decrease in total organic carbon. This is a clear demonstration of why a large barrier exists between research regarding photocatalysis and commercialization of photocatalytic water treatment systems. UV irradiation had some effect on contaminant removal, but the removal rates were often much lower than with the addition of the photocatalyst. This demonstrates the potential value in adding a photocatalyst to the UV water treatment setup. Additionally, it is also presumed that a contaminant more oppositely charged to the catalyst will have higher electrostatic interaction. The higher interactions should result in an increased photocatalytic removal. The charge of the photocatalyst was positive in the solutions studied and it was found that the charge of the pharmaceutical in solution had some effect on its removal. However, other properties of the pharmaceutical, including solubility may also have a large effect, especially in natural waters containing NOM. The high decrease in photocatalytic efficiency when completed in representative wastewater effluent relative to pure (Milli-Q) water demonstrates the need for laboratory testing to be completed using representative water matrices.

Future research in photocatalytic testing should consider commercialization at the beginning of the experimental design phase. The barriers associated with the marketing of photocatalytic water treatment are still vast but include the need to remove nanomaterials after treatment, low photocatalytic efficiency, and long treatment times required. However, the fast

removal of pharmaceuticals reported in this thesis and the environmental pressures imposed by emerging contaminants on the environment provide high motivation to continue research in photocatalytic water treatment.

Continuation of this research may involve fine-tuning of hydrothermal synthesis methods of plasmonic photocatalysts to continue optimization of efficiency. One must aim for simple synthesis methods for easier commercial production. Removal of the nanomaterials continues to be a challenge, and future researchers may consider the exploration of core-shell magnetic photocatalysts to create photocatalysts that may be removed by applying an electric field to the solution, or immobilization and filtering methods that do not result in a considerable loss in efficiency. The optimally manufactured plasmonic photocatalyst may also be tested in the removal of the emerging contaminants, such as pharmaceuticals, to confirm that the improved hydroxyl formation results in improved contaminant removal. An ideal photocatalytic setup would consider a specific contaminant that must be removed Alternatively, one may group contaminants by physical properties that indicate they may have similar mechanisms for removal. Charge of the contaminant and photocatalyst may be a strong consideration, as demonstrated by the improved degradation rate constants by electrostatic attraction. Alteration in pH may be explored to improve removal or target analytes.

There is also a challenge regarding the degradation byproducts. Some of the intermediates of pharmaceutical degradation are more harmful than the initial contaminant. Enhancement of analysis methods by inclusion of additional degradation intermediates may provide insight into whether the contaminant is fully mineralized, rather than just removed. This consideration may be made for pharmaceuticals as well as other emerging contaminants.

While vast improvements have been made in photocatalytic water treatment over the past forty years of research, there still exists ample opportunities to improve water treatment methods to ensure sustainable water sources. The need for novel treatment approaches will continue to grow as the diversity of contaminants and their risks continue to emerge.

References

Arlos, M. J. *et al.* (2015) 'Distribution of selected antiandrogens and pharmaceuticals in a highly impacted watershed', *Water Research*, 72, pp. 40–50. doi: 10.1016/j.watres.2014.11.008.

Arlos, M. J., Hatat-Fraile, M. M., *et al.* (2016) 'Photocatalytic decomposition of organic micropollutants using immobilized TiO 2 having different isoelectric points', *Water Research*. Elsevier Ltd, 101, pp. 351–361. doi: 10.1016/j.watres.2016.05.073.

Arlos, M. J., Liang, R., *et al.* (2016) 'Photocatalytic decomposition of selected estrogens and their estrogenic activity by UV-LED irradiated TiO2 immobilized on porous titanium sheets via thermal-chemical oxidation', *Journal of Hazardous Materials*. doi: 10.1016/j.jhazmat.2016.07.048.

Arlos, M. J. *et al.* (2017) 'Influence of methanol when used as a water-miscible carrier of pharmaceuticals in TiO2 photocatalytic degradation experiments', *Journal of Environmental Chemical Engineering*. Elsevier, 5(5), pp. 4497–4504. doi: 10.1016/j.jece.2017.08.048.

Arnold, K. E. *et al.* (2014) 'Medicating the environment: Assessing risks of pharmaceuticals to wildlife and ecosystems', *Philosophical Transactions of the Royal Society B: Biological Sciences*, 369(1656). doi: 10.1098/rstb.2013.0569.

Behnajady, M. A. *et al.* (2007) 'Photocatalytic degradation of C.I. Acid Red 27 by immobilized ZnO on glass plates in continuous-mode', *Journal of Hazardous Materials*, 140(1–2), pp. 257–263. doi: 10.1016/j.jhazmat.2006.07.054.

Bensalah, N. *et al.* (2014) 'Synthesis of supported silver nano-spheres on zinc oxide nanorods for visible light photocatalytic applications', *Materials Research Bulletin*, 63, pp. 134–140. doi: 10.1016/j.materresbull.2014.12.001.

Bielak, H. *et al.* (2016) 'Efficiency of UV-Oxidation in removal of pharmaceuticals from waste water samples and toxicological evaluation before and after the oxidative treatment', in Thompson, C., Gillespie, S., and Goslan, E. (eds) *Disinfection By-products in*

Drinking Water. Cambridge: Royal Society of Chemistry, pp. 180–188. doi: 10.1039/9781782622710-00180.

Bisesi, J. H., Bridges, W. and Klaine, S. J. (2014) 'Effects of the antidepressant venlafaxine on fish brain serotonin and predation behavior', *Aquatic Toxicology*, 148, pp. 130–138. doi: 10.1016/j.aquatox.2014.02.015.

Bohren, C. F. and Huffman, D. R. (1998) *Absorption and Scattering of Light by Small Particles*. 1st edn, *John Wiley & Sons, Inc.* 1st edn. Weinheim: Wiley-VCH Verlag GmbH & Co. KGaA. doi: 10.1080/716099663.

Bolton, J. R. *et al.* (2007) 'Figures-of-merit for the technical development and application of advanced oxidation technologies for both electric- and solar-driven systems (IUPAC Technical Report)', *Pure and Applied Chemistry*, 73(4), pp. 627–637. doi: 10.1351/pac200173040627.

Cates, E. L. (2017) 'Photocatalytic water treatment: So where are we going with this?', *Environmental Science and Technology*, 51(2), pp. 757–758. doi: 10.1021/acs.est.6b06035.

Černigoj, U., Kete, M. and Štangar, U. L. (2010) 'Development of a fluorescence-based method for evaluation of self-cleaning properties of photocatalytic layers', *Catalysis Today*, 151(1), pp. 46–52. doi: 10.1016/j.cattod.2010.03.043.

Chen, T. K., Ni, C. H. and Chen, J. N. (2003) 'Nitrification-denitrification of opto-electronic industrial wastewater by anoxic/aerobic process', *Journal of Environmental Science and Health - Part A Toxic/Hazardous Substances and Environmental Engineering*, 38(10), pp. 2157–2167. doi: 10.1081/ESE-120023346.

Chen, X. *et al.* (2016) 'Photocatalytic oxidation of methane over silver decorated zinc oxide nanocatalysts', *Nature Communications*. Nature Publishing Group, 7(12273), pp. 1–8. doi: 10.1038/ncomms12273.

Cheytt, T. *et al.* (2005) '1-Octanol / Water partition coefficients of 5 pharmaceuticals from human medical care: carbamazepine, clofibric acid, diclofenac, ibuprofenm and prophyphenazone', *Water Air and Soil Pollution*, 165(1–4), pp. 3–11. doi: 10.1007/s11270-005-3539-9.

Choi, J. *et al.* (2014) 'Heterogeneous photocatalytic treatment of pharmaceutical micropollutants: Effects of wastewater effluent matrix and catalyst modifications', *Applied Catalysis B: Environmental*. Elsevier B.V., 147(October 2017), pp. 8–16. doi: 10.1016/j.apcatb.2013.08.032.

Chong, M. N. *et al.* (2010) 'Recent developments in photocatalytic water treatment technology: A review', *Water Research*, 44(10), pp. 2997–3027. doi: 10.1016/j.watres.2010.02.039.

Christopher, P., Xin, H. and Linic, S. (2011) 'Visible-light-enhanced catalytic oxidation reactions on plasmonic silver nanostructures', *Nature Chemistry*, 3, pp. 467–472. doi: 10.1038/nchem.1032.

Cooper Langford (2004) *Applications and barriers to innovation in use of advanced oxidation processes (AOP) in management of wastewater*, *Canadian Water Network*. Available at: http://cwn-rce.ca/project/applications-and-barriers-to-innovation-in-use-of-advanced-oxidation-processes-aop-in-management-of-wastewater/.

Damodar, R. A., You, S. J. and Chou, H. H. (2009) 'Study the self cleaning, antibacterial and photocatalytic properties of TiO2 entrapped PVDF membranes', *Journal of Hazardous Materials*, 172(2–3), pp. 1321–1328. doi: 10.1016/j.jhazmat.2009.07.139.

Djurišić, A. B., Leung, Y. H. and Ng, A. M. C. (2014) 'Strategies for improving the efficiency of semiconductor metal oxide photocatalysis', *Materials Horizons*, 1(4), pp. 400–410. doi: 10.1039/c4mh00031e.

Drosos, M., Ren, M. and Frimmel, F. H. (2015) 'The effect of NOM to TiO2: Interactions and photocatalytic behavior', *Applied Catalysis B: Environmental*, 165, pp. 328–334. doi: 10.1016/j.apcatb.2014.10.017.

Eggins, B. R., Palmer, F. L. and Byrne, J. A. (1997) 'Photocatalytic treatment of humic substances in drinking water', *Water Research*, 31(5), pp. 1223–1226.

Eskandarian, M. R. *et al.* (2016) 'Effect of UV-LED wavelengths on direct photolytic and TiO2 photocatalytic degradation of emerging contaminants in water', *Chemical Engineering Journal*, 300, pp. 414–422. doi: 10.1016/j.cej.2016.05.049.

Fernández-Nieves, A., de las Nieves, F. J. and Richter, C. (1998) 'Point of zero charge estimation for a TiO2/water interface', in Koper, G. J. M. et al. (eds) *Trends in Colloid and Interface Science XII*. Heidelberg: Steinkopff, pp. 21–24.

Foote, C. S. *et al.* (1996) *Active Oxygen in Chemistry*. 1st edn. Dordrecht: Springer Science+Business Media Dordrecht. doi: 10.1007/978-94-007-0874-7.

Friedmann, D., Mendive, C. and Bahnemann, D. (2010) 'TiO2 for water treatment: Parameters affecting the kinetics and mechanisms of photocatalysis', *Applied Catalysis B: Environmental*. Elsevier B.V., 99(3–4), pp. 398–406. doi: 10.1016/j.apcatb.2010.05.014.

Fujishima, A. and Honda, K. (1972) 'Electrochemical photolysis of water at a semiconductor electrode', *Nature*, 238, pp. 37–38. doi: 10.1038/238037a0.

Government of Canada (2017) *Municipal wastewater treatment*. Available at: https://www.canada.ca/en/environment-climate-change/services/environmental-indicators/municipal-wastewater-treatment.html (Accessed: 27 May 2019).

van Grieken, R. *et al.* (2009) 'Photocatalytic inactivation of bacteria in water using suspended and immobilized silver-TiO2', *Applied Catalysis B: Environmental*, 93(1–2), pp. 112–118. doi: 10.1016/j.apcatb.2009.09.019.

Hashimoto, K., Irie, H. and Fujishima, A. (2005) 'TiO 2 photocatalysis: A historical overview and future prospects', *Japanese Journal of Applied Physics, Part 1: Regular Papers and Short Notes and Review Papers*, 44(12), pp. 8269–8285. doi: 10.1143/JJAP.44.8269.

He, L. *et al.* (2010) 'Magnetically recoverable core-shell nanocomposites with enhanced photocatalytic activity', *Chemistry - A European Journal*, 16(21), pp. 6243–6250. doi: 10.1002/chem.200903516.

Held, P. (2015) *An Introduction to Reactive Oxygen Species - Measurement of ROS in Cells*, *BioTek White Paper*. Available at: https://www.biotek.com/resources/white-papers/an-introduction-to-reactive-oxygen-species-measurement-of-ros-in-cells/.

Herrmann, J. M. (1999) 'Heterogeneous photocatalysis: Fundamentals and applications to the removal of various types of aqueous pollutants', *Catalysis Today*, 53(1), pp. 115–129. doi: 10.1016/S0920-5861(99)00107-8.

Hicks, K. A. *et al.* (2017) 'Reduction of Intersex in a Wild Fish Population in Response to Major Municipal Wastewater Treatment Plant Upgrades', *Environmental Science and Technology*, 51(3), pp. 1811–1819. doi: 10.1021/acs.est.6b05370.

Hofstadler, K. *et al.* (1994) 'New reactor design for photocatalytic wastewater treatment with TiO2 immobilized on fused-silica glass fibers: photomineralization of 4-chlorophenol', *Environmental Science and Technology*, 28(4), pp. 670–674. doi: 10.1021/es00053a021.

Jaciw-Zurakowsky, I. *et al.* (2019) 'Advanced Oxidation Processes Using Catalytic Nanomaterials for Air and Water Remediation', in *Nanomaterials in air and water remediations: Recent developments and future scope*. 1st edn. Elsevier.

Jiang, D. *et al.* (2014) 'Distinguishing localized surface plasmon resonance and schottky junction of Au-Cu2O composites by their molecular spacer dependence', *ACS Applied Materials and Interfaces*, 6(14), pp. 10958–10962. doi: 10.1021/am5023978.

Jones, O. A. H., Voulvoulis, N. and Lester, J. N. (2005) 'Human pharmaceuticals in wastewater treatment processes', *Critical Reviews in Environmental Science and Technology*, 35(4), pp. 401–427. doi: 10.1080/10643380590956966.

Jones, O. A., Lester, J. N. and Voulvoulis, N. (2005) 'Pharmaceuticals: A threat to drinking water?', *Trends in Biotechnology*, 23(4), pp. 163–167. doi: 10.1016/j.tibtech.2005.02.001.

Kamat, P. V. and Meisel, D. (2002) 'Nanoparticles in advanced oxidation processes', *Current Opinion in Colloid and Interface Science*, 7(5–6), pp. 282–287. doi: 10.1016/S1359-0294(02)00069-9.

Kanakaraju, D., Glass, B. D. and Oelgemo, M. (2014) 'Titanium dioxide photocatalysis for pharmaceutical wastewater treatment', *Environmental Chemistry Letters*, 12(1), pp. 27–47. doi: 10.1007/s10311-013-0428-0.

Kidd, K. A. *et al.* (2007) 'Collapse of a fish population after exposure to a synthetic estrogen', *Proceedings of the National Academy of Sciences of the United States of America*, 104(21), pp. 8897–8901. doi: 10.1073/pnas.0609568104.

Klavarioti, M., Mantzavinos, D. and Kassinos, D. (2009) 'Removal of residual pharmaceuticals from aqueous systems by advanced oxidation processes', *Environment International*. Elsevier Ltd, 35(2), pp. 402–417. doi: 10.1016/j.envint.2008.07.009.

Kotak, B. G. and Zurawell, R. W. (2007) 'Cyanobacterial toxins in Canadian freshwaters: A review', *Lake and Reservoir Management*, 23(2), pp. 109–122. doi: 10.1080/07438140709353915.

Kumar, A. (2017) 'A Review on the Factors Affecting the Photocatalytic Degradation of Hazardous Materials', *Material Science & Engineering International Journal*, 1(3), pp. 1–10. doi: 10.15406/mseij.2017.01.00018.

Li, G. *et al.* (2010) 'Effect of the agglomeration of TiO2 nanoparticles on their photocatalytic performance in the aqueous phase', *Journal of Colloid and Interface Science*, 348(2), pp. 342–347. doi: 10.1016/j.jcis.2010.04.045.

Linic, S., Christopher, P. and Ingram, D. B. (2011) 'Plasmonic-metal nanostructures for efficient conversion of solar to chemical energy', *Nature Materials*, 10, pp. 911–921. doi: 10.1038/nmat3151.

López, R. and Gómez, R. (2012) 'Band-gap energy estimation from diffuse reflectance measurements on sol-gel and commercial TiO 2: A comparative study', *Journal of Sol-Gel Science and Technology*, 61(1), pp. 1–7. doi: 10.1007/s10971-011-2582-9.

Mclaren, A. *et al.* (2009) 'Shape and Size Effect of ZnO nanocrystals on Photocatalytic Activity', *Journal of American Chemical Society*, 131, pp. 12540–12541. Available at: https://pubs.acs.org/doi/suppl/10.1021/ja9052703/suppl_file/ja9052703_si_001.pdf.

Mirzaei, A. *et al.* (2016) 'Removal of pharmaceuticals and endocrine disrupting compounds from water by zinc oxide-based photocatalytic degradation: A review', *Sustainable Cities and Society*. Elsevier B.V., 27, pp. 407–418. doi: 10.1016/j.scs.2016.08.004.

Mozzanega, H., Herrmann, J. M. and Pichat, P. (1979) 'Ammonia oxidation over UV-irradiated titanium dioxide at room temperature', *The Journal of Physical Chemistry*, 83(17),

pp. 2251–2255. doi: 10.1021/j100480a014.

Mubeen, S. *et al.* (2011) 'Plasmonic photosensitization of a wide band gap semiconductor: Converting plasmons to charge carriers', *Nano Letters*, 11(12), pp. 5548–5552. doi: 10.1021/nl203457v.

Nathonson, J. A. and Ambulkar, A. (2018) *Wastewater Treatment, Enclyclopaedia Britannica*. Encyclopædia Britannica, inc. Available at: Encyclopædia Britannica, inc. (Accessed: 27 May 2019).

Parrott, J. L. and Blunt, B. R. (2005) 'Life-cycle exposure of fathead minnows (Pimephales promelas) to an ethinylestradiol concentration below 1 ng/L reduces egg fertilization success and demasculinizes males', *Environmental Toxicology*, 20(2), pp. 131–141. doi: 10.1002/tox.20087.

Pavasupree, S. *et al.* (2006) 'Synthesis, characterization, photocatalytic activity and dye-sensitized solar cell performance of nanorods/nanoparticles TiO2 with mesoporous structure', *Journal of Photochemistry and Photobiology A: Chemistry*, 184(1–2), pp. 163–169. doi: 10.1016/j.jphotochem.2006.04.010.

Pekakis, P. A., Xekoukoulotakis, N. P. and Mantzavinos, D. (2006) 'Treatment of textile dyehouse wastewater by TiO2 photocatalysis', *Water Research*, 40(6), pp. 1276–1286. doi: 10.1016/j.watres.2006.01.019.

Pelaez, M. *et al.* (2012) 'A review on the visible light active titanium dioxide photocatalysts for environmental applications', *Applied Catalysis B: Environmental*, 125, pp. 331–349. doi: 10.1016/j.apcatb.2012.05.036.

Peral, J., Domènech, X. and Ollis, D. F. (1997) 'Heterogeneous photocatalysis for purification, decontamination and deodorization of air', *Journal of Chemical Technology and Biotechnology*, 70(2), pp. 117–140. doi: 10.1002/(SICI)1097-4660(199710)70:2<117::AID-JCTB746>3.0.CO;2-F.

Prairie, M. R. *et al.* (1993) 'An Investigation of TiO2 Photocatalysis for the Treatment of Water Contaminated with Metals and Organic Chemicals', *Environmental Science and Technology*, 27(9), pp. 1776–1782. doi: 10.1021/es00046a003.

Revised Statute of Canada (1985) *Food and Drugs Act*. Government of Canada. Available at: https://laws-lois.justice.gc.ca/eng/acts/F-27/page-1.html.

Romeiro, A. *et al.* (2018) 'Titanium Dioxide Nanoparticle Photocatalysed Degradation of Ibuprofen and Naproxen in Water : Competing Hydroxyl Radical Attack and Oxidative Decarboxylation by Semiconductor Holes', *ChemistrySelect*, 3(39), pp. 10915–10924. doi: 10.1002/slct.201801953.

Rusevova, K., Kopinke, F. and Georgi, A. (2012) 'Nano-sized magnetic iron oxides as catalysts for heterogeneous Fenton-like reactions — Influence of Fe (II)/ Fe (III) ratio on catalytic performance', *Journal of Hazardous Materials*. Elsevier B.V., 241–242, pp. 433–440. doi: 10.1016/j.jhazmat.2012.09.068.

Santoke, H. and Cooper, W. J. (2017) 'Environmental photochemical fate of selected pharmaceutical compounds in natural and reconstituted Suwannee River water: Role of reactive species in indirect photolysis', *Science of the Total Environment*. Elsevier B.V., 580, pp. 626–631. doi: 10.1016/j.scitotenv.2016.12.008.

Sayes, C. M. *et al.* (2009) 'The relationship between pH and zeta potential of similar to 30 nm metal oxide nanoparticle suspensions relevant to in vitro toxicological evaluations', *Nanotoxicology*. doi: Doi 10.3109/17435390903276941.

Shafaei, A., Nikazar, M. and Arami, M. (2010) 'Photocatalytic degradation of terephthalic acid using titania and zinc oxide photocatalysts : Comparative study', *Desalination*. Elsevier B.V., 252(1–3), pp. 8–16. doi: 10.1016/j.desal.2009.11.008.

Sponza, D. T. and Güney, G. (2017) 'Photodegradation of some brominated and phenolic micropollutants in raw hospital wastewater with CeO2 and TiO2 nanoparticles', *Water Science and Technology*, 76(10), pp. 2603–2622. doi: 10.2166/wst.2017.433.

Srikant, V. and Clarke, D. R. (1998) 'On the optical band gap of zinc oxide', *Journal of Applied Physics*, 83(10), pp. 5447–5451. doi: 10.1063/1.367375.

Ternes, T. A., Joss, A. and Siegrist, H. (2004) 'Scrutinizing Pharmaceuticals and Personal Care Products in Wastewater Treatment', *Environmental Science and Pollution Research*, pp. 393A-399A.

Tetreault, G. R. *et al.* (2011) 'Intersex and reproductive impairment of wild fish exposed to multiple municipal wastewater discharges', *Aquatic Toxicology*. Elsevier B.V., 104(3–4), pp. 278–290. doi: 10.1016/j.aquatox.2011.05.008.

Thomann, I. *et al.* (2011) 'Plasmon enhanced solar-to-fuel energy conversion', *Nano Letters*, 11(8), pp. 3440–3446. doi: 10.1021/nl201908s.

Tibbetts, J. (1995) 'Whats in the water: The disinfectant dilemma', *Environmental Health Perspectives*, 103(1), pp. 30–34.

Tokode, O. *et al.* (2016) 'Controlled periodic illumination in semiconductor photocatalysis', *Journal of Photochemistry and Photobiology A: Chemistry*. Elsevier B.V., 319–320, pp. 96–106. doi: 10.1016/j.jphotochem.2015.12.002.

Turchi, C. S. and Ollis, D. F. (1990) 'Photocatalytic degradation of organic water contaminants: Mechanisms involving hydroxyl radical attack', *Journal of Catalysis*, 122(1), pp. 178–192. doi: 10.1016/0021-9517(90)90269-P.

Tušar, N. N. *et al.* (2011) 'Manganese Functionalized Silicate Nanoparticles as a Fenton-Type Catalyst for Water Purifi cation by Advanced Oxidation Processes (AOP)', *Advanced Functional Materials*, 22(4), pp. 820–826. doi: 10.1002/adfm.201102361.

Wang, H. *et al.* (2014) 'Semiconductor heterojunction photocatalysts: Design, construction, and photocatalytic performances', *Chemical Society Reviews*, 43(15), pp. 5234–5244. doi: 10.1039/c4cs00126e.

Wang, Z., Liu, J. and Chen, W. (2012) 'Plasmonic Ag/AgBr nanohybrid: Synergistic effect of SPR with photographic sensitivity for enhanced photocatalytic activity and stability', *Dalton Transactions*, 41(16), pp. 4866–4870. doi: 10.1039/c2dt12089e.

Yildirim, Ö. A., Unalan, H. E. and Durucan, C. (2013) 'Highly efficient room temperature synthesis of silver-doped zinc oxide (ZnO: Ag) nanoparticles: Structural, optical, and photocatalytic properties', *Journal of the American Ceramic Society*, 96(3), pp. 766–773. doi: 10.1111/jace.12218.

Zepp, R. G., Baughman, G. L. and Schlotzhauer, P. F. (1981) 'Comparison of photochemical behavior of various humic substances in water: I. Sunlight induced reactions of

aquatic pollutants photosensitized by humic substances', *Chemosphere*, 10(1), pp. 109–117. doi: 10.1016/0045-6535(81)90174-0.

Zhang, X. *et al.* (2013) 'Plasmonic photocatalysis', *Reports on Progress in Physics*, 76(4). doi: 10.1088/0034-4885/76/4/046401.

Zhang, Y. and Mu, J. (2007) 'One-pot synthesis, photoluminescence, and photocatalysis of Ag/ZnO composites', *Journal of Colloid and Interface Science*. Academic Press, 309(2), pp. 478–484. doi: 10.1016/J.JCIS.2007.01.011.

Zhdanov, V. P., Hägglund, C. and Kasemo, B. (2005) 'Relaxation of plasmons in nm-sized metal particles located on or embedded in an amorphous semiconductor', *Surface Science*, 599(1–3), pp. L372–L375. doi: 10.1016/j.susc.2005.10.001.

Appendix A: Standard Operating Procedures

This appendix outlines the standard operating procedures that were used for the work completed in this thesis. The procedures include those for Chapter 2 including photocatalytic activity (the TPA test), the synthesis methods used for the plasmonic photocatalysts, and the measurement of the bandgap. The remainder of this section refer to the protocols used in Chapter 3, including the collection of wastewaters, the pharmaceutical degradation test and the solid phase extraction of the pharmaceuticals.

A1: TPA to HTPA Conversion Protocol

1. Make 1L of TPA Solution: 0.0831 g TPA (sigma) dissolved in 6 mL of 1 M NaOH in a volumetric flask, then filled to the 1 L mark with Milli-Q water. Sonicate 10 minutes.
2. Prepare beaker solutions accordingly: add 30mg of powder to each beaker, use thinnest beakers available for better sonication
3. Sonicate Beaker powdered solutions (without stir bar) for 5 minutes
4. Calibrate the pH meter and measure pH
5. Measure the Power output of each individual light
6. Program: PM100/200 Utility
7. Press Meas Config>Zero Adjust>Cover Sensor
8. Press Log Config> Select Log File: Save to folder Ivana as a .txt with the default name plus '_2_Uvx' (2 is for setup 2, x is light one two or three)
9. Turn on each lamp individually, place sensor in middle of light and press 'Start Log'
10. Once complete (dates will appear instead of sample #s along bottom of display plot) press export data and select the log file you made, press okay
11. Switch UV lights, press reset/clear, then 'Start Log'
12. Once complete, 'export data' and save with same name as UV1, just change UV#.
13. Repeat for UV 3
14. With beakers under foil, stir samples for 60 minutes in the dark
15. Turn on the UV light at T=0.
16. Take 1mL samples of each beaker into micro centrifuge tubes at T= -60, 0, 1, 5, 10, 20, 40, 60, 90, 120, 180, 240, 300 min
17. Can cover samples in foil to be safe

18. Make standards of HTPA from 60 uM stock solution for the standard curve. Make a serial dilution.

Table A 1: Serial dilution of HTPA calibration curve.

C (uM)	Volume of the Higher Concentration (mL)	Volume of Water/ solution (mL)
20	0.333	0.667
10	0.5	0.5
6	0.6	0.4
2	0.333	0.667
1	0.5	0.5
0.5	0.5	0.5
0.25	0.5	0.5
0.1	0.4	0.6

19. For the blank, mix 2uL of 1 M NaOH in 998 uL of Water/ solution
20. Centrifuge the samples at 1600g and 24 degrees Celsius (default temperature) for 10 minutes to remove the TiO_2, P25, and other particles
21. Add 300 uL of each samples and the stock to a black plate, record the chosen layout
22. Use the plate reader at the following settings:
    a. Fluorescence Spectrum
    b. Excitation: 315 nm
    c. Range: 350 nm- 55 0nm
    d. Step Size: 1
    e. No cutoff
    f. Shake 5 Seconds before 1st read
    g. 6 flashes per second, auto gain
23. Measure final pH of each beaker

A2: Hydrothermal Synthesis

1. Add 1 g P25 into 125 mL acid digester containing 60 mL of Acid Digester
2. For the acid digester, measure out 60mL of Milli-Q and add the appropriate amount of Silver Nitrate and HMTA
    a. AgNO3 (1 mM – 10.2 mg) and HMTA (2 mM – 16.8 mg).
3. Heat acid digester to 100°C for 4h in a pressurized vessel.
4. Ag ions in solution were removed by washing with ultrapure water, centrifuging samples, and decanting the supernatant
    a. First from the oven, remove the contents into a 400 ml beaker, rinsing the containers with Milli-Q and placing in the beaker until there are no traces left (2-3 rinses with squirt bottle).
    b. Next leave that beaker to stir for about 5 minutes
    c. Aliquot about 25 mL of the solution into eight separate 50ml conical tubes. Continue adding to each tube bit by bit until the beaker is empty. Rinse the beaker and add to 50 mL conical tubes
    d. My centrifuge process is 3500 rpm. Complete three cycles. The first Is 30 minutes, followed by 20 then 10 minutes.
5. In between cycles, dump the supernatant into the waste, refill the tubes with Milli-Q and resuspend the pellet (vortex in at 3000 for 15 seconds does most of the trick, add some manual shaking to complete if necessary)
6. After the last cycle, dump out supernatant and resuspend only in about 25 ml Milli-Q. The dump all tubes into a single beaker and rinse tubes with Milli-Q also dumping into beaker. We then perform suction filtration, rinsing with ethanol three times. Ensure you get all of the particles from the beaker.
7. After Suction filtration, Dry the Ag solution (can leave on filter paper at 80°C for 8 h (or overnight).
8. Weigh and label a glass scintillation vial
9. Once particles are dried overnight, scrape them into the labelled scintillation vial
10. Mass yield= Mass With Particles- Mass Empty Vial
11. Record the mass in your lab book

A3: UV- Diffuse Reflectance Spectroscopy

Samples are prepared by sonicating a small about (about 2 mg) in ethanol. The samples were then filtered through 2 µm filter paper. The filter paper was dried in the oven overnight.

The DRS spectra was collected using a Shimadzu UV-2501PC UV-Visible-NIR spectrophotometer equipped with an integrating sphere accessory, using $N_{2(g)}$ as the reference.

The bandgap was calculated using the following equations (López and Gómez, 2012): R is the measured reflectance, and $\alpha(hv)$ is proportional to the extinction coefficient. Plotting $\alpha(hv)$ provides a linear change. The bandgap E_g is calculated using the slope (m) and the intercept (b) of the line of best fit.

$$F(R) = \frac{(1-R)^2}{2R}$$

$$\alpha(hv) = (hv * F(R))^{0.5}$$

$$E_g = \frac{1239.84 \times m}{-b}$$

A4: Collection of Wastewater from Waterloo Wastewater Treatment Plant

1. Talk to Technician, book the truck and have someone who has sampled there before attend with you
2. Ensure the truck has the required equipment
    a. Generator
    b. pump
    c. gas for generator
    d. pickaxes
    e. hose
    f. hard hats, steel-toed boots, safety vests
    g. gloves

h. cooler with ice
i. 500 mL amber bottles
j. Maxxam bottles (if not in storage we will stop by Maxxam in the morning and pick some up)
k. Markers

At the plant, you must be wearing steel toes, hard hats, and safety vests

3. Sign in at the desk
4. Drive to the manhole cover. Use the pick axe to open it up.
5. Ensure the pump is well tied off and lower it into the manhole. Turn the pump on and collect the samples into the required 1 L amber glass bottles. You may also have containers from Maxxaam that you need to fill. Ensure you follow those instructions closely.
6. Keep the samples on ice.
7. Sign out at the treatment plant office before leaving the site.
8. You may drive straight to Maxxam to drop off their samples, then return to the University.
9. Store the samples in the fridge until needed. If you are not preserving them, they should be used within 48 hours of sampling.
10. Clean up the truck

A5: Pharmaceutical Degradation Test

Reactor Settings: UV-LED; 2 ug/L suspension; -60 min dark, 0, 5, 10, 20, 40, 60, 90, 120 min UV-LED

1. Prepare spike solution and apparatus ahead of time.
    a. Ensure availability of 10 mg/L regular standard stock solution.
    b. Ensure availability of 100 µg/L deuterated standard stock solution.
    c. Ensure availability of reconstitution solution.
2. Check UV-LEDs and ensure they are working properly.
3. Pipette 60 uL of stock solution in 3 beakers
4. Turn on laminar flow hood and place the beakers in the fume hood. Wait until solution dries.
5. Meanwhile, measure three 30 mg of designated TiO_2 powder in a paper weighing boat.
6. If the stock solution is dry, fill the beakers with either 300mL of Milli-Q or Wastewater Effluent (filtered). Place the beakers on the stir plate. Add P25. Stir high for 5 min.
7. Take the first set of samples by pipetting 4.5 mL into labelled test tubes (-60 min dark in this case). Set timer for 60 min.
8. Place samples in test tube racks covered with aluminum foil in the glass fridge (4^oC).
9. Take the 2^{nd} set of samples at time=0 min and turn on UV-LED lamps.
10. Take the next set of samples at the following time intervals:
    a. -60, 0, 5, 10, 20, 40, 60, 90, 120
11. Meanwhile, centrifuge the samples and transfer 4 mL into another set of test tubes.
12. At time = 60 min, prepare the MS1, MS2, and blank. Here are the components of each:
    a. MS1 & MS2 – 4 mL Milli-Q water, add 32 µL of 100 µg/L regular standard and 32 µL of 100 µg/L deuterated standard.
    b. Blank – just 4 mL Milli-Q

13. Once all the sample sets are complete, spike new 4mL aliquots with 32 µL of 100 µg/L standard.
14. Prepare for SPE. See different SOP for SPE.

A6: Solid Phase Extraction of Pharmaceuticals

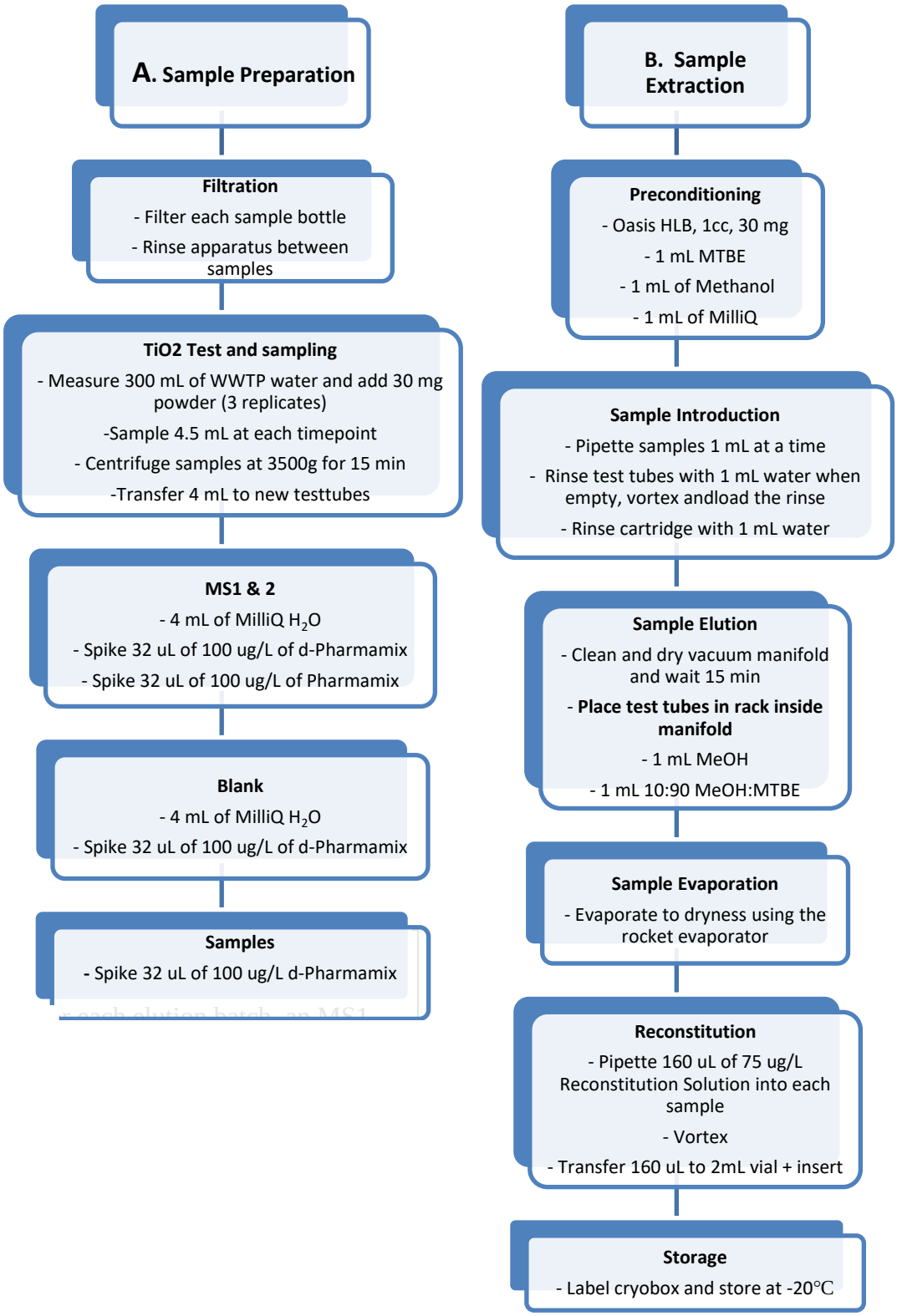

Appendix B: Additional Characterization of Ag-ZnO Particles

B1: SEM Images and XPS Data

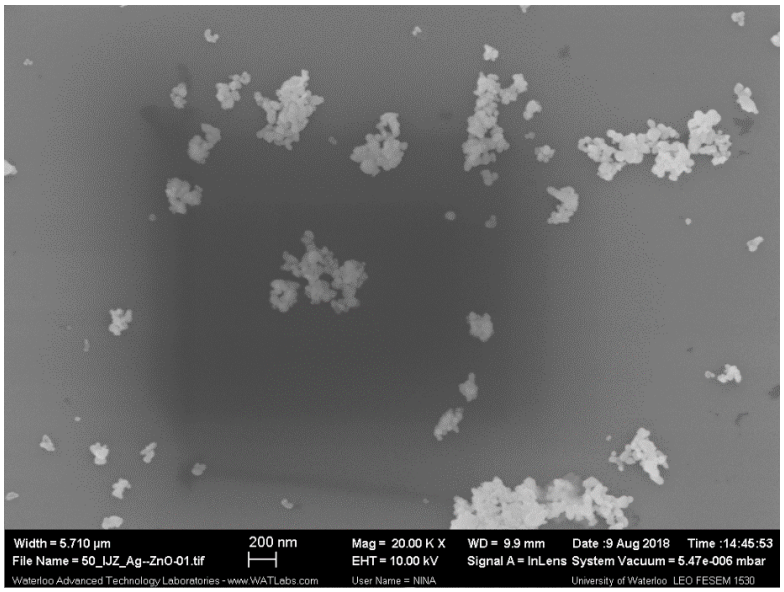

Figure B 1: SEM image of a 50 molar percent loading of silver.

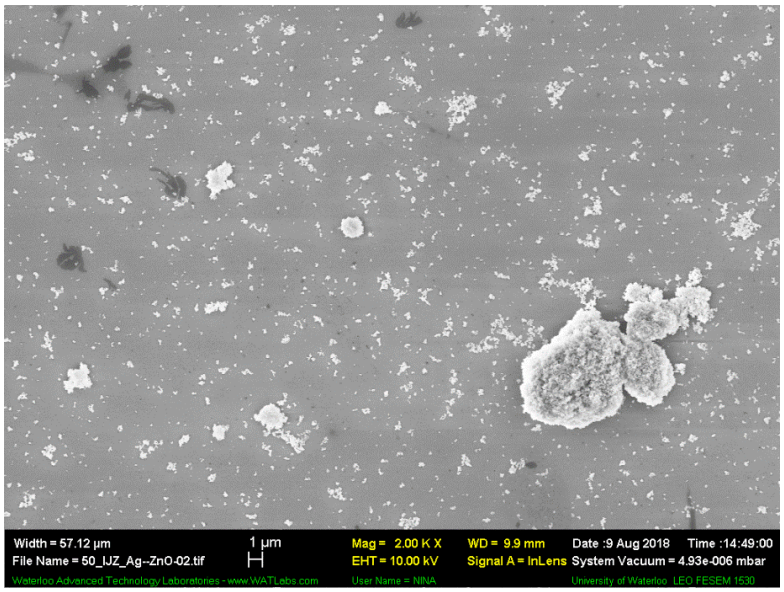

Figure B 2: SEM image of 50 molar percentage silver loading at a lower magnification (2000x).

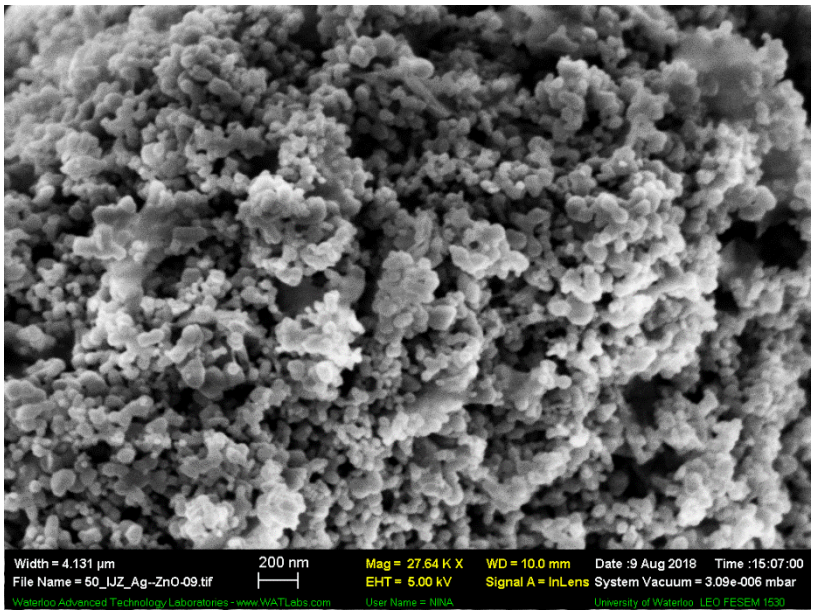

Figure B 3: SEM image of agglomerate of 50 molar % silver loading at a high magnification.

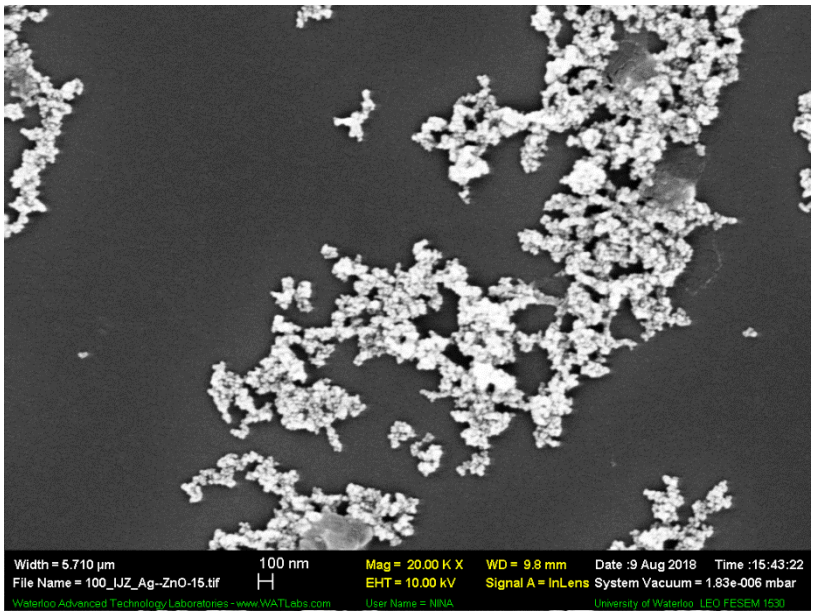

Figure B 4: SEM image of 100 molar percent silver loading.

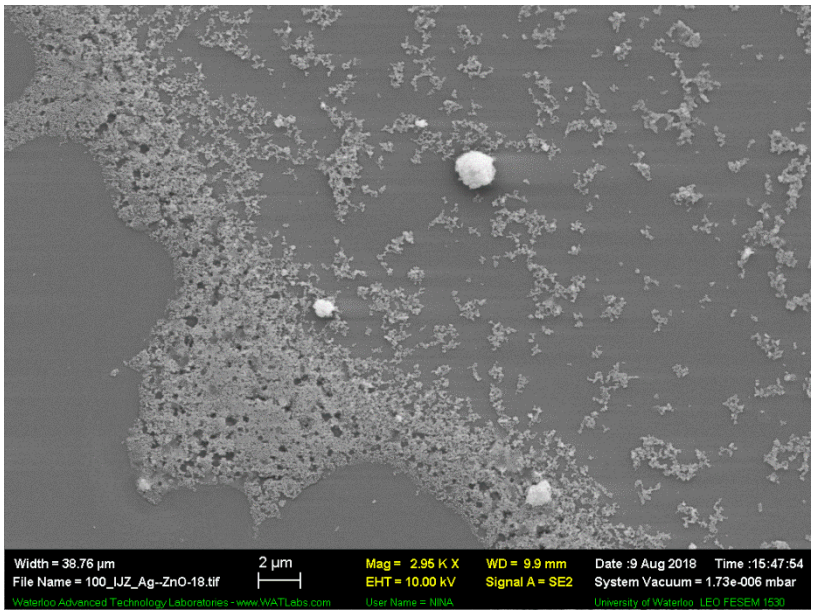

Figure B 5: SEM image of 100 molar percent silver loading at low magnification.

Table B 1: The XPS data of the 50 molar percentage Ag-ZnO nanoparticles. No silver was detected.

Element	Line Type	Apparent Concentration	k Ratio	Wt.%	Wt.% Sigma	Standard Label	Factory Standard
O	K series	0.04	0.00014	18.36	1.29	SiO2	Yes
Si	K series	0.00	0.00002	2.24	0.65	SiO2	Yes
Zn	L series	0.07	0.00073	79.41	1.39	Zn	Yes
Total:				100.00			

Table B 2: XPS for a 100 molar % Ag-ZnO nanoparticle. Even with a search for Ag, none was detected.

Element	Line Type	Apparent Concentration	k Ratio	Wt.%	Wt.% Sigma	Standard Label	Factory Standard
O	K series	0.18	0.00059	17.46	0.59	SiO2	Yes
Si	K series	0.00	0.00003	0.95	0.27	SiO2	Yes
Zn	L series	0.34	0.00342	81.59	0.63	Zn	Yes
Ag	L series	0.00	0.00000	0.00	0.82	Ag	Yes

B3: DRS Data

The following data from the line of best fit is tabulated below, with the calculated bandgap. A linear regression found no significant change in bandgap.

Table B 3: Diffuse Reflectance Spectroscopy lines of best fit and calculated adsorption bandgap.

Molar Percentage	Slope	Intercept	Bandgap	R^2
1	9.36	-30.77	377.35	0.96
3	11.57	-37.76	379.81	0.93
5	13.63	-43.78	385.99	0.93
10	12.43	-40.56	379.94	0.93
15	11.06	-36.30	377.81	0.93
25	11.44	-37.26	380.49	0.93
50	13.28	-43.37	379.70	0.94
100	12.81	-41.77	380.23	0.92
14000	13.53	-44.01	381.03	0.93
42000	14.54	-47.29	381.12	0.93
70000	17.38	-56.71	380.07	0.92

Molar Percentage	Slope	Intercept	Bandgap	R^2
140000	16.92	-55.33	379.21	0.92
210000	13.77	-44.86	380.46	0.93
350000	17.78	-58.25	378.46	0.94
700000	6.65	-20.90	394.23	0.88
1050000	17.08	-55.72	380.03	0.86
1400000	36.05	-121.33	368.41	0.99
		Average:	380.26	0.93

B4: Failure of pseudo- first order TPA conversion model

Typically, the conversion of HTPA is modelled using a pseudo-first order reaction kinetics model, Equation B1. This reaction model was appropriate for low silver concentrations (Figure B6) but failed to properly represent the conversion experienced at high silver ratios (Figure B7). It is estimated that at a high silver ratio, the rate of degradation becomes dominant. At this stage the HTPA is further degraded into different by-products, which were not identified by our tests.

$$[\boldsymbol{HTPA}] = \frac{\boldsymbol{k_1}}{\boldsymbol{k_2}}(\mathbf{1} - \boldsymbol{e}^{-\boldsymbol{k_2}\cdot\boldsymbol{t}})$$ **Equation 2-6** (Černigoj, Kete and Štangar, 2010)

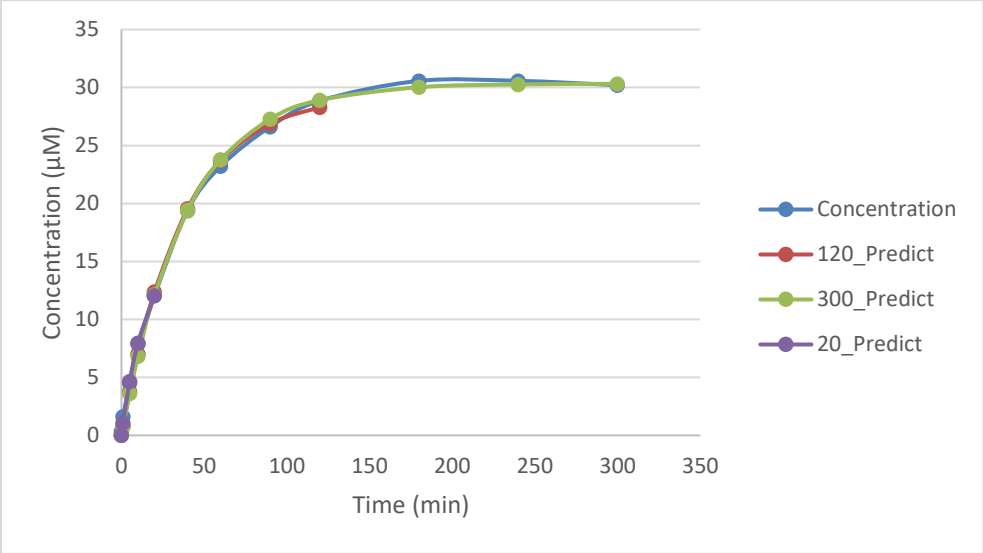

Figure B 6: The conversion of TPA into 2-HTPA by 0.0018 wt.% AgZnO photocatalyst over time. The curve of fit normally used for TPA tests succeeds here, even when the model is fit to 300 minutes.

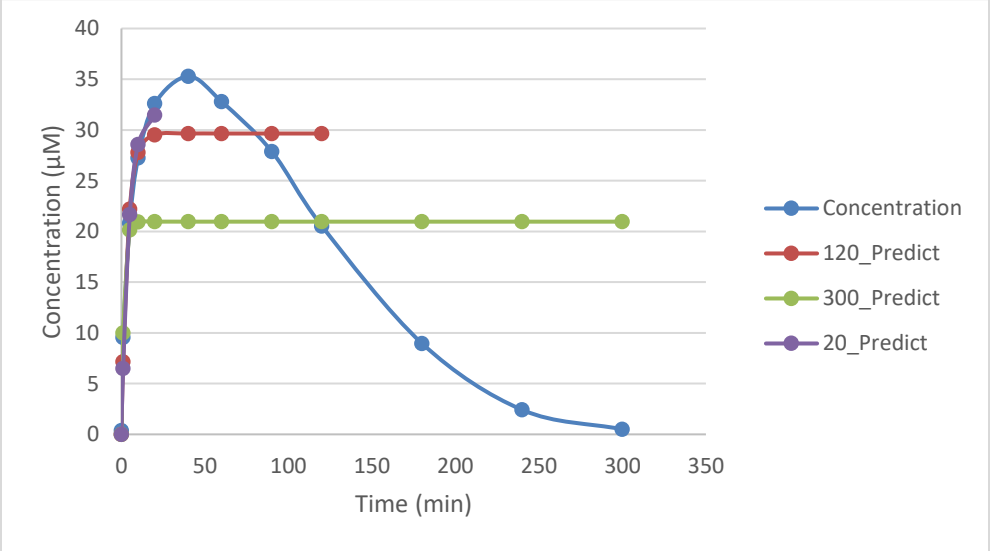

Figure B 7: The conversion of TPA into 2-HTPA over time using a 10.13 wt.% AgZnO composite. The pseudo-first order reaction rate model fails here. There is a clear formation of TPA, which proceeds to degrade after 60 min.

Appendix C: Pharmaceutical Data

C1: Degradation Plots

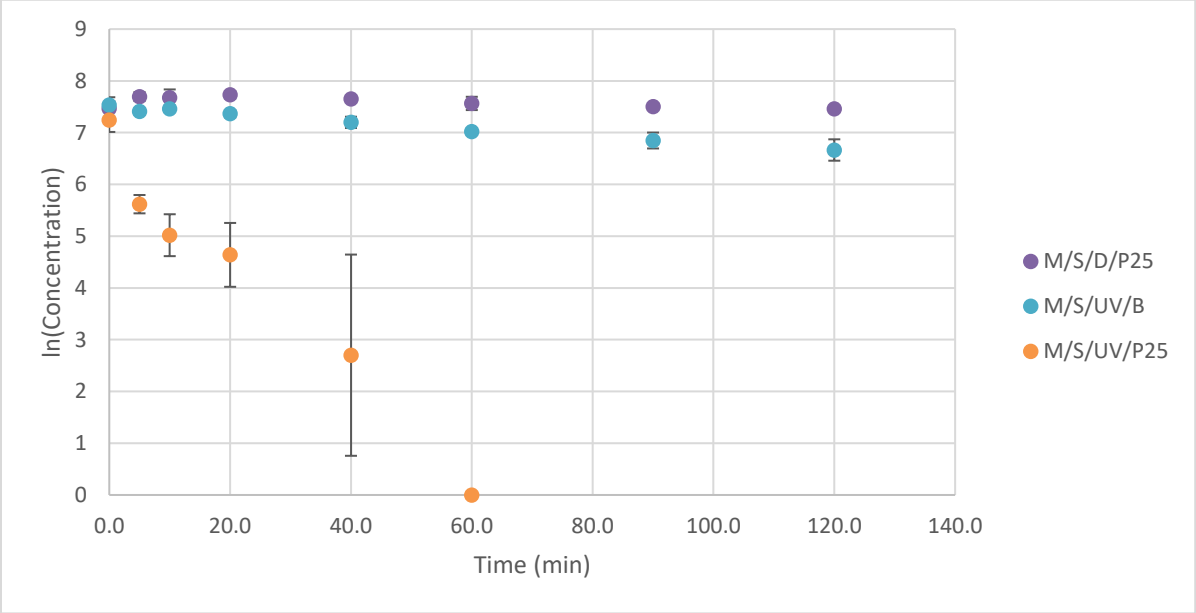

Figure C 1: Degradation of acetaminophen in Milli-Q.

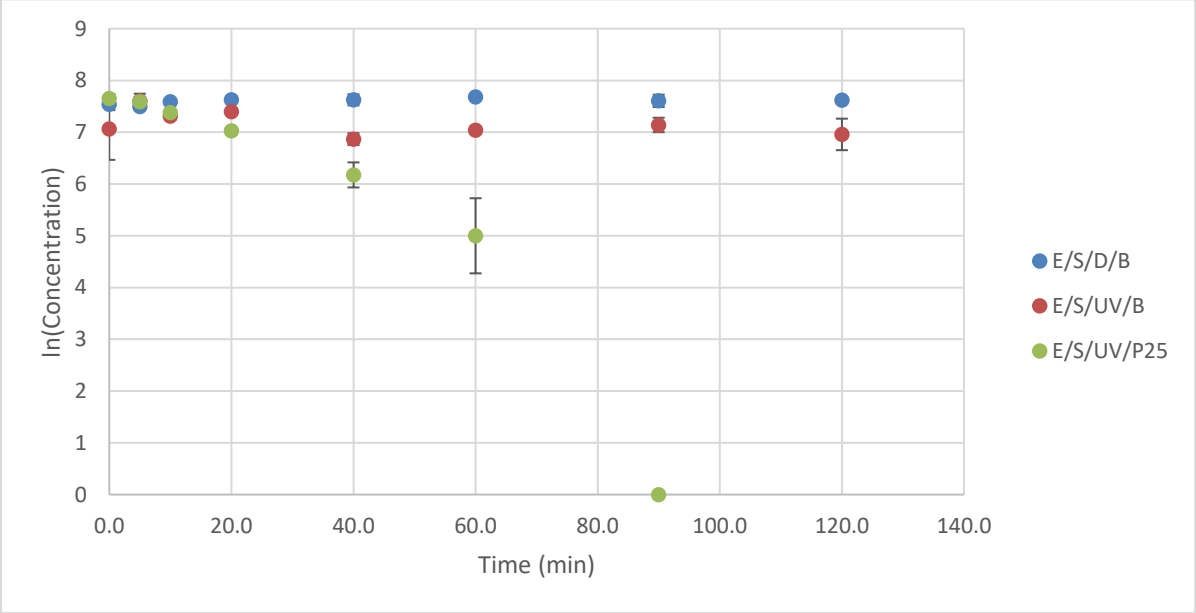

Figure C 2: Degradation of acetaminophen in wastewater effluent.

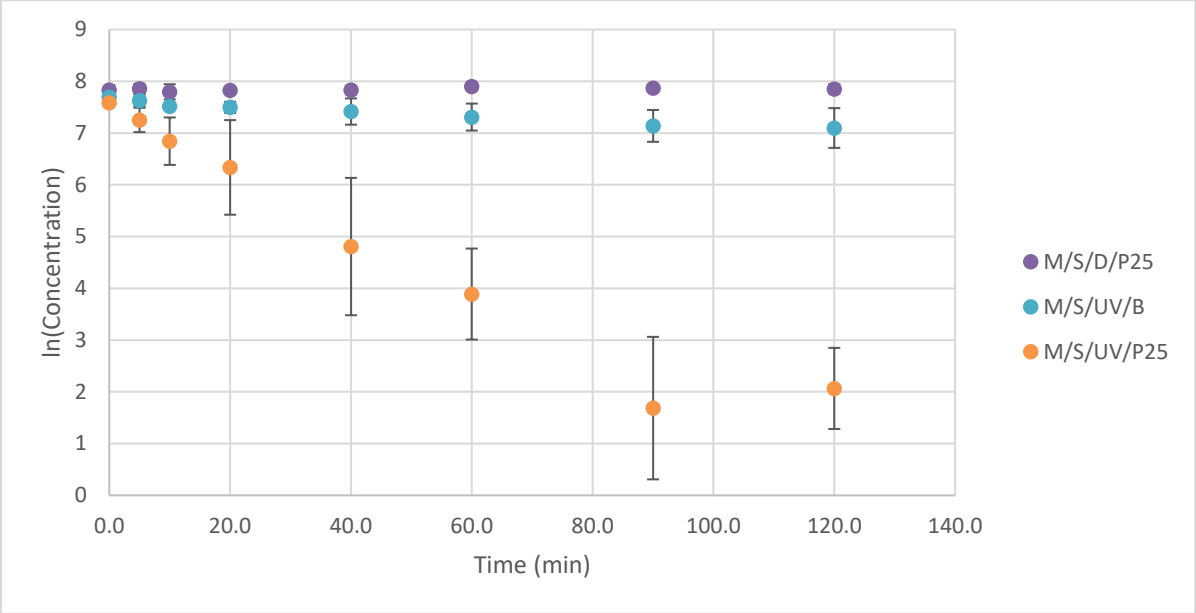

Figure C 3: Degradation of atenolol in Milli-Q.

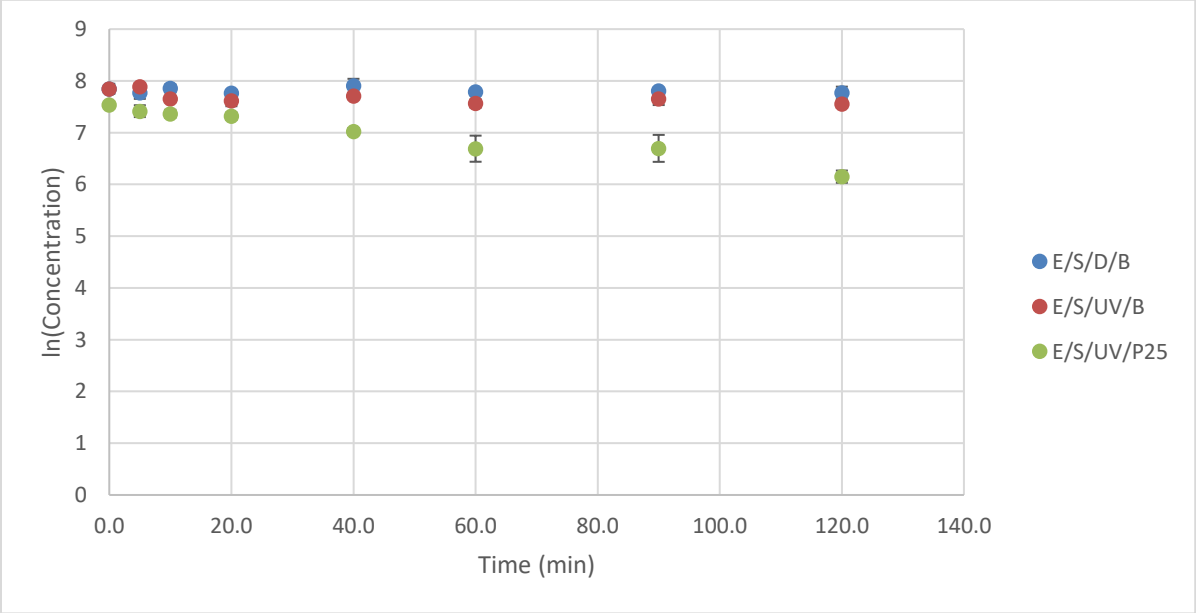

Figure C 4: Degradation of atenolol in wastewater effluent.

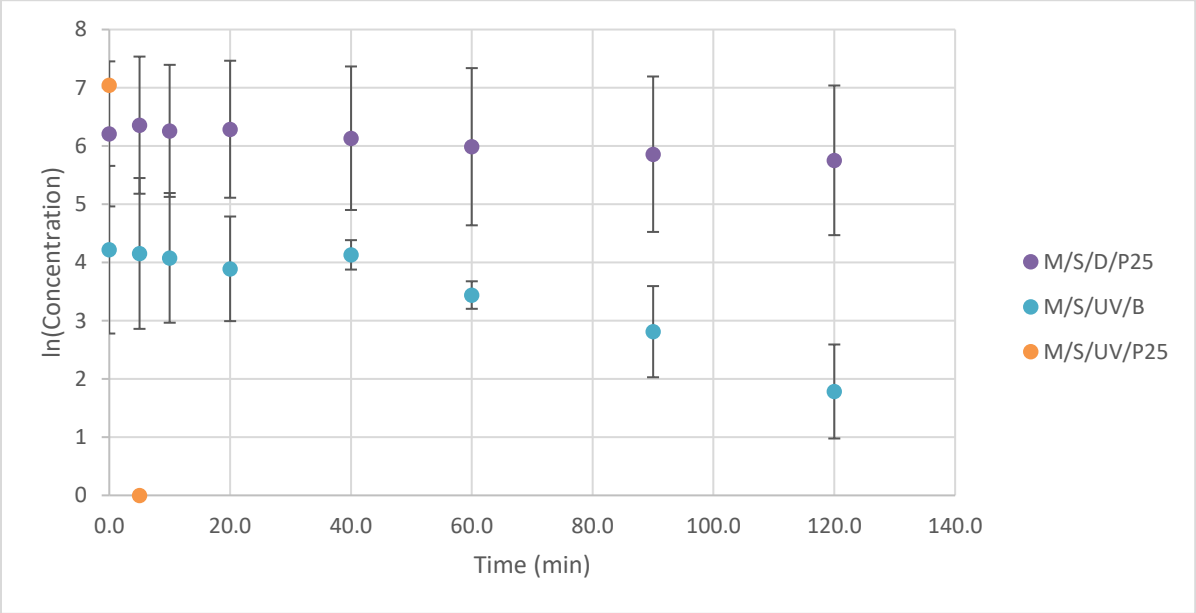

Figure C 5: Degradation of atorvastatin in Milli-Q.

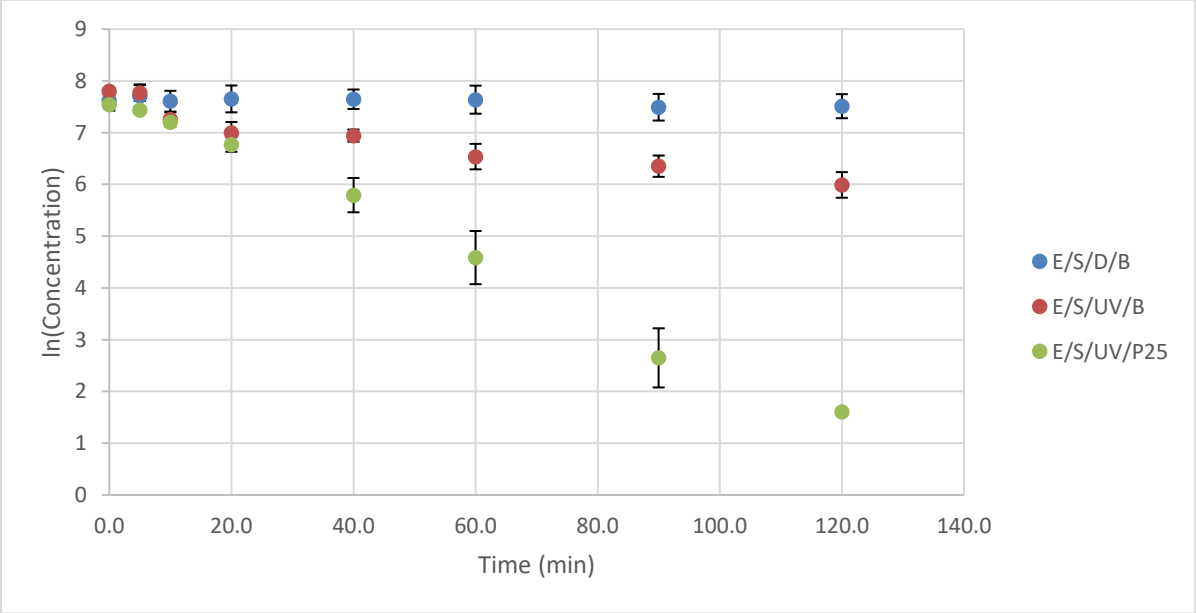

Figure C 6: Degradation of atorvastatin in wastewater effluent.

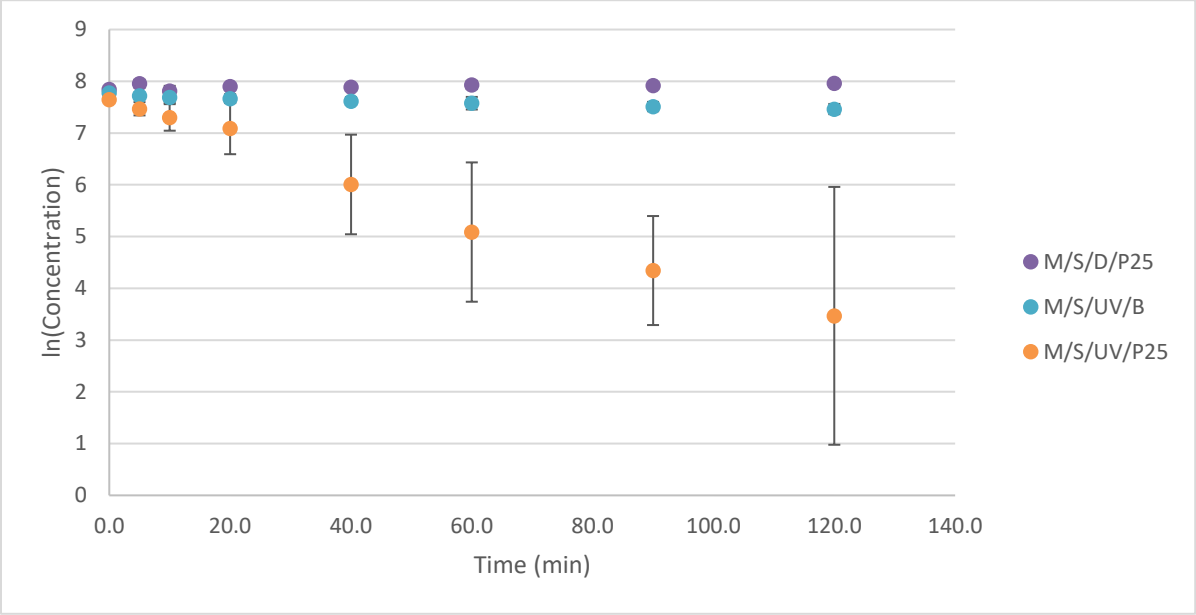

Figure C 7: Degradation of atrazine in Milli-Q.

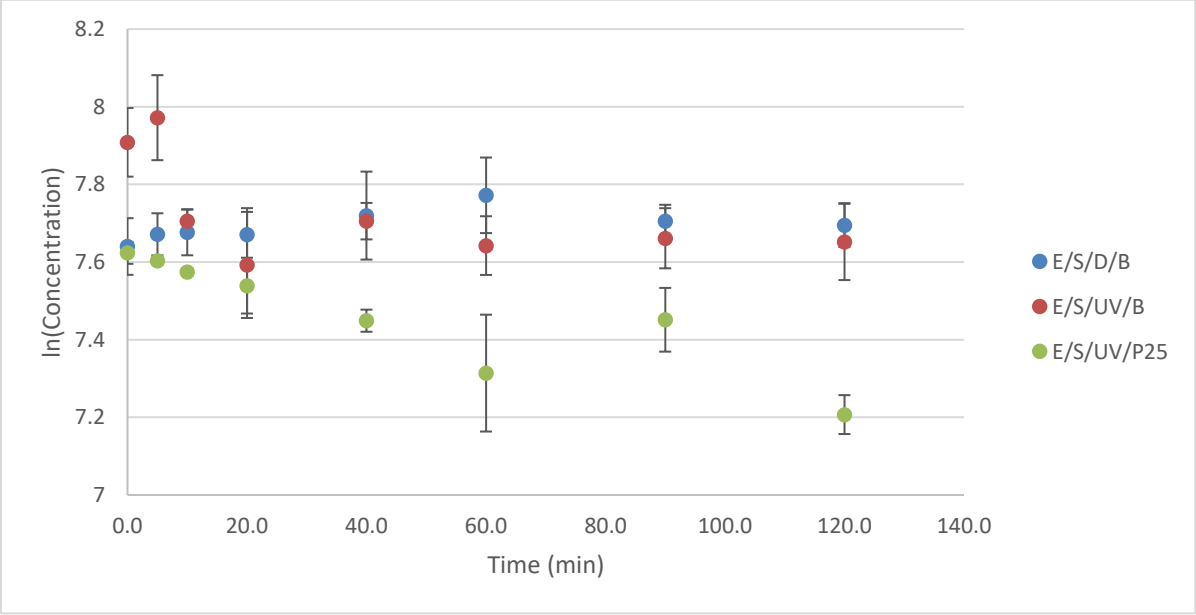

Figure C 8: Degradation of atrazine in wastewater effluent.

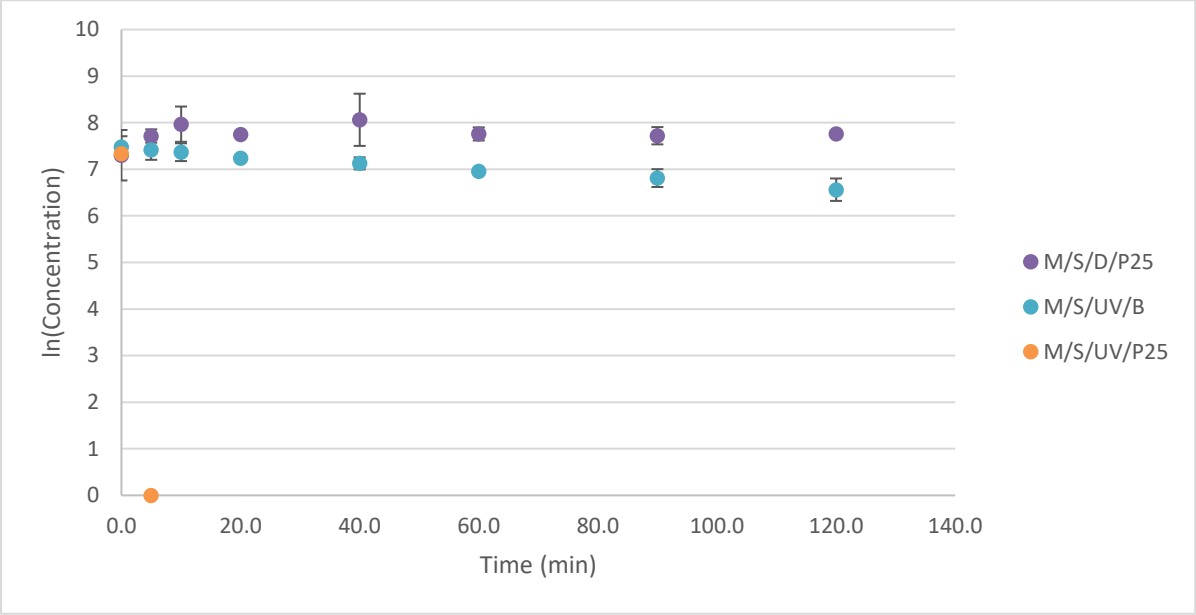

Figure C 9: Degradation of bisphenol a in Milli-Q.

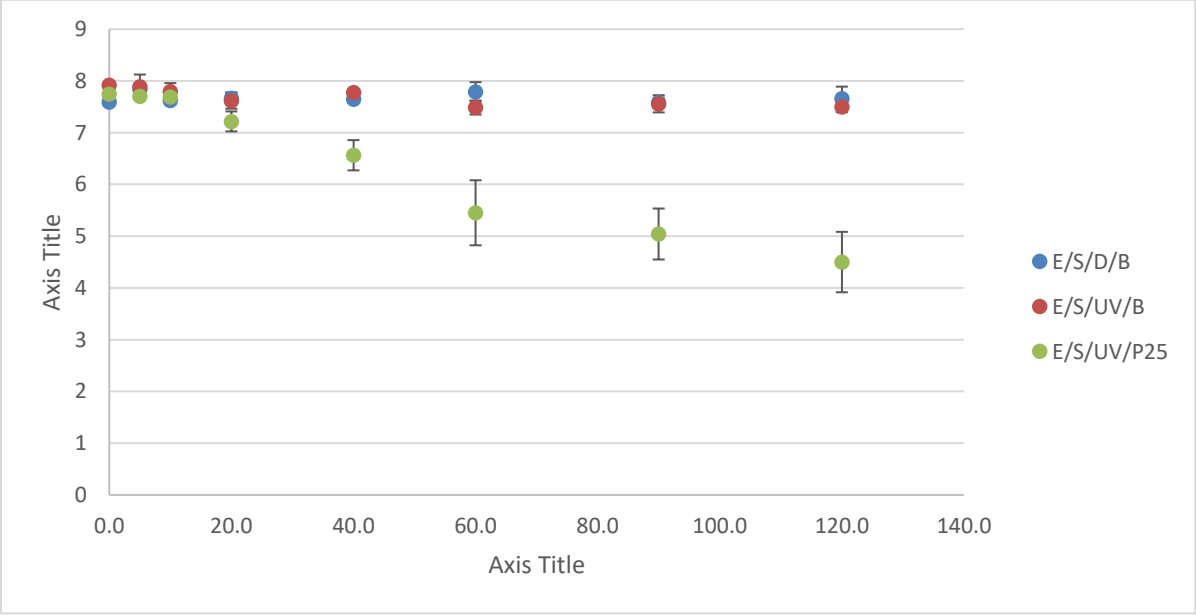

Figure C 10: Degradation of bisphenol a in wastewater effluent.

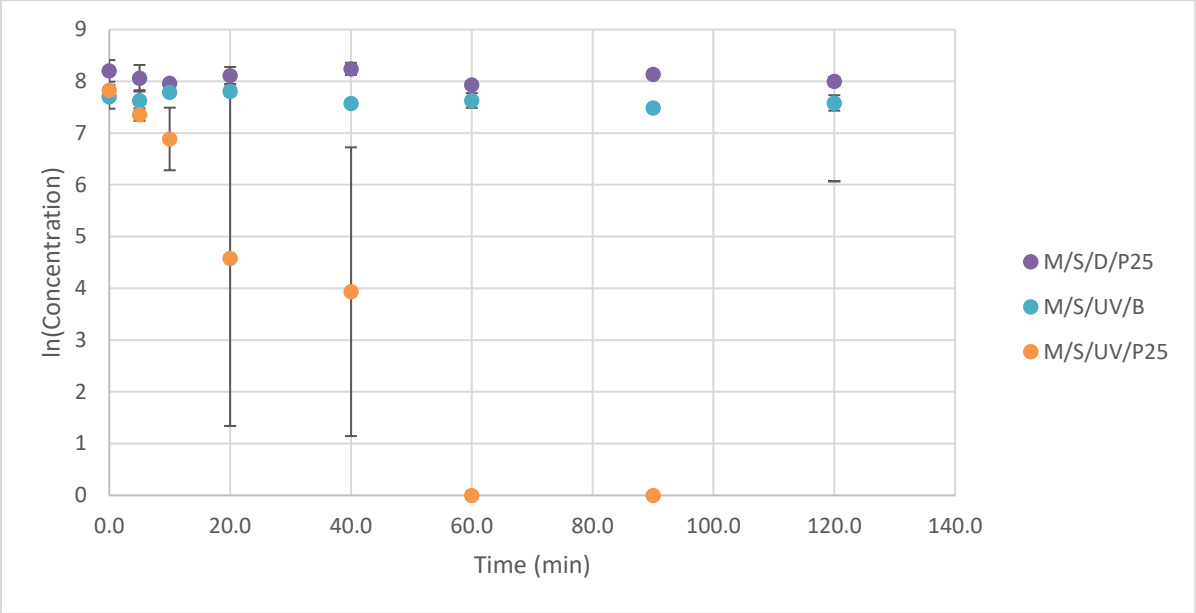

Figure C 11: Degradation of caffeine in Milli-Q.

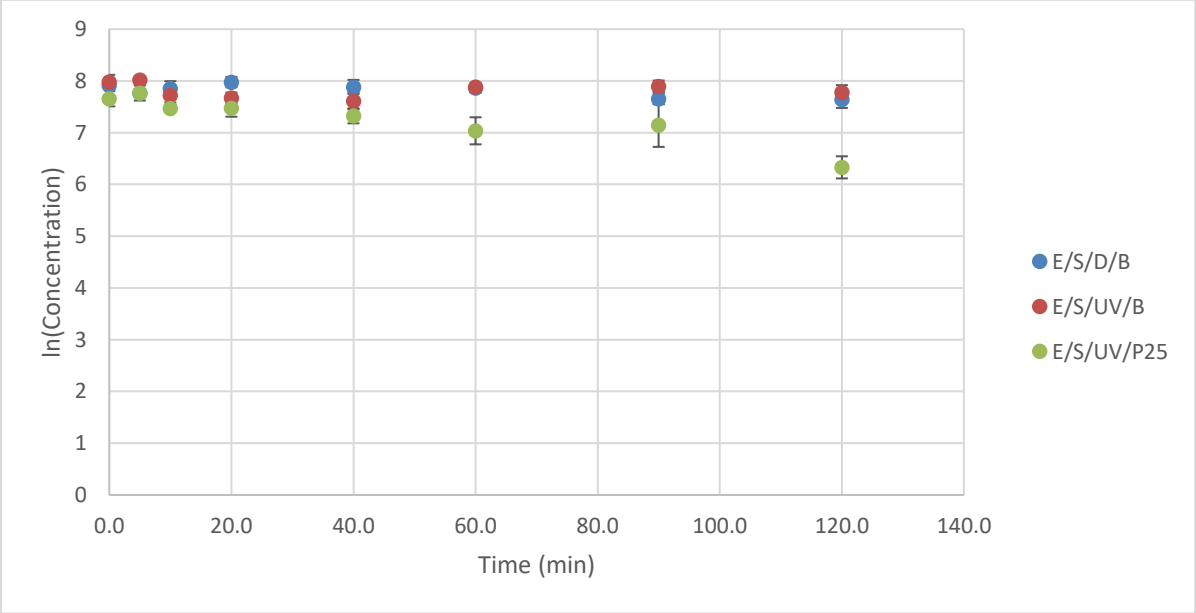

Figure C 12: Degradation of caffeine in wastewater effluent.

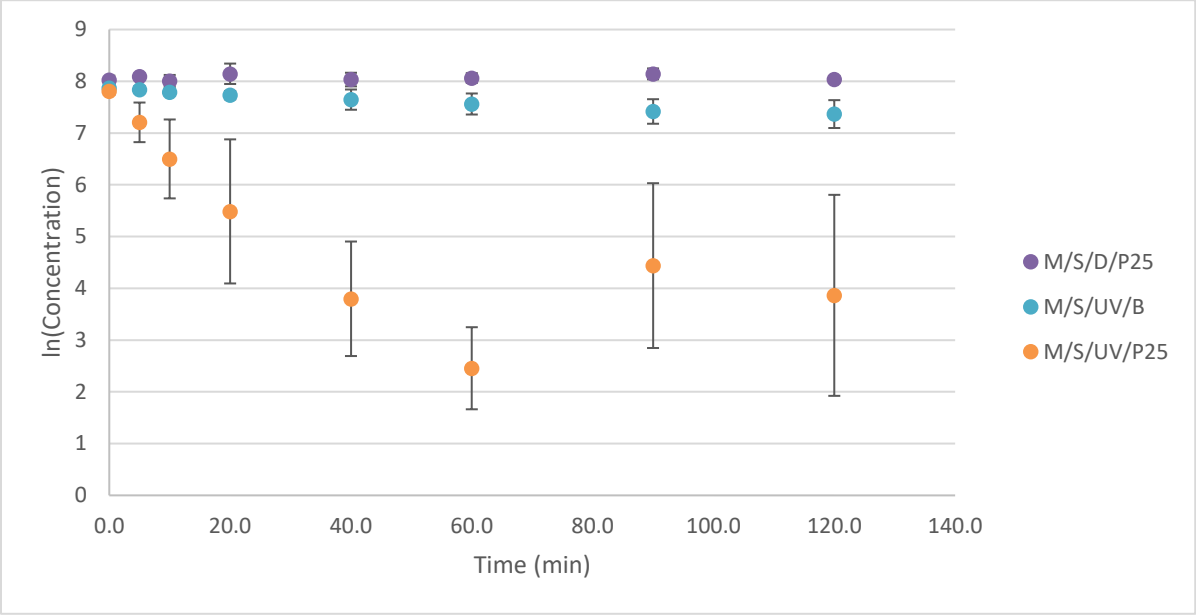

Figure C 13: Degradation of carbamazepine in Milli-Q.

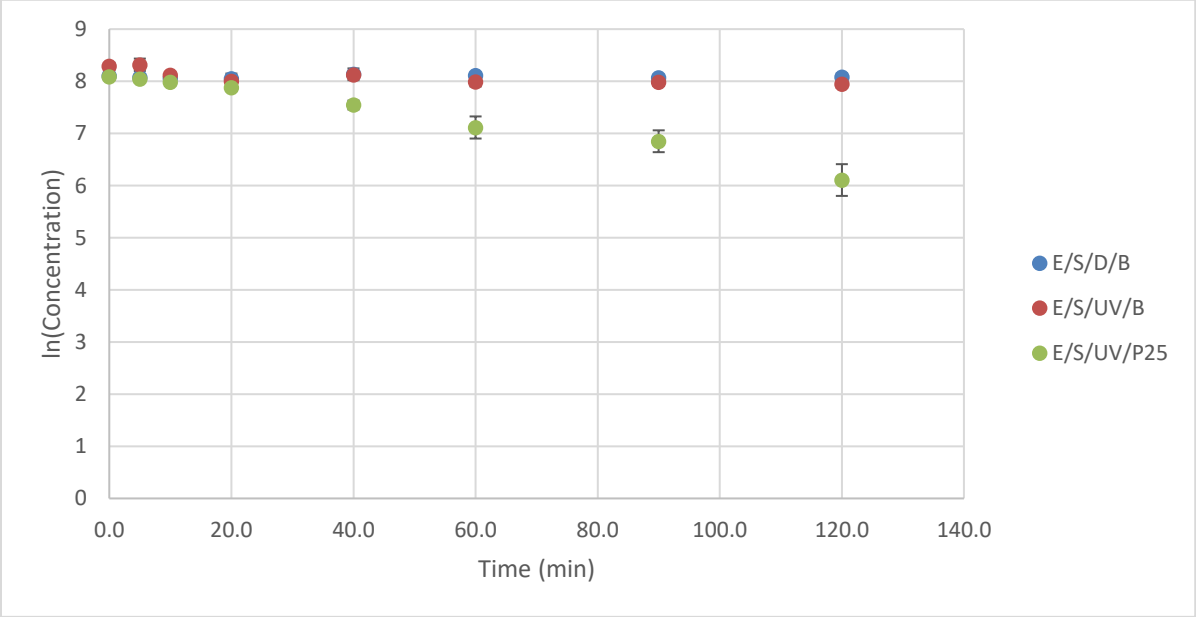

Figure C 14: Degradation of carbamazepine in wastewater effluent.

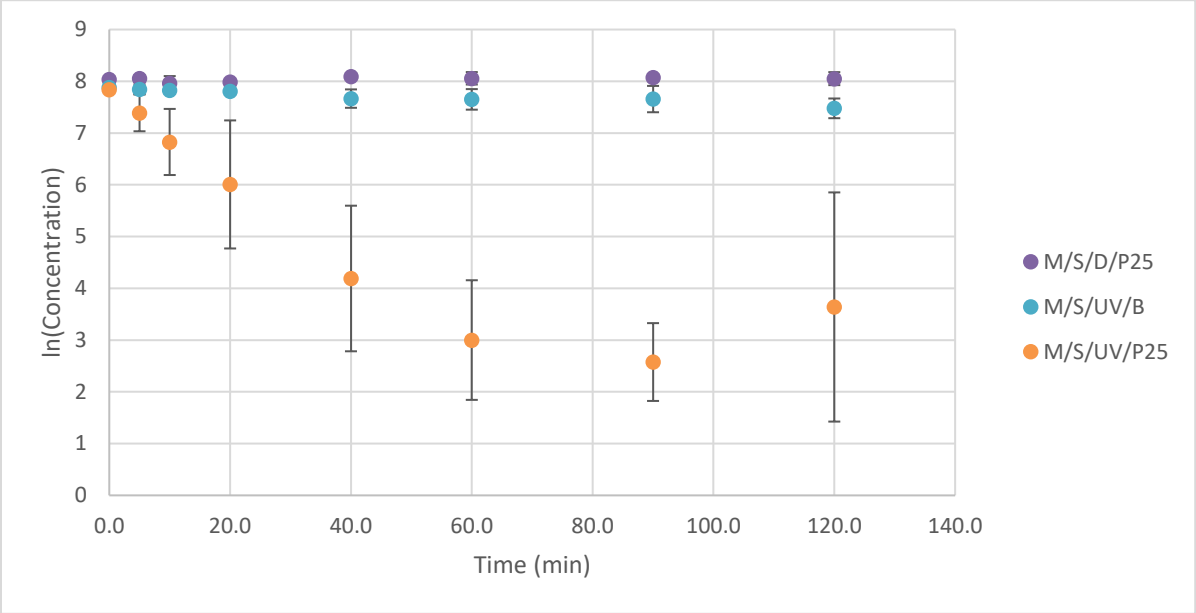

Figure C 15: Degradation of carbamazepine- 10,11- epoxide in Milli-Q.

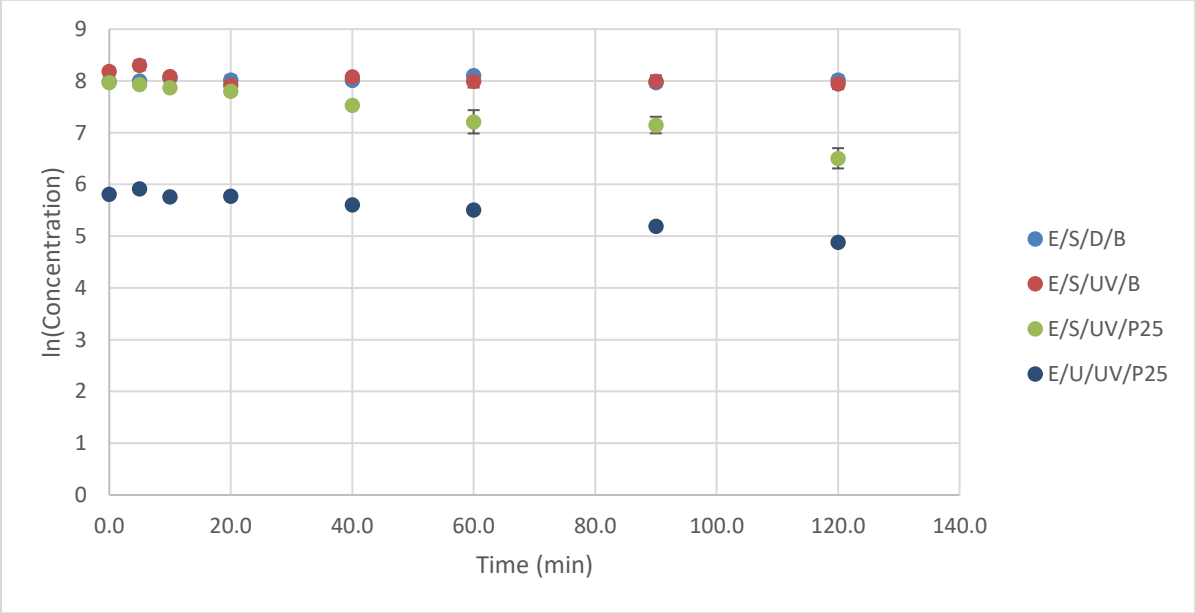

Figure C 16: Carbamazepine- 10,11- epoxide in effluent degradation.

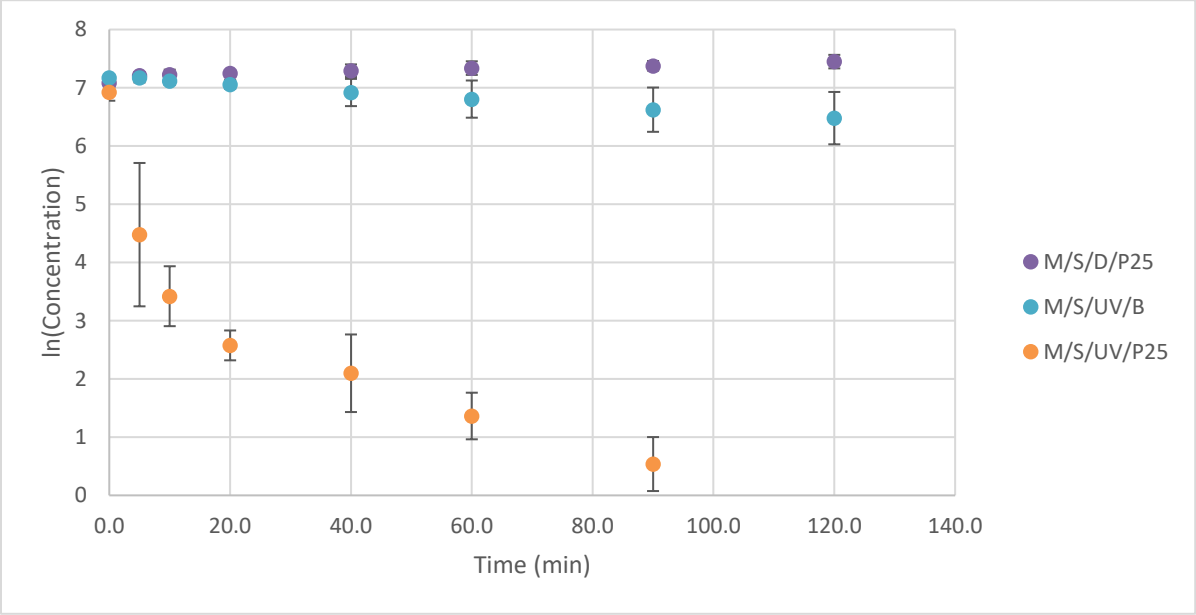

Figure C 17: Degradation of desvenlafaxine in Milli-Q.

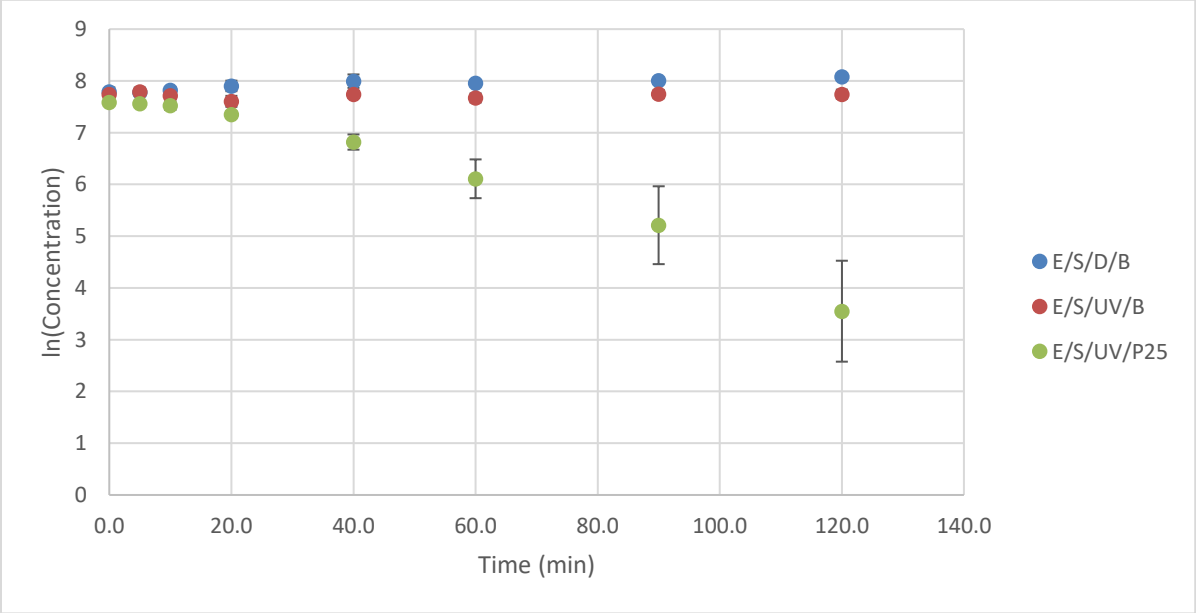

Figure C 18: Degradation of desvenlafaxine in wastewater effluent.

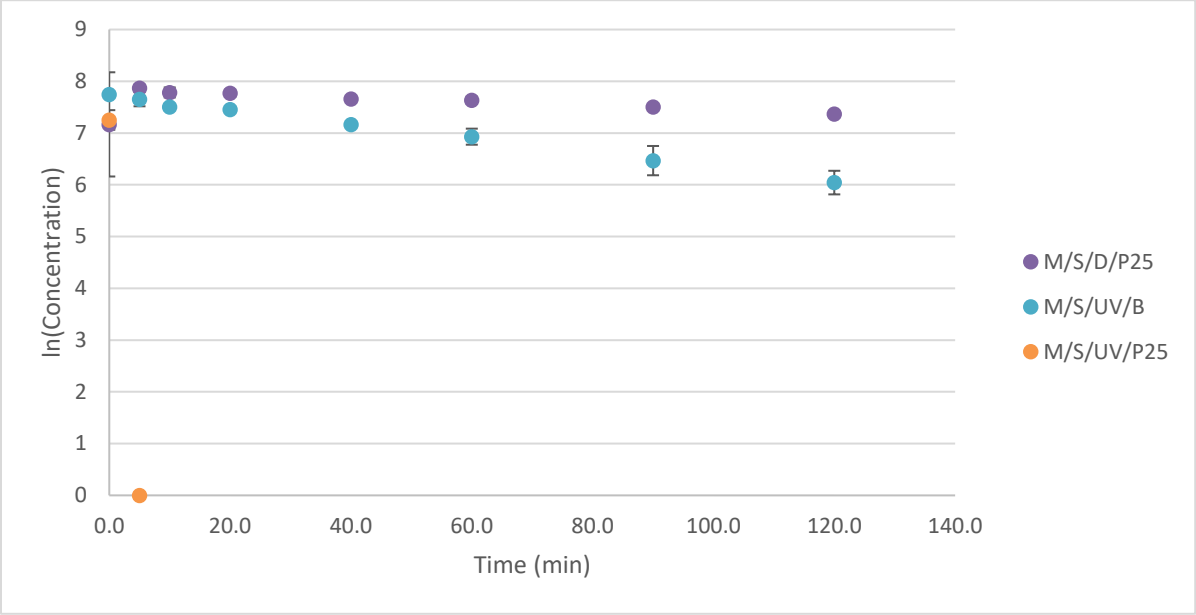

Figure C 19: Degradation of diclofenac in Milli-Q.

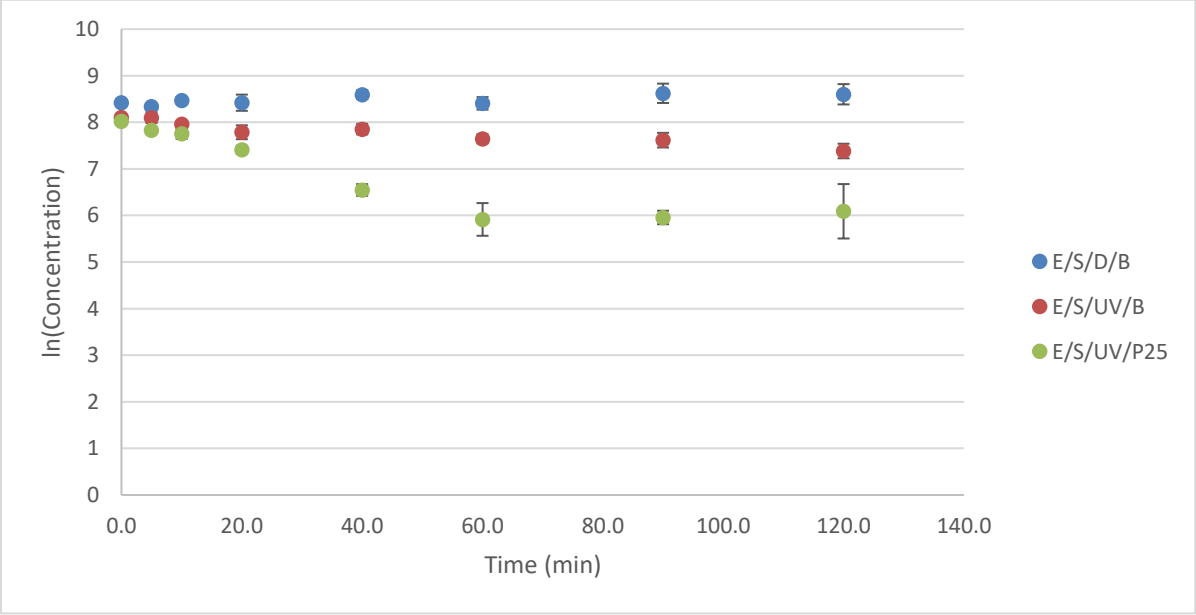

Figure C 20: Degradation of diclofenac in wastewater effluent.

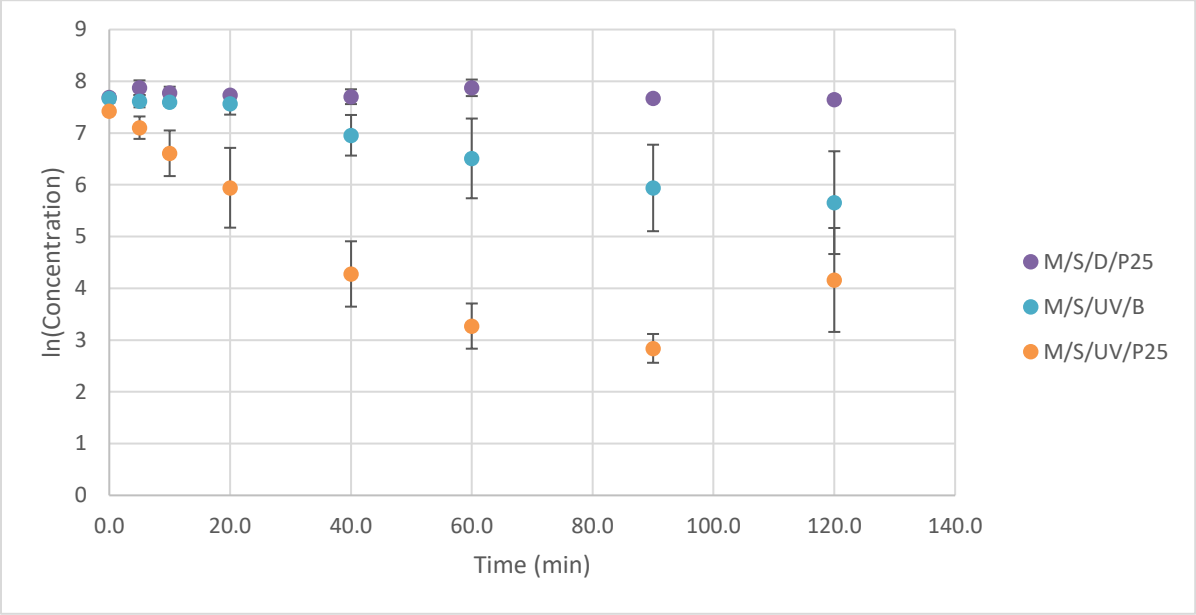

Figure C 21: Degradation of fluoxetine in Milli-Q.

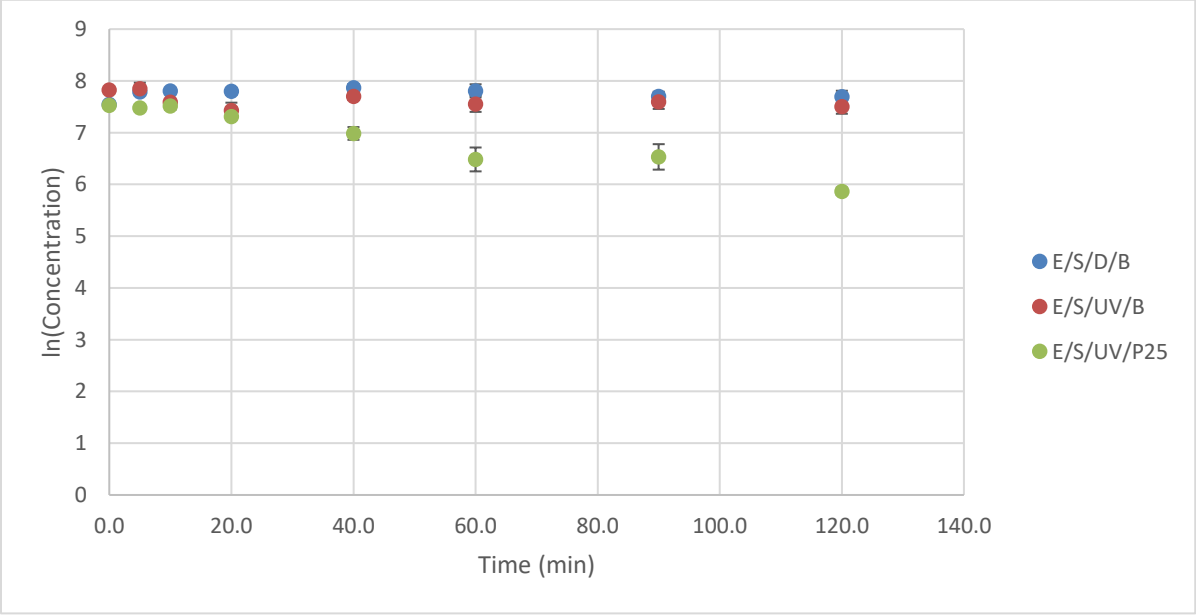

Figure C 22: Degradation of fluoxetine in wastewater effluent.

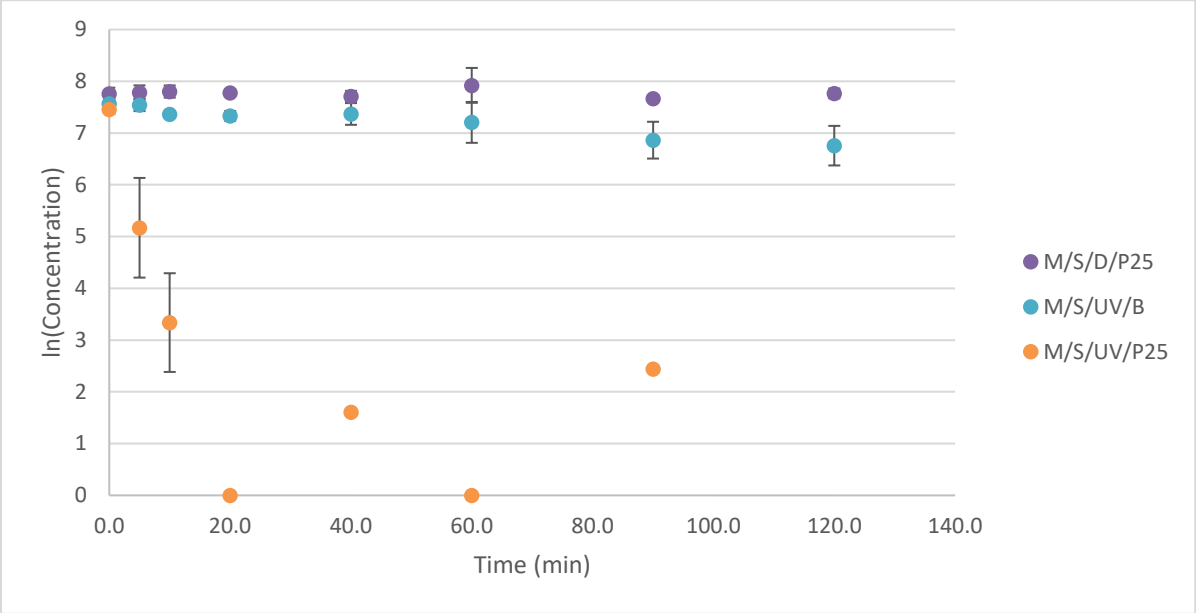

Figure C 23: Degradation of gemfibrozil in Milli-Q.

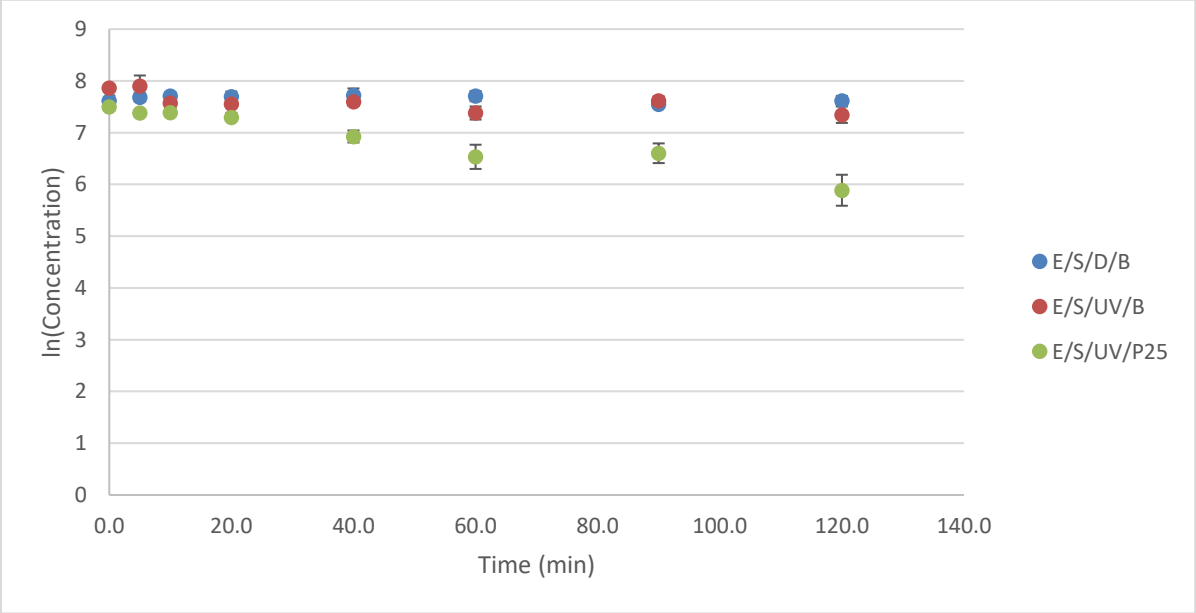

Figure C 24: Degradation of gemfibrozil in wastewater effluent.

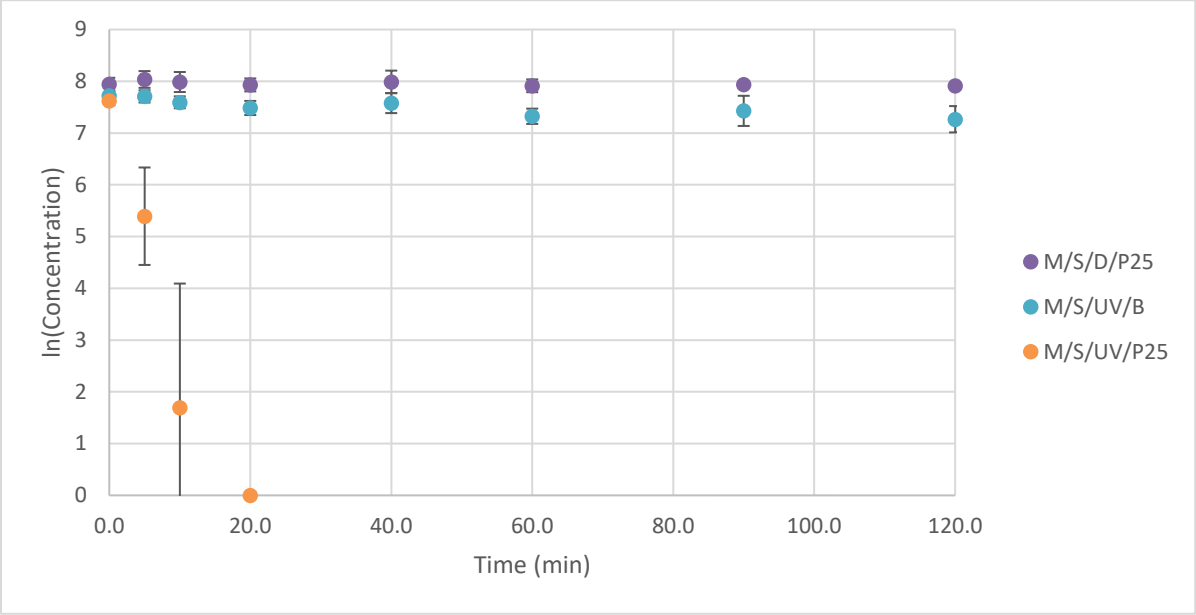

Figure C 25: Degradation of ibuprofen in Milli-Q.

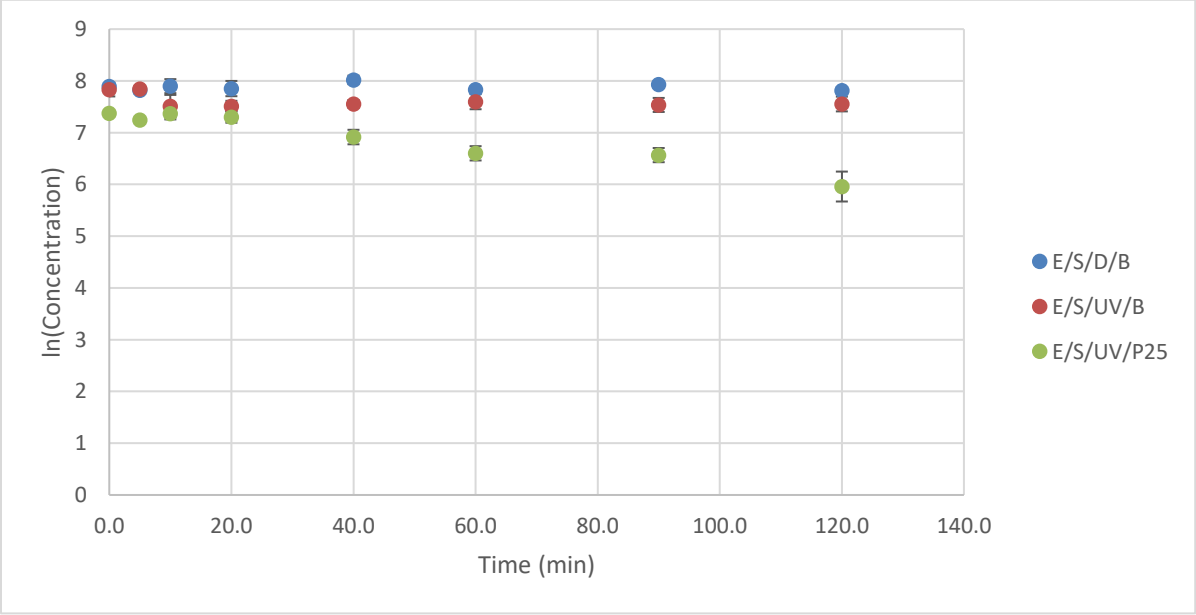

Figure C 26: Degradation of ibuprofen in wastewater effluent.

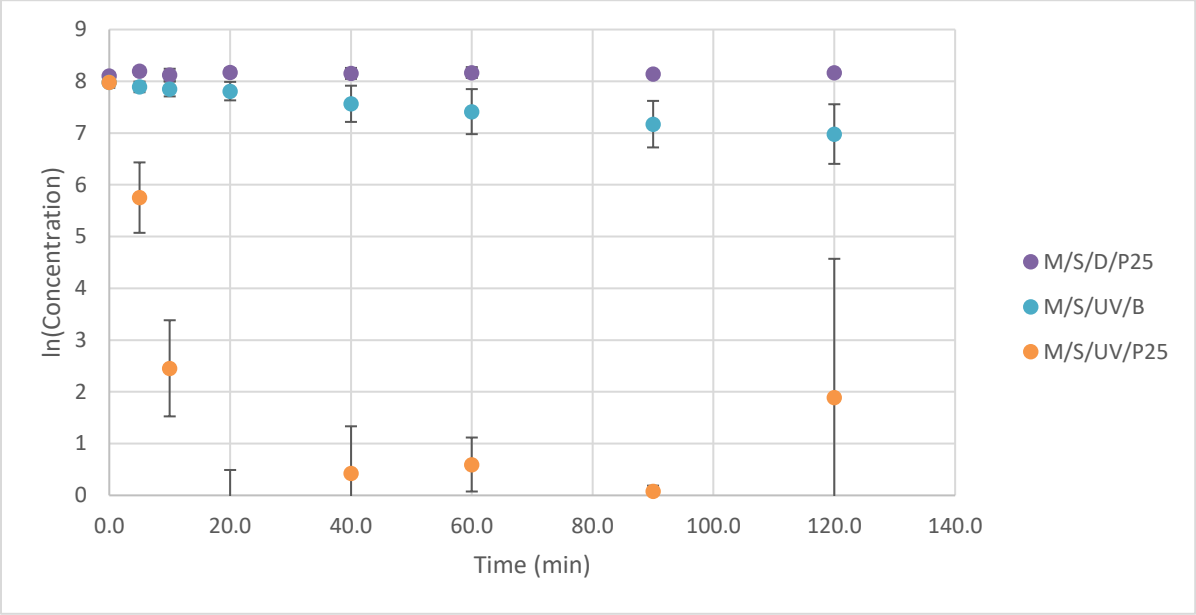

Figure C 27: Degradation of lincomycin in Milli-Q.

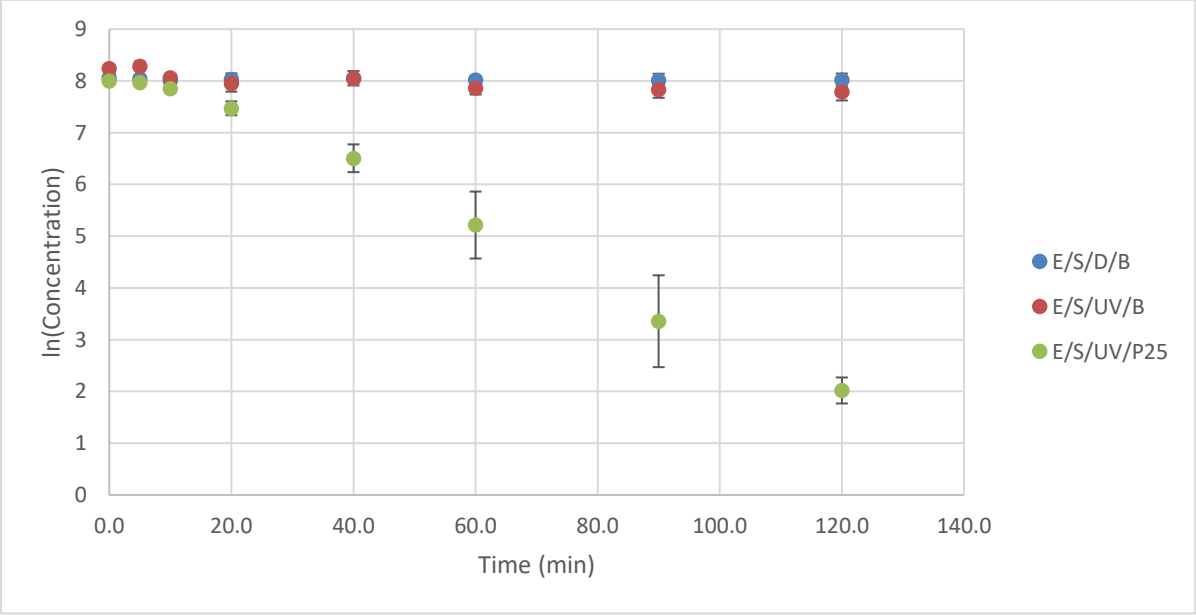

Figure C 28: Degradation of lincomycin in wastewater effluent.

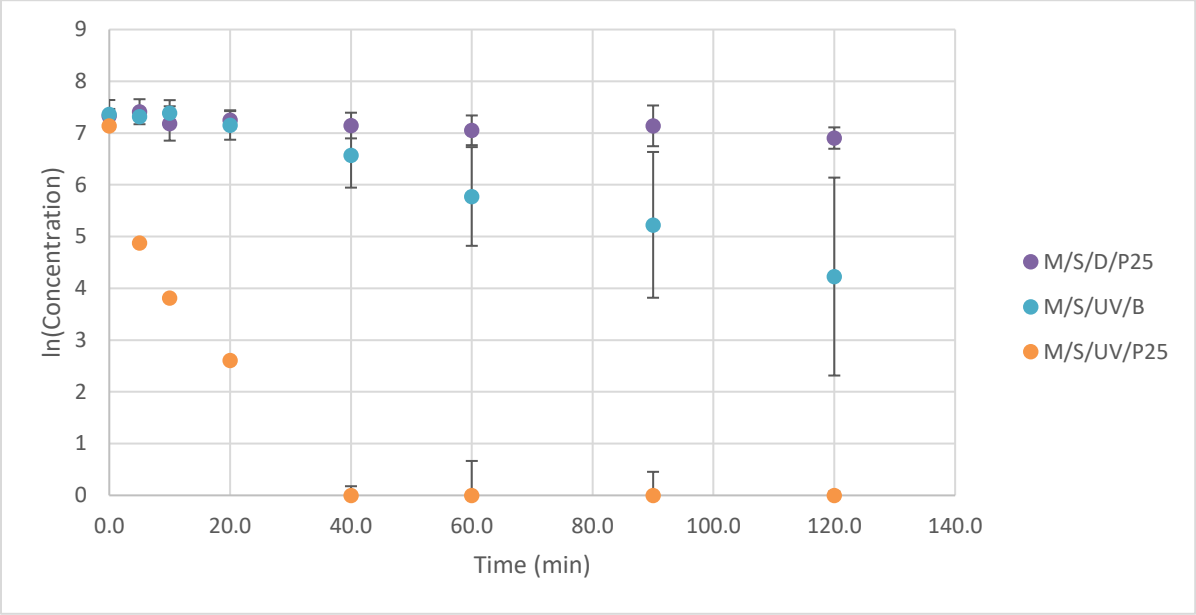

Figure C 29: Degradation of monensin in Milli-Q.

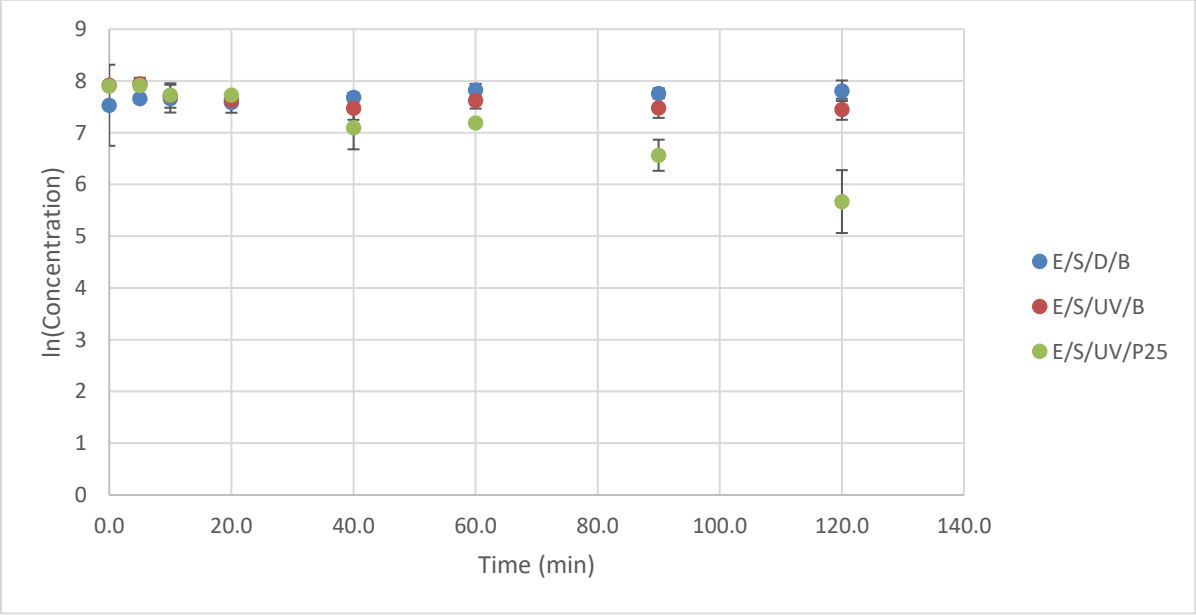

Figure C 30: Degradation of monensin in wastewater effluent.

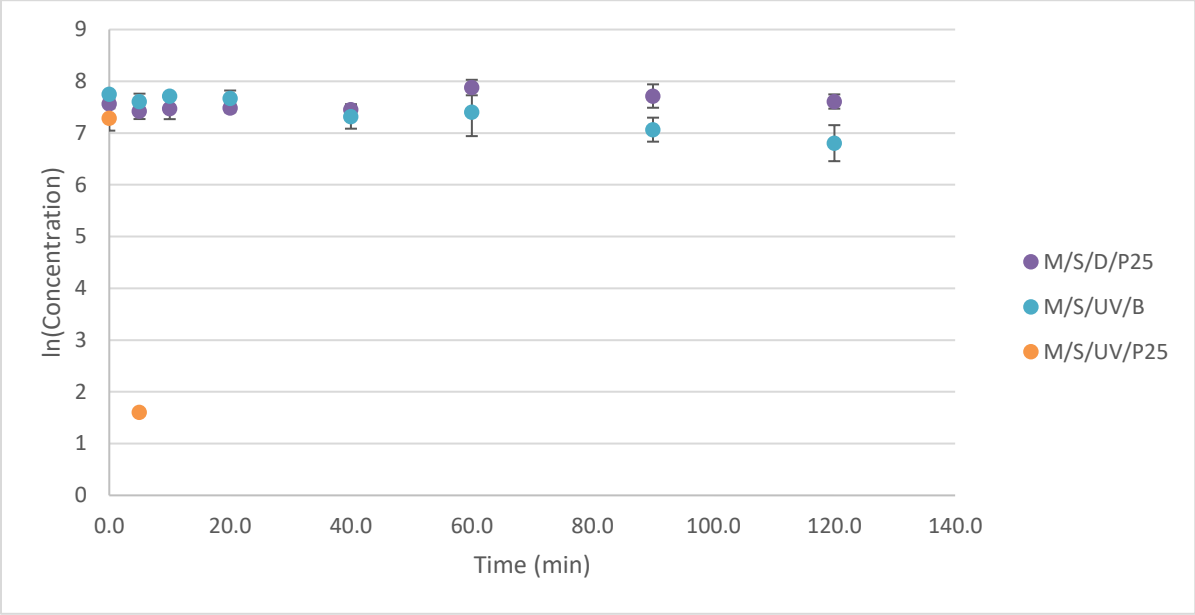

Figure C 31: Degradation of naproxen in Milli-Q.

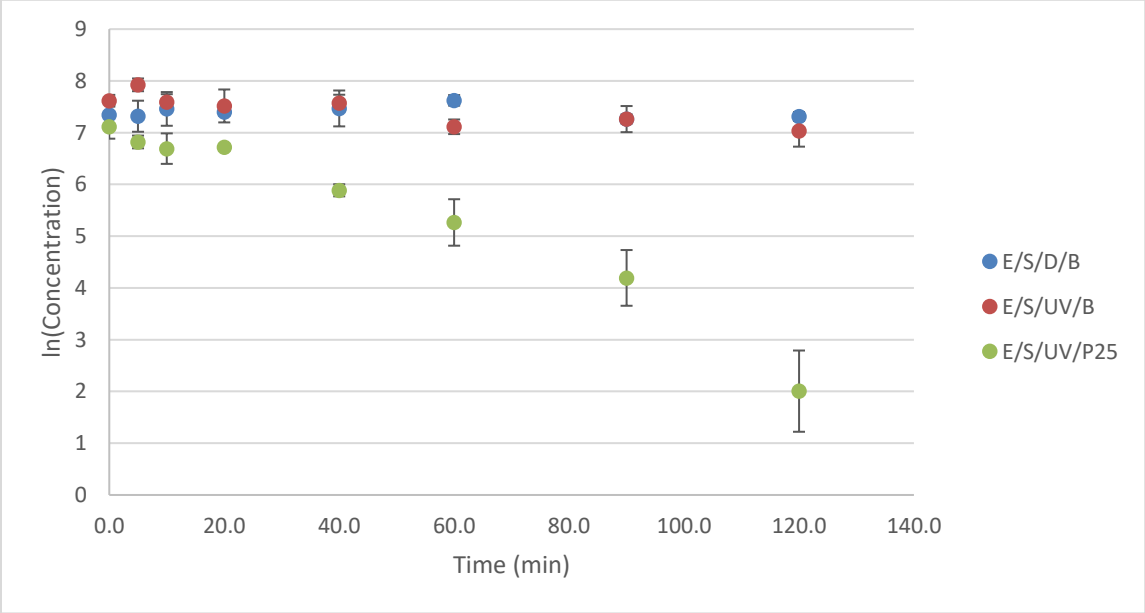

Figure C 32: Degradation of naproxen in wastewater effluent.

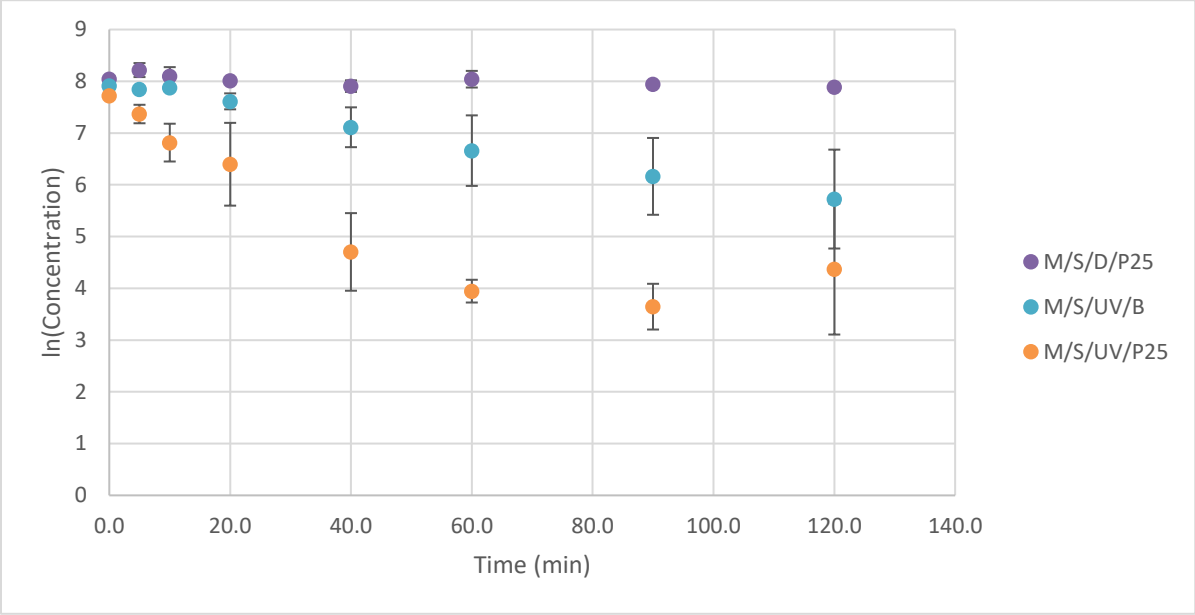

Figure C 33: Degradation of norfluoxetine in Milli-Q.

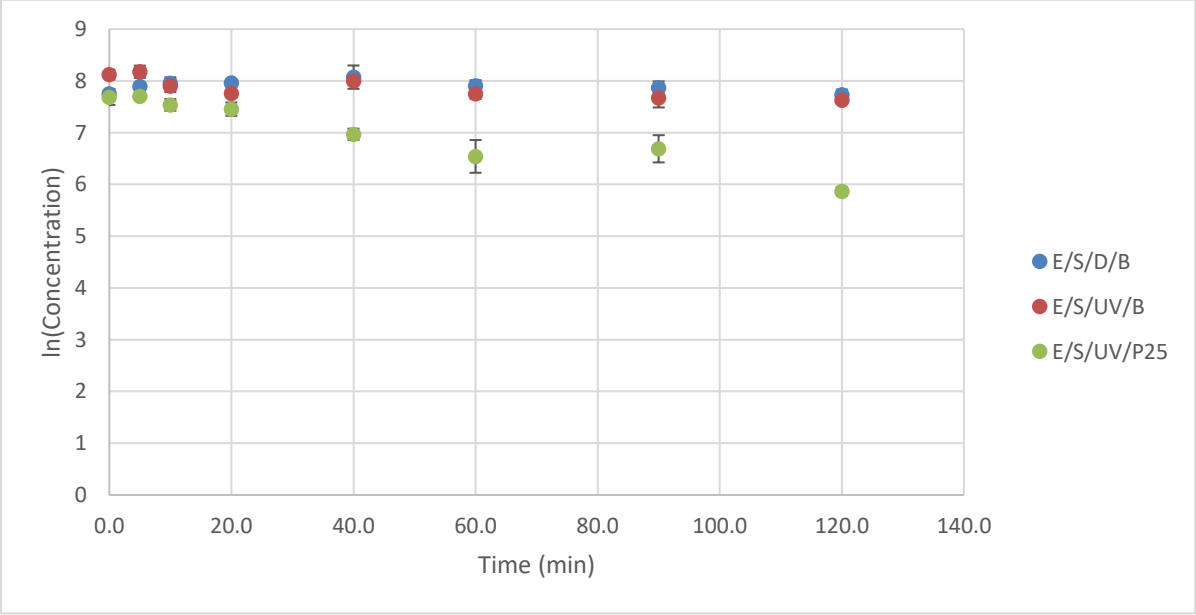

Figure C 34: Degradation of norfluoxetine in wastewater effluent.

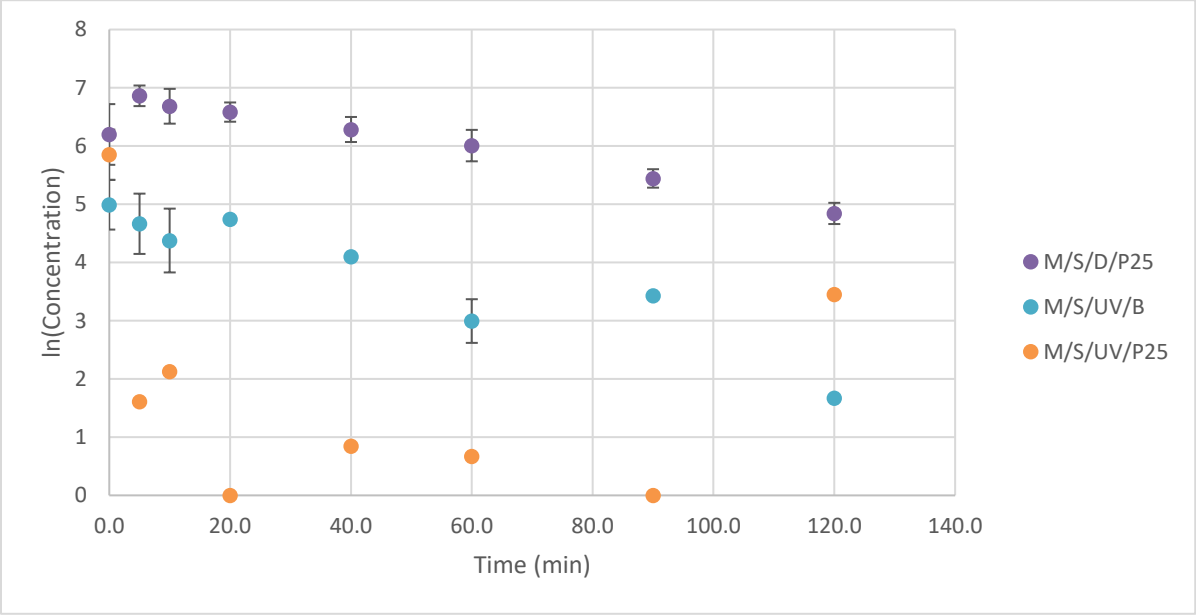

Figure C 35: Degradation of o-atorvastatin in Milli-Q.

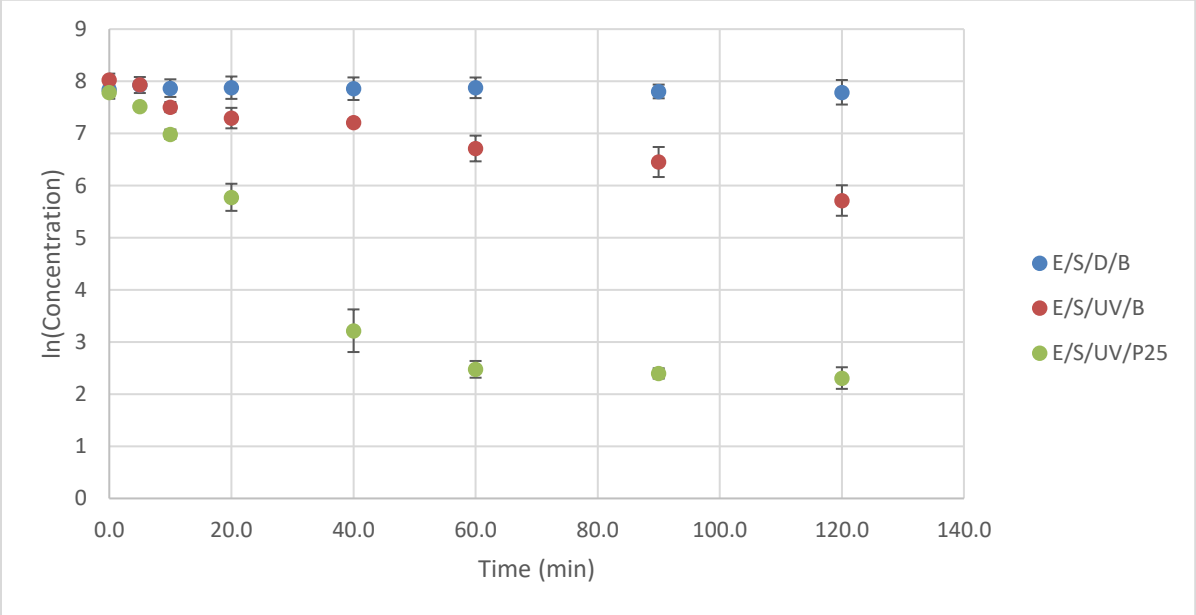

Figure C 36: Degradation of o-atorvastatin in wastewater effluent.

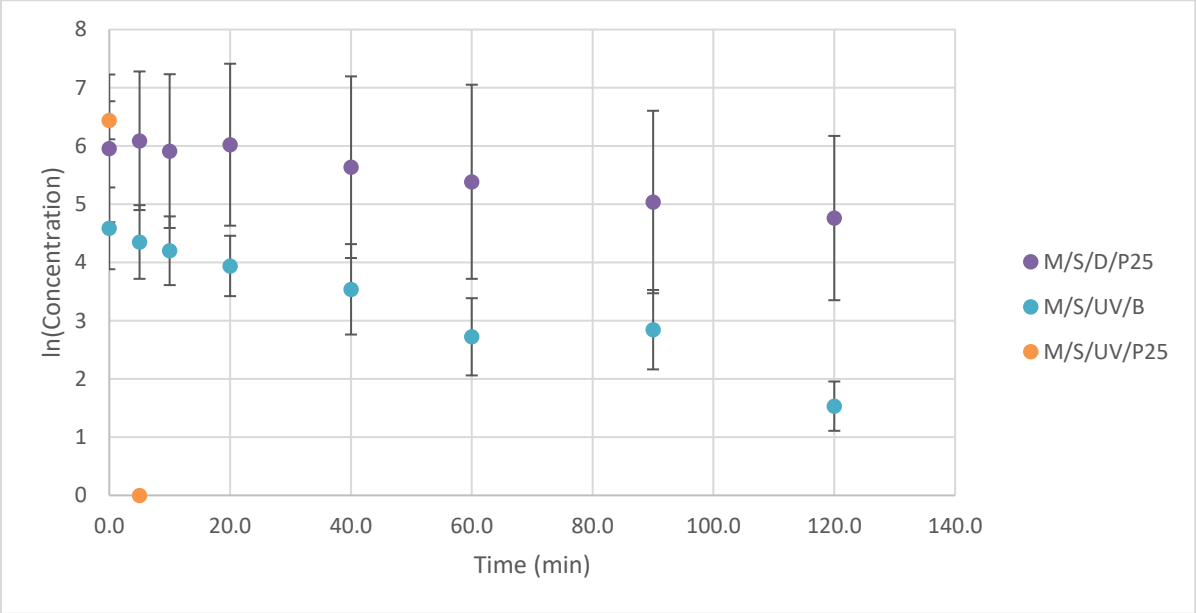

Figure C 37: Degradation of p-atorvastatin in Milli-Q.

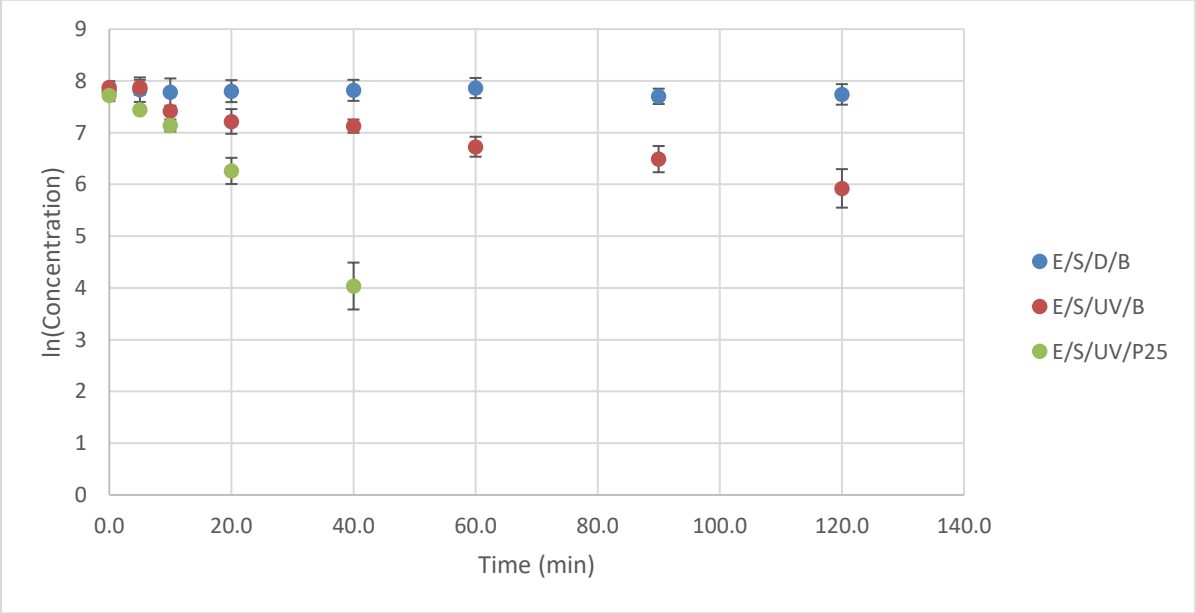

Figure C 38: Degradation of p-Atorvastatin in wastewater effluent.

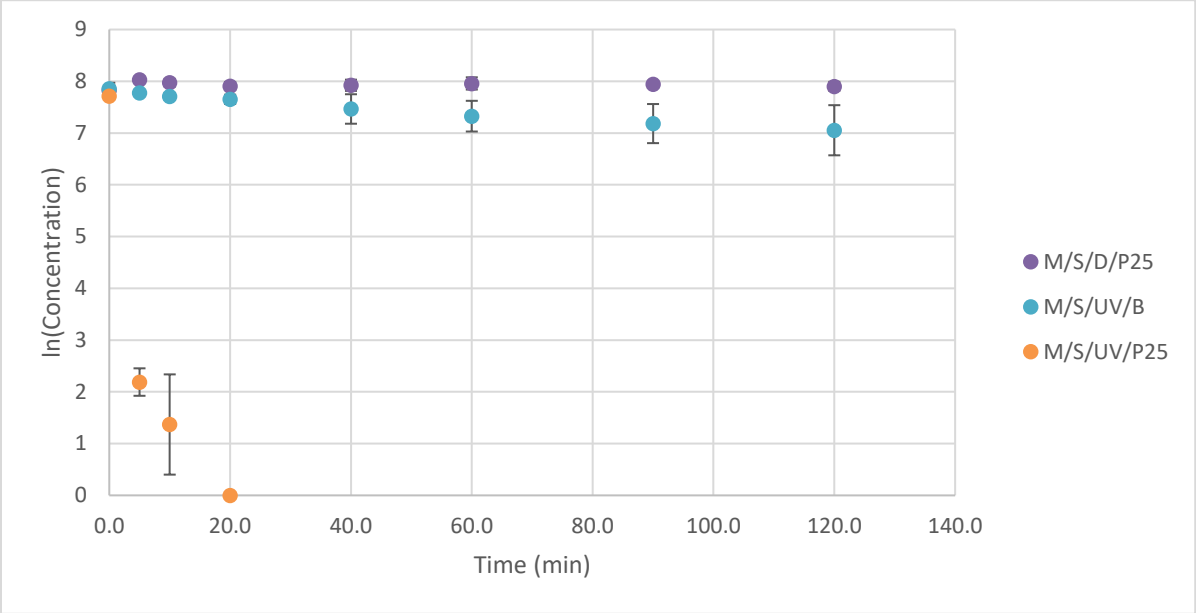

Figure C 39: Degradation of sulfamethoxazole in Milli-Q.

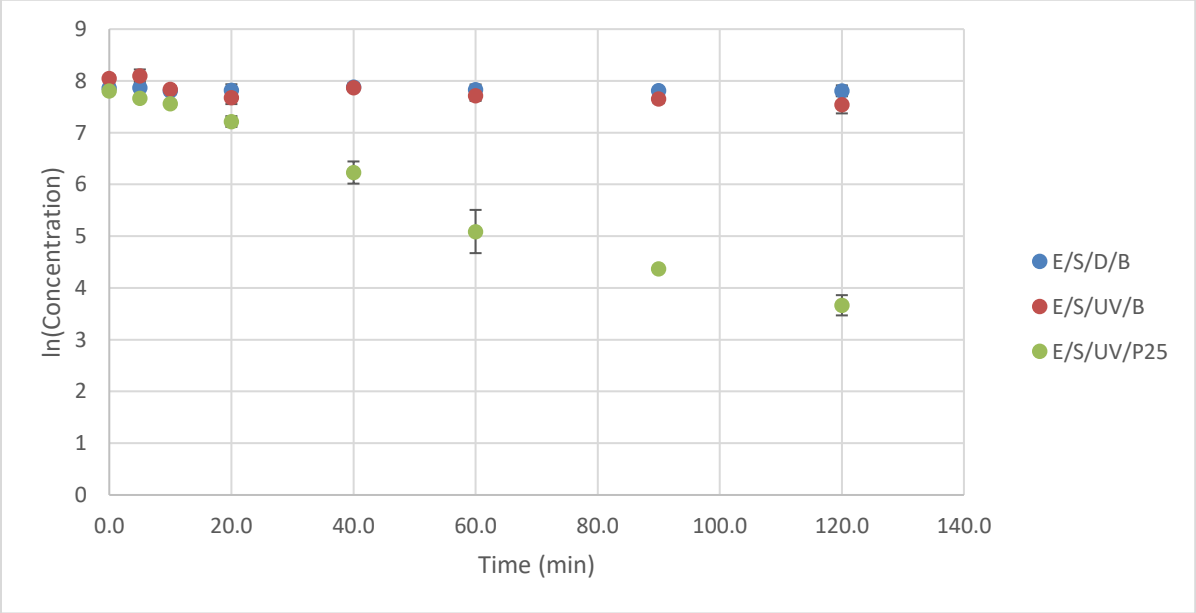

Figure C 40: Degradation of sulfamethoxazole in wastewater effluent.

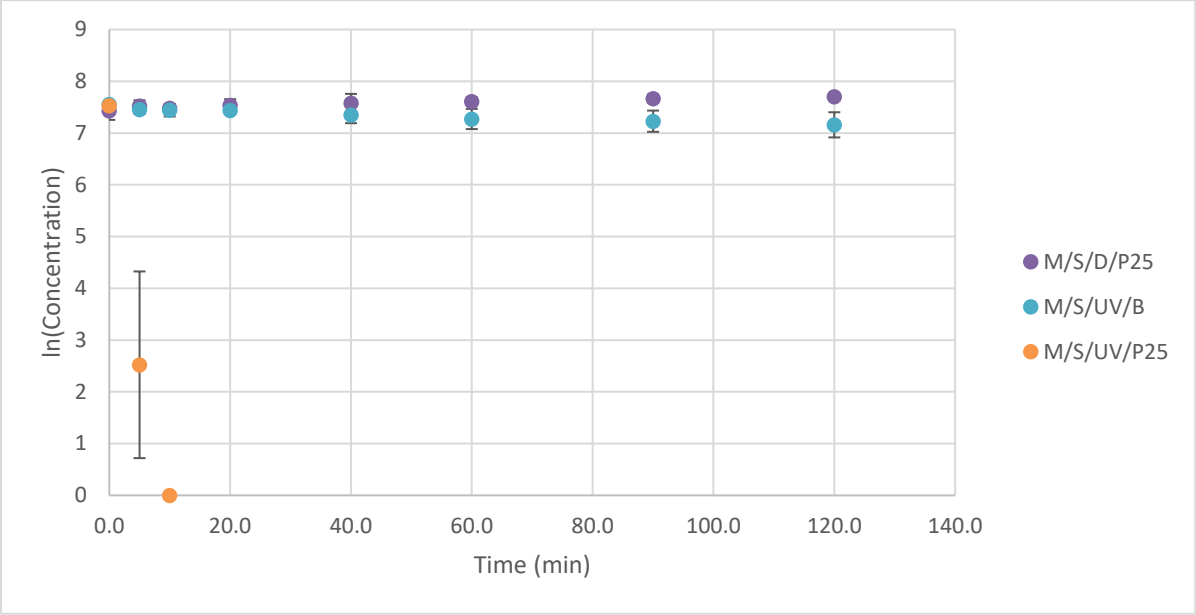

Figure C 41: Degradation of sulfanilamide in Milli-Q.

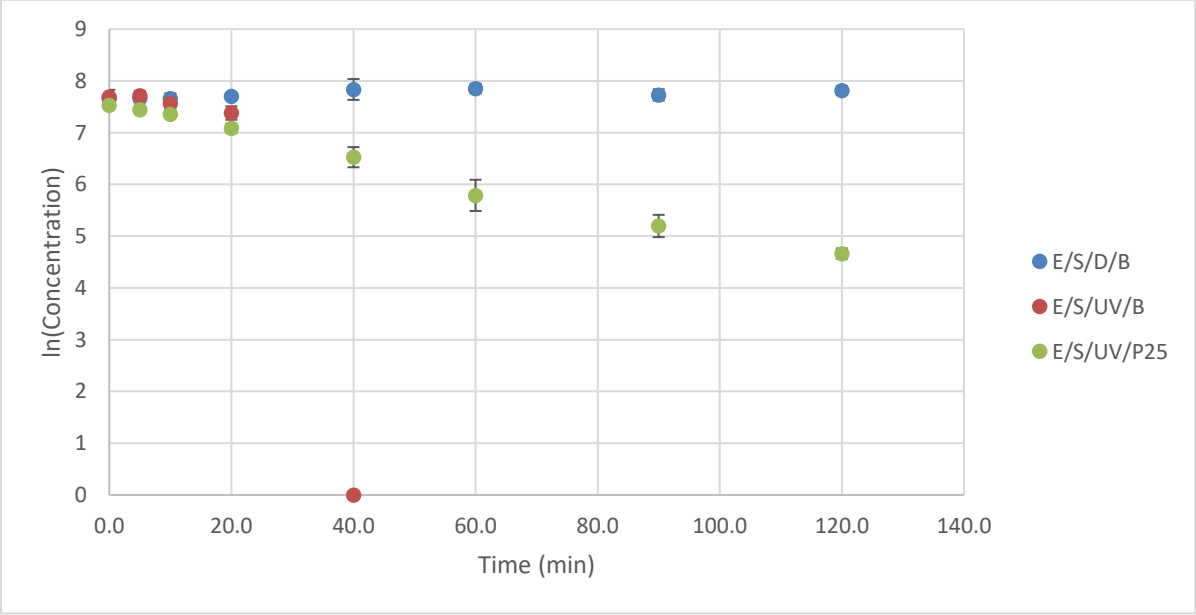

Figure C 42: Degradation of sulfanilamide in wastewater effluent.

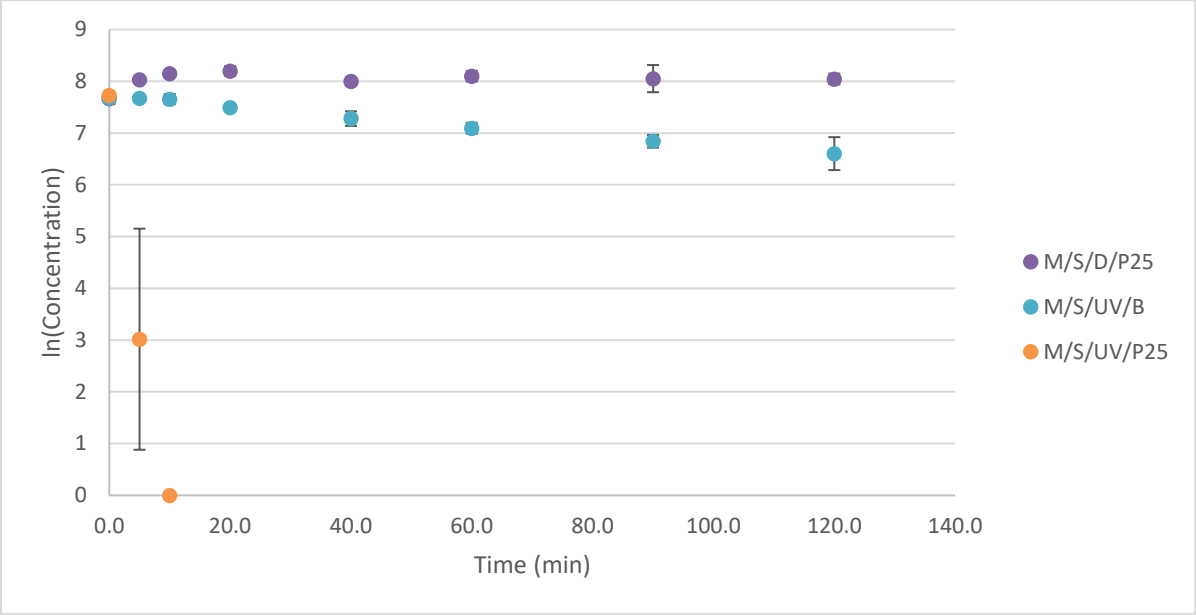

Figure C 43: Degradation of triclosan in Milli-Q.

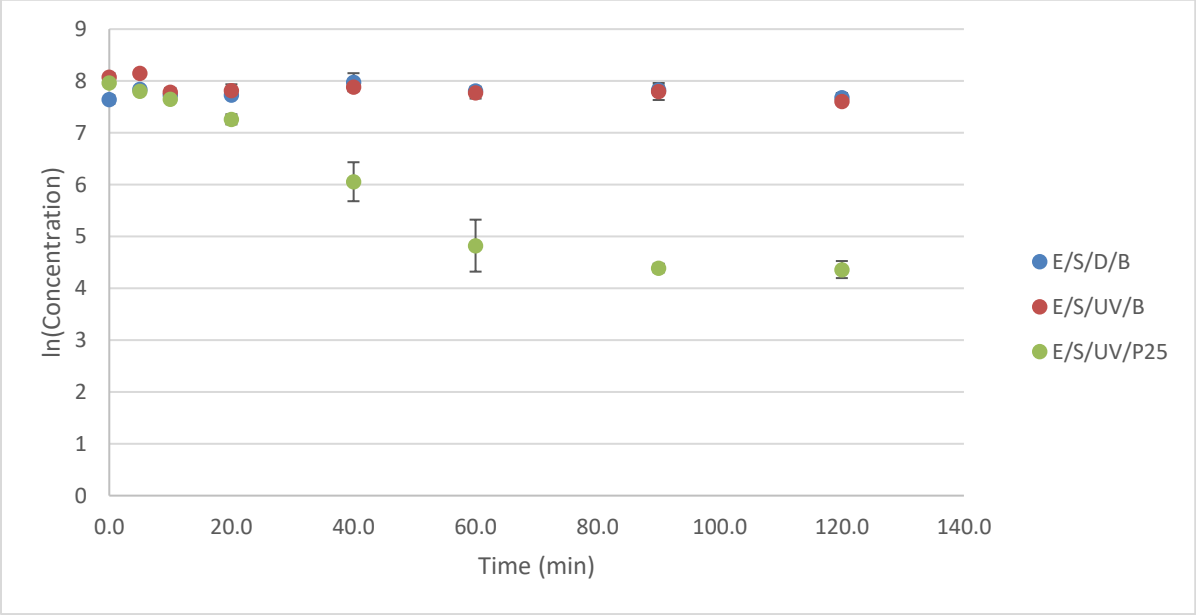

Figure C 44: Degradation of triclosan in wastewater effluent.

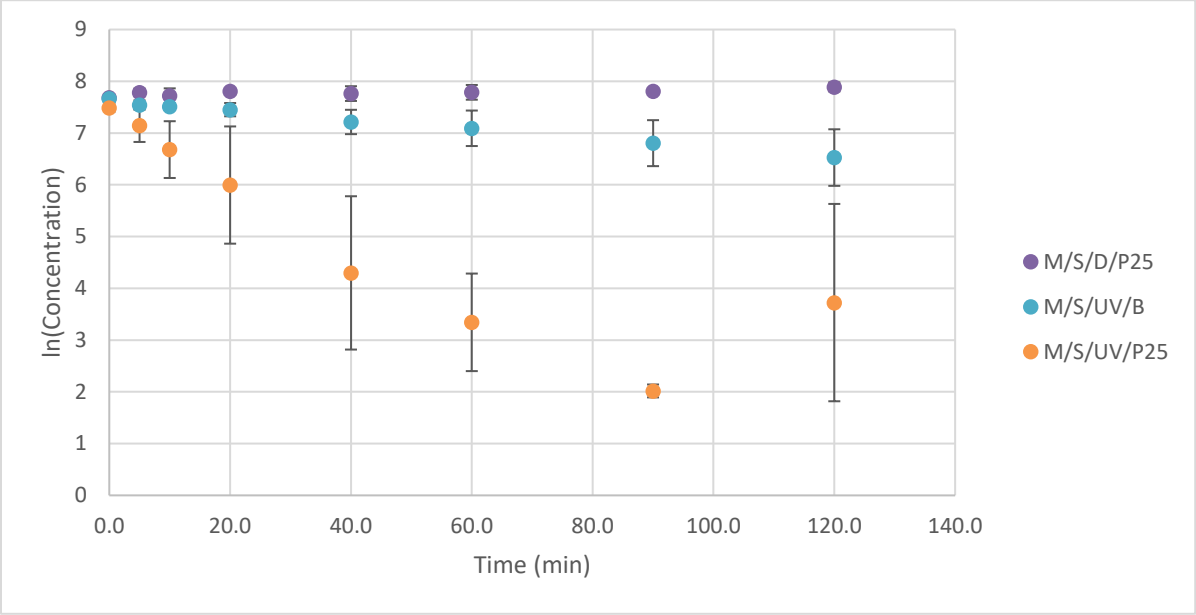

Figure C 45: Degradation of trimethoprim in Milli-Q.

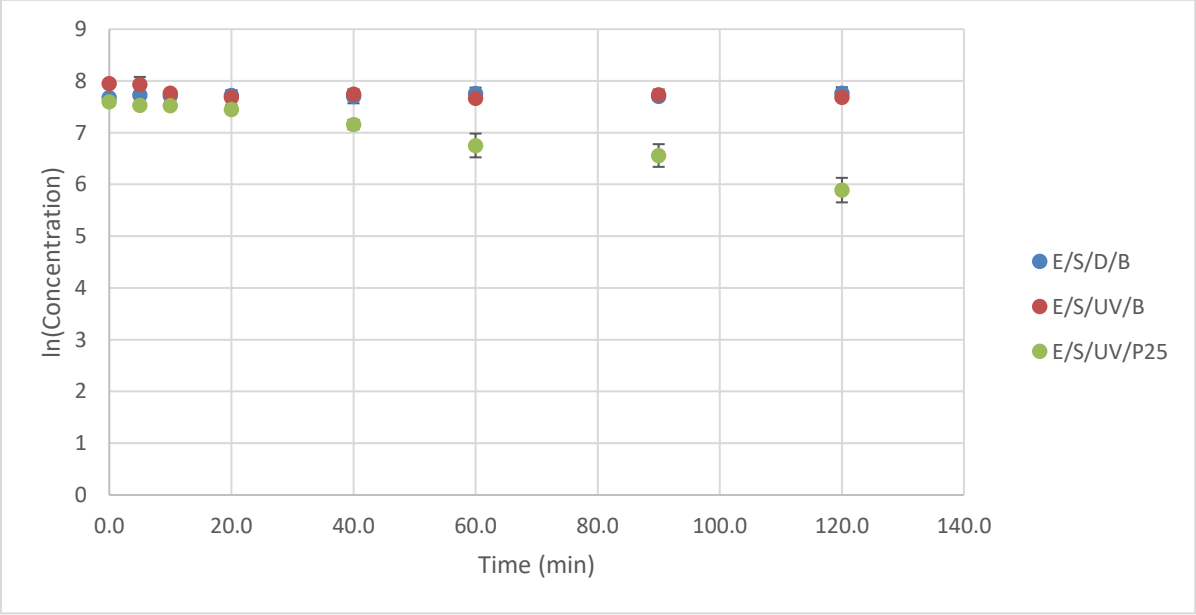

Figure C 46: Degradation of trimethoprim in wastewater effluent.

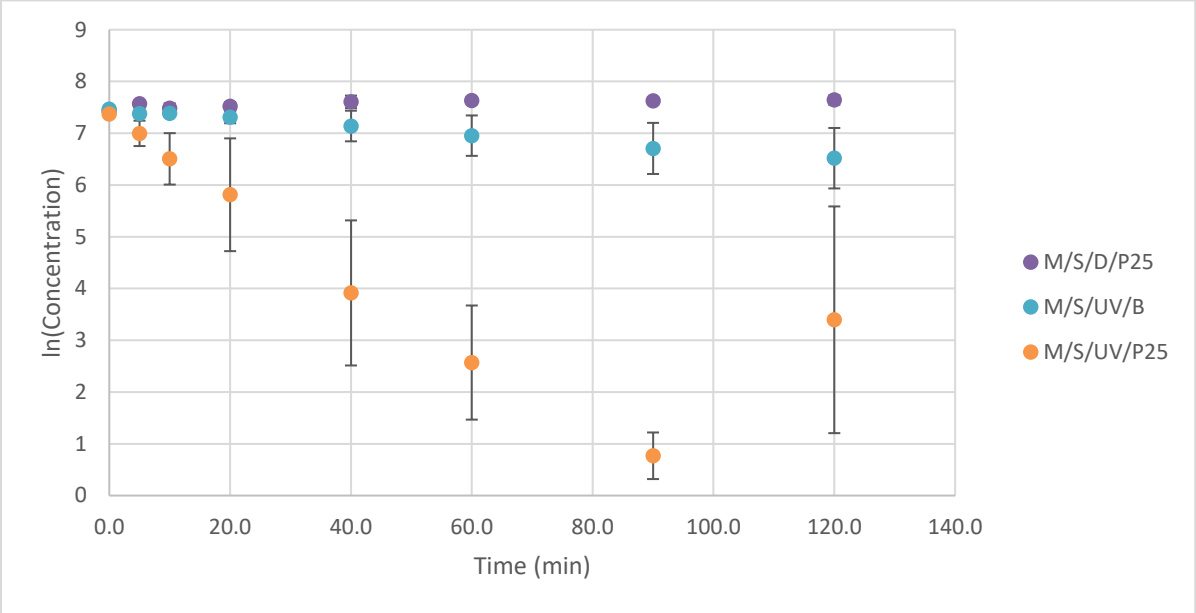

Figure C 47: Degradation of venlafaxine in Milli-Q.

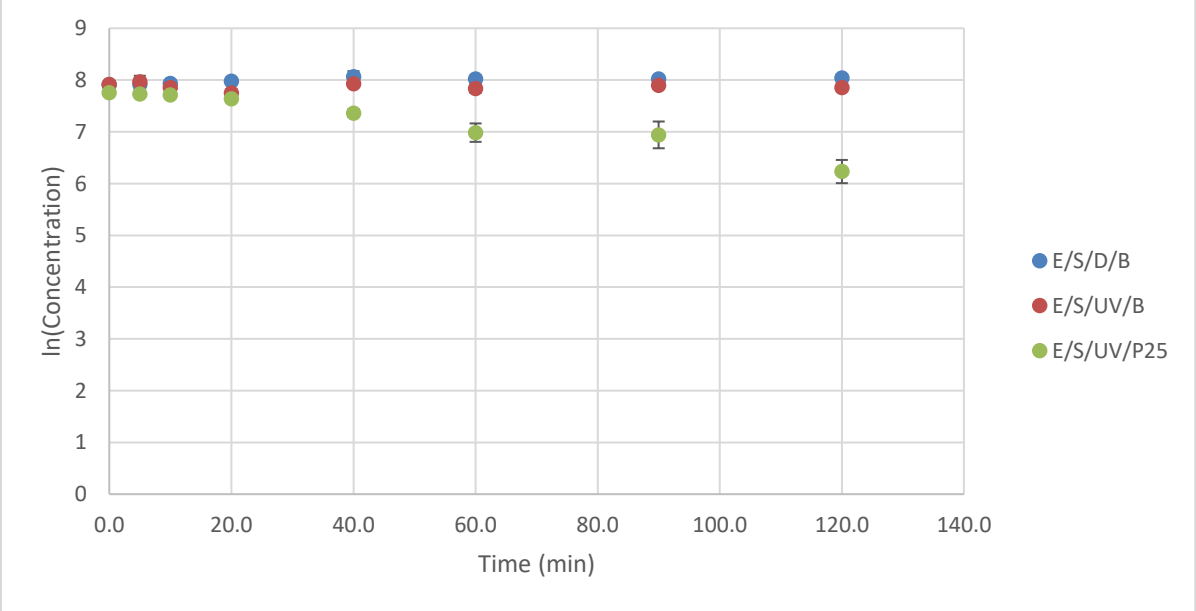

Figure C 48: Degradation of venlafaxine in wastewater effluent.

C2: Statistical Data

SAMPLE NAME	*TEST*	*E/S/D/B*	*E/S/UV/B*	*E/S/UV/P25*	*M/S/D/P25*	*M/S/UV/B*	*M/S/UV/P25*
Acetaminophen	k	-7.06E-04	3.05E-03	-	1.48E-03	7.15E-03	-
	r^2	2.81E-01	2.95E-01	-	3.50E-01	9.88E-01	-
	F	2.34E+00	2.51E+00	-	3.23E+00	5.04E+02	-
	Statistical Pass?	Fail	Fail	N/A	Fail	Pass	N/A
Atrazine	k	-4.62E-04	1.76E-03	3.03E-03	-6.88E-04	2.39E-03	3.62E-02
	r^2	2.56E-01	3.22E-01	8.09E-01	3.38E-01	9.54E-01	9.87E-01
	F	2.07E+00	2.85E+00	2.54E+01	3.07E+00	1.23E+02	4.43E+02
	Statistical Pass?	Fail	Fail	Pass	Fail	Pass	Pass
Atenolol	k	3.46E-04	1.90E-03	1.07E-02	-3.79E-04	4.84E-03	5.16E-02
	r^2	8.93E-02	4.66E-01	9.61E-01	2.67E-01	9.51E-01	9.40E-01
	F	5.88E-01	5.24E+00	1.47E+02	2.19E+00	1.16E+02	9.38E+01
	Statistical Pass?	Fail	Fail	Pass	Fail	Pass	Pass
Atorvastatin	k	1.36E-03	1.41E-02	5.22E-02	4.80E-03	1.88E-02	1.41E+00
	r^2	6.47E-01	9.00E-01	9.94E-01	9.30E-01	9.07E-01	1.00E+00
	F	1.10E+01	5.42E+01	9.62E+02	7.97E+01	5.83E+01	-
	Statistical Pass?	Pass	Pass	Pass	Pass	Pass	N/A
BisphenolA	k	3.29E-04	3.29E-03	2.96E-02	-9.16E-04	7.35E-03	1.47E+00
	r^2	2.39E-02	6.84E-01	9.64E-01	3.21E-02	9.89E-01	1.00E+00
	F	1.47E-01	1.30E+01	1.62E+02	1.99E-01	5.43E+02	-!
	Statistical Pass?	Fail	Pass	Pass	Fail	Pass	N/A
Caffeine	k	2.06E-03	4.24E-04	9.67E-03	5.94E-04	1.70E-03	3.73E-02
	r^2	5.49E-01	1.59E-02	8.72E-01	5.43E-02	4.43E-01	2.72E-01
	F	7.31E+00	9.69E-02	4.08E+01	3.45E-01	4.77E+00	2.25E+00
	Statistical Pass?	Pass	Fail	Pass	Fail	Fail	Fail
Carbamazepine	k	-2.31E-05	2.52E-03	1.61E-02	-1.82E-04	4.29E-03	3.14E-02

	r^2	1.25E-03	5.98E-01	9.86E-01	2.22E-02	9.77E-01	5.38E-01
	F	7.48E-03	8.94E+00	4.36E+02	1.36E-01	2.53E+02	6.98E+00
	Statistical Pass?	Fail	Pass	Pass	Fail	Pass	Pass
Carbamazepine-10,11-Epoxide	k	3.06E-05	1.90E-03	1.15E-02	-4.44E-04	3.00E-03	4.10E-02
	r^2	1.04E-03	4.10E-01	9.68E-01	2.05E-01	9.11E-01	7.41E-01
	F	6.28E-03	4.16E+00	1.81E+02	1.55E+00	6.15E+01	1.72E+01
	Statistical Pass?	Fail	Fail	Pass	Fail	Pass	Pass
Desvenlafaxine	k	-2.38E-03	-9.85E-05	3.26E-02	-2.40E-03	5.98E-03	-
	r^2	8.54E-01	5.64E-03	9.68E-01	8.69E-01	9.97E-01	-
	F	3.50E+01	3.40E-02	1.84E+02	3.97E+01	1.76E+03	-
	Statistical Pass?	Pass	Fail	Pass	Pass	Pass	N/A
Diclofenac	k	1.74E-03	5.47E-03	1.84E-02	1.76E-03	1.38E-02	1.45E+00
	r^2	5.49E-03	9.03E-01	7.89E-01	1.06E-01	9.97E-01	1.00E+00
	F	3.31E-02	5.58E+01	2.25E+01	7.10E-01	1.72E+03	-!
	Statistical Pass?	Fail	Pass	Pass	Fail	Pass	N/A
Flouxitine	k	1.34E-04	1.75E-03	1.37E-02	8.96E-04	1.85E-02	3.39E-02
	r^2	3.47E-03	2.62E-01	9.55E-01	1.97E-01	9.79E-01	6.87E-01
	F	2.09E-02	2.13E+00	1.26E+02	1.47E+00	2.78E+02	1.32E+01
	Statistical Pass?	Fail	Fail	Pass	Fail	Pass	Pass
Gemfibrozil	k	6.98E-04	3.24E-03	1.25E-02	2.93E-04	6.58E-03	-
	r^2	2.52E-01	5.11E-01	9.47E-01	2.93E-02	9.36E-01	-
	F	2.02E+00	6.27E+00	1.07E+02	1.81E-01	8.84E+01	-
	Statistical Pass?	Fail	Pass	Pass	Fail	Pass	N/A
Ibuprofen	k	0.00E+00	1.57E-03	1.14E-02	5.89E-04	3.34E-03	3.88E-01
	r^2	1.34E-02	2.43E-01	9.51E-01	3.55E-01	7.63E-01	9.14E-01
	F	8.18E-02	1.92E+00	1.16E+02	3.30E+00	1.93E+01	2.13E+01
	Statistical Pass?	Fail	Fail	Pass	Fail	Pass	Pass
Lincomycin	k	2.32E-04	3.64E-03	5.25E-02	-1.34E-04	8.35E-03	3.63E-02
	r^2	2.61E-01	7.44E-01	9.92E-01	4.23E-02	9.92E-01	2.86E-01
	F	2.11E+00	1.74E+01	7.52E+02	2.65E-01	7.47E+02	2.40E+00

	Statistical Pass?	Fail	Pass	Pass	Fail	Pass	Fail
Monensin	k	-1.99E-03	3.56E-03	1.76E-02	3.17E-03	2.70E-02	-
	r^2	6.85E-01	6.46E-01	9.56E-01	7.60E-01	9.87E-01	-
	F	1.31E+01	1.10E+01	1.29E+02	1.90E+01	4.48E+02	-
	Statistical Pass?	Pass	Pass	Pass	Pass	Pass	N/A
Naproxen	k	4.40E-04	5.86E-03	3.92E-02	-1.95E-03	7.58E-03	1.14E+00
	r^2	2.72E-02	7.48E-01	9.60E-01	3.02E-01	9.43E-01	1.00E+00
	F	1.68E-01	1.78E+01	1.45E+02	2.60E+00	9.87E+01	-!
	Statistical Pass?	Fail	Pass	Pass	Fail	Pass	N/A
Norfluoxetine	k	8.32E-04	3.83E-03	1.46E-02	1.80E-03	1.94E-02	3.21E-02
	r^2	1.06E-01	6.53E-01	9.32E-01	5.24E-01	9.90E-01	7.40E-01
	F	7.12E-01	1.13E+01	8.19E+01	6.61E+00	5.94E+02	1.71E+01
	Statistical Pass?	Fail	Pass	Pass	Pass	Pass	Pass
O-Atorvastatin	k	7.61E-04	1.75E-02	4.99E-02	1.45E-02	2.40E-02	-
	r^2	5.71E-01	9.59E-01	7.92E-01	8.71E-01	8.81E-01	-
	F	7.98E+00	1.42E+02	2.29E+01	4.04E+01	4.43E+01	-
	Statistical Pass?	Pass	Fail	Pass	Pass	Pass	Pass
P-Atorvastatin	k	6.78E-04	1.51E-02	-	1.11E-02	2.31E-02	-
	r^2	3.36E-01	9.49E-01	-	9.70E-01	9.49E-01	-
	F	3.04E+00	1.12E+02	-	1.92E+02	1.11E+02	-
	Statistical Pass?	Fail	Pass	N/A	Pass	Pass	N/A
Sulfamethoxazole	k	3.38E-04	3.68E-03	3.69E-02	7.65E-05	6.63E-03	-
	r^2	2.36E-01	6.69E-01	9.79E-01	3.14E-03	9.72E-01	-
	F	1.85E+00	1.21E+01	2.77E+02	1.89E-02	2.12E+02	-
	Statistical Pass?	Fail	Pass	Pass	Fail	Pass	N/A
Sulfonamide	k	-1.26E-03	-	2.52E-02	-2.04E-03	2.97E-03	-
	r^2	4.44E-01	-	9.89E-01	9.18E-01	9.38E-01	-
	F	4.78E+00	-	5.49E+02	6.70E+01	9.13E+01	-
	Statistical Pass?	Pass	N/A	Pass	Pass	Pass	N/A

Triclosan	k	-6.07E-05	3.05E-03	3.44E-02	-8.51E-04	9.38E-03	7.73E-01
	r^2	6.27E-04	5.82E-01	9.05E-01	5.26E-02	9.93E-01	9.84E-01
	F	3.77E-03	8.36E+00	5.72E+01	3.33E-01	8.57E+02	6.25E+01
	Statistical Pass?	Fail	Pass	Pass	Fail	Pass	Pass
Trimethoprim	k	-3.80E-04	1.62E-03	1.38E-02	-1.13E-03	9.10E-03	3.98E-02
	r^2	3.13E-01	4.05E-01	9.80E-01	6.47E-01	9.95E-01	7.47E-01
	F	2.73E+00	4.09E+00	2.87E+02	1.10E+01	1.19E+03	1.78E+01
	Statistical Pass?	Fail	Fail	Pass	Pass	Pass	Pass
Venlafaxine	k	-1.06E-03	2.12E-04	1.21E-02	-1.42E-03	7.98E-03	4.54E-02
	r^2	5.95E-01	1.92E-02	9.59E-01	6.46E-01	9.96E-01	7.02E-01
	F	8.82E+00	1.17E-01	1.41E+02	1.10E+01	1.47E+03	1.42E+01
	Statistical Pass?	Pass	Pass	Pass	Pass	Pass	N/A